Michael Chimaeze Ekeogu Jensen

Numerical study on roll damping, relevant for FPSO platforms

Master's thesis in Marine Technology
Supervisor: Marilena Greco
February 2019

Master's thesis

NTNU
Norwegian University of Science and Technology
Faculty of Engineering
Department of Marine Technology

NTNU
Norwegian University of
Science and Technology

Michael Chimaeze Ekeogu Jensen

Numerical study on roll damping, relevant for FPSO platforms

Master's thesis in Marine Technology
Supervisor: Marilena Greco
February 2019

Norwegian University of Science and Technology
Faculty of Engineering
Department of Marine Technology

NTNU
Norwegian University of
Science and Technology

NTNU Trondheim
Norwegian University of Science and Technology
Faculty of Engineering Science and Technology
Department of MarineTechnology

MASTER THESIS IN MARINE TECHNOLOGY

Fall 2018

FOR

Michael Chimaeze Ekeogu Jensen

Numerical study on roll damping, relevant for FPSO platforms

(Et numerisk studie på rulle dempning, relevant for FPSO-plattformer)

For advancing vessels and for ships used as FPSO platforms, roll damping is highly nonlinear and comes from several contributions. Among them, the linear wave radiation damping is generally quite small compared to the total damping in the system. An adequate estimate of the roll damping near resonance is very important, to ensure stable and safe conditions for the vessels. For example, the damping is one of the parameter that affects occurrence of parametric resonance in roll.
This master thesis is the logical continuation of a project thesis as preparation of a numerical investigation of the topic.

Objective
The present master thesis aims to enhance knowledge on the physical phenomena governing the roll damping mechanisms. The investigation tool is an open-source Computational Fluid Dynamic (CFD) solver.

The work should be carried out in steps as follows:

1. Summarize major findings/outcomes from the project thesis and complement the literature survey in order to identify state-of-the-art on the roll damping mechanisms for ship and FPSO cross-sections, without and with bilge keels.
2. Describe the CFD method selected during the project and complete its validation and numerical convergence studies initiated during the project work. Define the assumptions that you intent to use within this numerical study.
3. Select a FPSO platform. Apply the CFD method to investigate the mid-FPSO section without and with bilge keels. Examine at least two bilge-keel widths, within the range relevant for FPSO platforms. Forced oscillatory roll motion at the roll resonance should be studied, with at least three oscillation amplitudes to investigate the effect of KC number on the roll damping. To do this, the natural roll period should be identified from free-decay simulations. However, it is more efficient to perform numerical-convergence studies for the different bilge-keel arrangements in forced roll motion. Therefore, an iterative process is suggested, using preliminary results from step 4, to identify the roll natural period and then carrying on the parameter analysis on the converged grids obtained from the forced-roll studies.
4. Free-decay simulation in roll for the same ship section (without and with bilge keels) should be studied as 1-DOF system, with three initial roll angles (equal to the steady state amplitudes used in the force-roll studies in step 3). Examine quantitative importance of linear and second-order damping in roll for the different section arrangements and initial roll amplitudes. Compare the linearized roll damping estimated in the forced-roll and roll free-decay simulations. For selected cases,

analyse the sensitivity of the results to the grid choices made, for example near sharp corners.
5. Draw the conclusions from the studies and discuss possible future steps in the context of this topic.

The work may show to be more extensive than anticipated. Some topics may therefore be left out after discussion with the supervisor without any negative influence on the grading.
The candidate should in his report give a personal contribution to the solution of the problem formulated in this text. All assumptions and conclusions must be supported by mathematical models and/or references to physical effects in a logical manner.

The candidate should apply all available sources to find relevant literature and information on the actual problem.

The thesis should be organised in a rational manner to give a clear presentation of the work in terms of exposition of results, assessments, and conclusions. It is important that the text is well written and that tables and figures are used to support the verbal presentation. The thesis should be complete, but still as short as possible. In particular, the text should be brief and to the point, with a clear language. Telegraphic language should be avoided.

The thesis must contain the following elements: the text defining the scope (i.e. this text), preface (outlining project-work steps and acknowledgements), abstract (providing the summary), table of contents, main body of thesis, conclusions with recommendations for further work, list of symbols and acronyms, references and (optional) appendices. All figures, tables and equations shall be numerated.

The supervisor may require that the candidate, in an early stage of the work, present a written plan for the completion of the work. The plan should include budget for the use of computer and laboratory resources that will be charged to the department. Overruns shall be reported to the supervisor.

From the thesis it should be possible to identify the work carried out by the candidate and what has been found in the available literature. It is important to give references to the original source for theories and experimental results.

Supervisor : Marilena Greco
Co-supervisor : Giuseppina Colicchio
Co-supervisor : Andrea Califano

Submitted : September 6th 2018
Deadline : February 18th 2019

Marilena Greco
Supervisor

Preface

This work was carried out during the final year of my M.Sc. in Marine Hydrodynamics at the Department of Marine Technology, NTNU Trondheim. This work introduces and addresses the difficulties and methods for roll damping estimation in general and how numerical methods can be applied to determine the damping coefficients for marine structures such as FPSO platforms fitted with bilge keels. The numerical tool used in the work is OpenFOAM, which is an open source toolbox used in a broad range of computational fluid dynamics (CFD) related problems. My goal with this work was do get a deeper understanding and knowledge of the hydrodynamic problems related to roll motion. I also wanted to perform a case study by using a numerical tool, to strengthen my interest and skills within CFD.

Throughout the project, supervisor Marilena Greco has been available and open for discussions, and I thank her very much for her contribution and guidance when I have been in need of both knowledge and motivation. I am very grateful for her help. Further, Giuseppina Colicchio has also been very helpful in every part regarding questions and problems with the simulations in OpenFOAM.

In addition, PhD candidate Mohd Atif Siddiqui should be mentioned as he has been my greatest support with the simulations. He has thought me everything I need to know about performing a study like this with OpenFOAM, and spent several hours after his working hours helping me. I would also like to thank my co-supervisor Andrea Califano from DNV-GLs department in Trondheim for taking time to assist me besides his own work, and Tufan Arslan from the computer department at NTNU for help and guidance with parallel computing with hpc at Vilje.

Trondheim, 2017-12-19

Michael Chimaeze Ekeogu Jensen

Abstract

Ship motions are described by six degrees of freedom. Five of these can be estimated fairly well by use of linear potential theory. Rolling however, cannot be predicted accurately by use of this, as it is connected to non-linearities.

The case study performed during this work has been conducted with the open source computational fluid dynamics (CFD) toolbox OpenFOAM. A lot of time has been used in the preparatory work, as OpenFOAM can be tricky to use, and it demands quite some time to understand the program.

Based on the available literature and experiments done, a validation study has been performed. This is done to ensure that the CFD software is suitable for the current work, as it was discovered in the project thesis that particularly roll damping was not estimated well. Due to the low damping ratio, estimation of roll damping are sensitive to numerical properties and discretization techniques, which should be carefully considered.

Roll damping has then been estimated for a 2D section of a floating, production, storage and offloading (FPSO) platform. Four different configurations in terms of bilge keels has been investigated, where the effect of the bilge keel width on the damping coefficient showed a linear relation. The difference with and without bilge keels is significant, with up to 400% increase in the damping when equipped with larger than usual bilge keels.

Forced roll simulations and free decay tests have been performed and compared against each other. It was found that comparison of these two methods are possible if one consider the mean roll angle during the first roll cycles for the free decay test. Due to this, forced roll motions are to prefer as the amplitude is held constant.

In terms of Keulegan-Carpenter (KC) number, which is a function of the roll amplitude for one specific cross section, the damping showed to have a strong dependence on this. This confirms that the damping phenomena is strongly connected with non linear terms, as the KC dependence is connected to the quadratic damping term.

Contents

List of Figures

List of Tables

Nomenclature

α	Bilge keel angle to vertical
$\ddot{\theta}$	Roll acceleration
$\dot{\theta}$	Roll velocity
∇	Displacement
ω_n	Natural frequency
ω_n^*	Non dimensional natural frequency
ρ	Density of water
θ	Roll amplitude
ζ	Damping ratio
A_{44}	Added mass moment of inertia
$B_{44,1}$	Linear roll damping coefficient
$B_{44,2}$	Quadratic roll damping coefficient
$B_{44,eq}$	Equivalent roll damping coefficient
B_{44}	Roll damping coefficient
B_{44}^*	Non dimensional roll damping coefficient
B_{BKN}	Bilge keel normal force damping
B_{BKS}	Bilge keel hull pressure damping
B_{BKW}	Bilge keel wave making damping
b_{bk}	Bilge keel width

B_{crit} Critical damping

C_D Drag coefficient

C_M Inertia coefficient

C_P Pressure coefficient

C_{44} Restoring coefficient in roll

GM_T Transverse metacentric height

I_4 Roll moment of inertia

L_{bk} Bilge keel width

l_{bk} Bilge keel length

n_1 Surge motion

n_2 Sway motion

n_3 Heave motion

n_4 Roll motion

n_5 Pitch motion

n_6 Yaw motion

r_{44} Roll radius of gyration

2D Two Dimensional

a Acceleration

B Beam/breadth

BM Distance from buoyancy center to metacenter

CFD Computational Fluid Dynamics

D Draft

FDPSO Floating, Drilling, Production Storage and Offloading

FEM Finite Element Method

FPSO	Floating, Production, Storage and Offloading
FSO	Floating, Storage and Offloading
FSRU	Floating, Storage, Regasification Unit
FVM	Finite Volume Method
g	Gravitational constant
KB	Distance from keel to centre of buoyancy
KG	Distance from eel to centre of gravity
M	Mass
M(t)	Roll moment
T_n	Roll natural period
u	Velocity
VOF	Volume Of Fluid

Chapter 1

Introduction

Background

I have grown up spending a lot of time on our family's boat. Boats, and ships in general have influenced many of my choices through my life, becoming a naval architect included. The choice of focusing on ships on my project and masters degree was something I really wanted. The motivation behind this project was to get more familiar with the complex physical aspects of ship rolling motions. For ships, rolling plays an important role for both physical aspects regarding the ship, in addition to the experience for crew, passengers or cargo on board. The intended plan was to focus on roll damping for advancing vessels, but as the preparatory work was delayed and challenges with the numerical solver was discovered these plans were discarded. A new scope was set where a through investigation of the numerical solver would be performed, and then continue with analysis of a FPSO (Floating, Production, Storage and Offloading) platform.

Estimation of ship motions in roll are somewhat difficult to obtain by the well known potential theory, since rolling is highly dependent on non-linear phenomena. To give good predictions of the roll motion of a ship, experiments are necessary to give accurate results. In the recent time, with increasing computational power, CFD has become an important tool for estimating ship motions, which can be done early in the design phase, and are time- and cost saving compared to experiments. The damping plays an important role when considering roll motion, and will influence the roll motion. Damping devices are present on ships with the aim of increasing the damping coefficient, such that the roll amplitude is decreased. The focus in the thesis will be on the roll damping coefficients, and particularly how the Keulegan-Carpenter (KC) number and bilge keels will affect the roll damping.

Related work

Rolling has been a tricky subject for naval architects due to strong, nonlinear effects. A big scope of this work is based on the research by the Japanese scientist *Ikeda, Himeno and Tanaka*, which in many ways still is the industry standard for estimation of roll damping for ships.

Motivation

In the preparatory work for this thesis, a literature review and a simple case study was conducted. The experiments by Vugts [4] was reproduced with the open source CFD toolbox OpenFOAM. However, these findings gave indications that there may be some problems regarding roll damping analysis based on OpenFOAM simulations. This gave motivation to not only proceed with other types of simulations, but also to investigate in a thorough manner how the user specified controls are playing an important role in order to achieve satisfactory results.

Outline

The outline of the report is as follows:

- A literature study identifying the state-of-the-art on roll damping components and how they are found based on empirical formulas. Work from project thesis.
- Theoretical background for the CFD simulations and roll damping estimation.
- A validation case to investigate and validate if the solver is applicable for the current studies.
- A case study where the parameter dependence of bilge keel width and KC number is investigated.
- A discussion about the results, and a conclusion is drawn.

Chapter 2

Background

2.1 Ship motions

A freely floating body has six degrees of freedom. Three oscillatory rigid body motions (surge, sway, heave) and three oscillatory angular motions (roll, pitch, yaw). These motions leads to six equations of motions, which describes the total motion of the body. For ships, vertical accelerations and relative vertical motion are of interest, as these will impact loads on the vessel and is of interest what regards seasickness. Rolling is also identified as the most critical motion, and can cause severe accidents or capsizing.

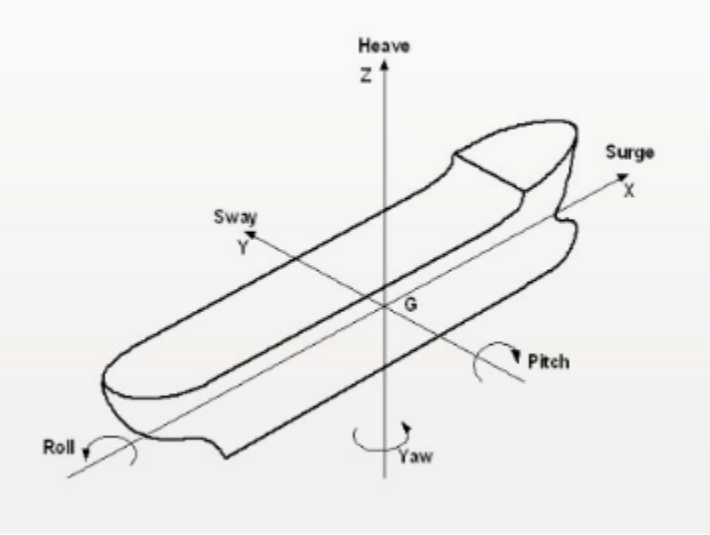

- $\eta 1 - surge$
- $\eta 2 - sway$
- $\eta 3 - heave$
- $\eta 4 - roll$
- $\eta 5 - pitch$
- $\eta 6 - yaw$

Figure 2.1: Degrees of freedom for a ship

For a ship, when modelling these motions, roll is the one which is strongly dependent on non-linear terms, making it difficult to determine based on linear, potential theory. η_4 which de-

scribes the roll motion, will be referred to as θ from now on, as it is an angular motion.

2.1.1 Roll motion

Motions for a ship are coupled to each other. As Faltinsen [1] stated, the advantage for ships having lateral symmetry is that the heave-surge-pitch motions can be decoupled from the sway-roll-yaw motion. By further assumptions and the simplicity, the roll motion can be explicit described as an equation of single degree.
In general, a linearized model of the motion equation may be used in calculating response and loads on ships. By linear, it is meant output is proportional to input. Assuming a slender body, harmonic and small oscillations, linear potential theory can be used by calculating the loads for a 2D-strip, and integrate over the body's length (Strip theory). In regular waves, the hydrodynamic forces acting may be divided into two sub-problems,

- Forces on restrained body from incident waves
- Forced oscillating motion

where the restrained body problem will lead to what we call wave excitation forces, and are coupled to diffraction and Froude-Kryloff forces.
Since a freely floating body will move in the case of incident waves, this is dealt with assuming no incident waves, and force the body to oscillate with the wave frequency in the specific body motion of interest. We identify these loads as added mass, damping and restoring from the radiated waves from the body.

The linearized single roll motion equation is written like a mass-springer-dashspot system;

$$(I_4 + A_{44})\dot{\theta} + B_{44,w}\dot{\theta} + C_{44}\theta = M(t) \tag{2.1}$$

where, $\ddot{\theta}$, $\dot{\theta}$ and θ denotes the angular acceleration, angular velocity and angular motion respectively. I_4 and A_{44} are the moment of inertia and added mass moment, B_{44}, w the linear, wave damping coefficient and C_{44} is the restoring term. $M(t)$ represents the roll excited moment.

The natural frequency of the body, can then be obtained by the following expression;

$$\omega_n = \sqrt{\frac{C_{44}}{I_4 + A_{44}}} \tag{2.2}$$

with the critical damping given as:

$$\zeta = \frac{B_{44}}{2(I_4 + A_{44})\omega_n} \tag{2.3}$$

Including terms

It can be seen that the damping B_{44}, w is connected to the velocity, and it's physical aspect when considering linear wave damping is energy dissipating from the body, as it generates outgoing waves. Linear wave damping for a 2D section is strongly connected to the beam/draft ratio, shown by Vugts [4] and can be clearly shown in 2.2. Faltinsen [1] explains this by cancellation effects. Cancellation happens when the roll moment caused by pressure forces along the ship side tends to counteract the roll moment from pressure forces at the ship bottom. The damping loads, expressed in equation (2.1) will be further discussed in the thesis, as non linear effects will be of importance, and an improved model is introduced.

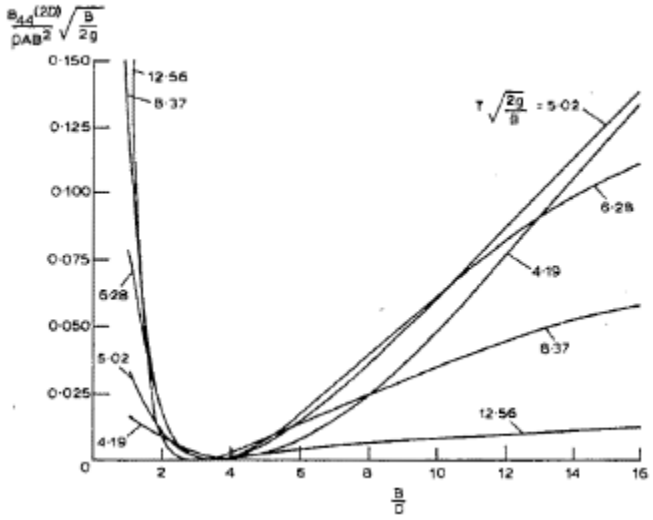

Figure 2.2: 2D roll damping with respect to B/D ratio [4]

Restoring

The restoring term C_{44} is connected to roll motion, θ and represents a force from the change in centre of buoyancy. From stability analysis, a change in buoyancy will lead to a restoring

moment, and physically this is the body's ability to return to it's initial position. The restoring coefficient in roll is defined;

$$C_{44} = \rho g V \overline{GM_T} \tag{2.4}$$

with $\overline{GM_T}$ as the transverse metacentric height and V volume displacement.

Mass and inertia

The mass forces are coupled to the accelerations. A physical understanding is that when a body is accelerated, it has to move some volume of fluid surrounding it as well. The added mass term can be calculated by e.g. use of strip theory or forced oscillation tests. The inertia coefficient can be obtained as

$$I_4 = M r_{44}^2 \tag{2.5}$$

which is the mass multiplied by the roll radius of gyration squared. A general guidance is that for ships, r_{44} is given as 0.35 times the beam according to Faltinsen [1].

2.2 On roll damping in general

In order to predict the roll damping for ships advancing in waves, a natural step is to first investigate how roll damping at zero speed is estimated, and get familiar with the characteristics of the different damping components account for the total roll damping. The focus presented in the following text is based on displacement type ship bodies, and for other types of structure like platforms, modifications to the presented work may apply.

As equation (2.1) only includes the linear wave damping component, it is not sufficient to cover all the mechanisms contributing to roll damping. Roll damping can physically be explained as a transfer of roll energy to the surrounding fluid. As previously discussed, the linear wave damping shows to only be one of many mechanisms to transfer the roll energy, and viscous effects will be of great importance. Prediction of roll motions by potential theory is therefore highly inaccurate, and overestimates the amplitudes near resonance region [10].

In order to predict roll motions precisely, equation (2.1) should be modified to include non linear effects. We may rewrite it on the form,

$$(I_4 + A_{44})\dot{\theta} + B_{44}(\dot{\theta}) + C_{44}\theta = M(t) \tag{2.6}$$

where $B_{44}(\dot{\theta})$ is the damping term including non-linear contributions. This damping term can further be expressed as an series expansion of the roll velocity, as a sum of a linear, quadratic and cubic term.

$$B_{44}(\dot{\theta}) = B_{44,1}\dot{\theta} + B_{44,2}\dot{\theta}|\dot{\theta}| + B_{44,3}\dot{\theta}^3 + ... \tag{2.7}$$

Equation (2.7) shows, we get different damping components connected to orders of the roll velocity. The first order term includes e.g. the linear wave making damping and lift effects, as well as some frictional effects. What these terms represent will be further discussed. For practical reasons, the non-linear damping equation is often approximated by an linear equivalent term, as it is difficult to analyze.

$$B_{44}(\dot{\theta}) = B_{44,eq}\dot{\theta} \tag{2.8}$$

$B_{44,eq}$ can be expressed in several ways. A common way, presented in [10] is to represent it with the same damping components as in equation (2.7).

$$B_{44,eq} = B_{44,1} + B_{44,2}\frac{8}{3\pi}\omega\theta + B_{44,3}\frac{3}{4}(\omega\theta)^2 \tag{2.9}$$

Here, it is assumed that the energy loss due to damping during a half cycle of roll is the same when nonlinear and linear damping are used [6]. Flow separation leads to a drag force, and is presented as a function of velocity squared in Morrison equation.

2.3 On FPSO

A floating production, storage and offloading platform (FPSO) is a unit used by the energy industry, to produce and process hydrocarbons as well as storage. FPSO platforms are convenient in remote or deep waters, as they eliminates the need of pipelines from the production site to onshore terminals for processing. FPSO platforms also have the advantage that they can easily be moved between different locations. There are different types of FPSOs whereas many are converted oil tankers and some are custom built. Further, one can classify the platforms in different types as FPSO, FSO, FDPSO and FSRU. These platforms are characterized by their capabilities, where a FSO does not have the capability of processing the hydrocarbons it self. FDPSO is an FPSO which also can do drilling operations, and the FSRU is a regasification unit.

For ships, installation of bilge keels is a compromise of stability and cost, as the bilge keels increases the drag. A FPSO, which is mostly moored at site does not have the same compromise so that the bilge keels often can be significant larger than for corresponding ships. Other constraints for FPSOs are more structural constraints, as the hull must withstand the forces from the bilge keels, as well as outfitting constraints related to dry-docking and maintenance. In addition, location for the planned operation can also affect the dimensions of the bilge keels, and the general platform requirements. E.g, West Africa deep water developments are exposed to mild environmental conditions, with most of the swell coming from south-west (FPSO heading)

[36]. That means the vessel is exposed to smaller roll excitation motions, and the bilge keels may be smaller compared to other FPSO platforms. In the Mexican gulf and the north sea the conditions are categorized as harsh, which demands quite different requirements. Large roll angles will limit both the comfort and operational time, hence roll is an important parameter also for FPSO platforms.

Figure 2.3: The FPSO Bleo Holm [48]

2.4 Damping components

As a summary of the project work, the damping components and how they are estimated according to the present state are presented in the following section.

Roll damping for ships are in general dealt with by dividing the damping contributions into different components, as presented in Ikeda [5]. As Chakrabarti [8] says, this subdivision is not necessary justified from a hydrodynamic point of view, since interactions among the components will occur.
In general, the damping components for ships are a function of velocity, roll amplitude and frequency of motion, Taylan [9]. Since the viscous contributions are related to drag, the equivalent damping models are presented as quadratic from now on.

$$B_{44} = B_{44}(\omega, \theta, V) \tag{2.10}$$

By introducing Ikeda's method, we identify the components of roll damping as

- Wave making damping, B_W

- Eddy making damping, B_E
- Skin friction damping, B_F
- Lift damping, B_L
- Bilge keel damping, $B_B K$

Of these terms, only the wave making damping and the lift damping can be said to be linear and inviscid. As shown later, a part of the bilge keel damping can also be considered as linear and inviscid. The other three components can be regarded as viscous, and nonlinear. It shows that all the damping components are dependant on the angular oscillating frequency and velocity [10]. All terms presented in the following text will be based on (2.9), the equivalent linearized damping term. The nonlinear terms in the following text will be described by the quadratic term. Due vortex shedding, the bilge keel components and eddy making component will depend on the roll amplitude as well, due their dependencies of KC number.

2.4.1 Wave making

Wave making damping, as first introduced in (2.1) relates to the radiation problem, and is considered linear and inviscid. An oscillating body will generate waves, and by that transfer energy to the surrounding fluid. The wave damping term is the only of five damping terms that can be calculated satisfactory by use of potential theory. According to ITTC [10], the wave making damping accounts for somewhere between 5% to 30% of the roll damping for a general cargo ship. The Wave making damping contribution is strongly connected to the Beam/Draft ratio as shown in figure (2.2). In means of this, examples for a full ($C_B = 0.8$) & one slender ship($C_B = 0.5$) is shown, and the wave making damping distribution.

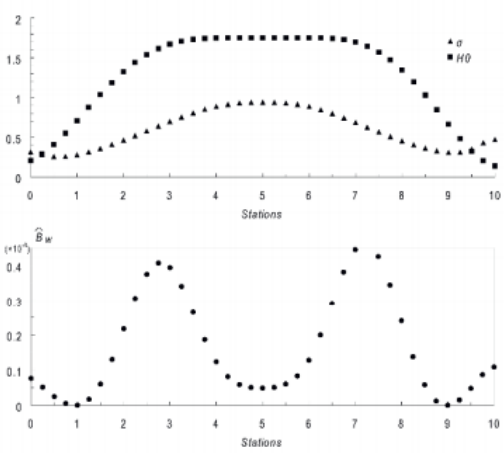

Figure 2.4: 1

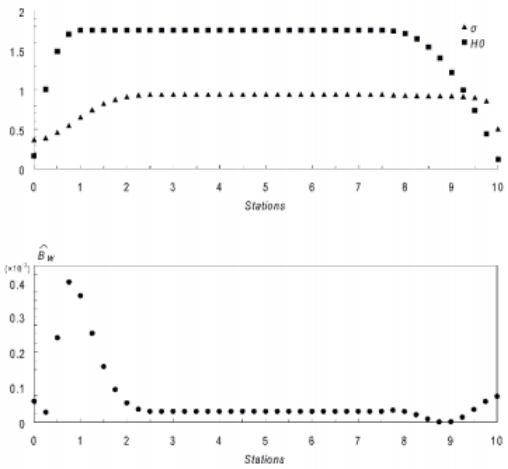

Figure 2.5: 2

Figure 2.6: Wave making roll damping at different locations [7]

There are presented several ways of estimating this component, as introduced by Ikeda, and also the one found in the ITTC procedures. The formula can be rather complex, and for some cases it will include coupling terms with e.g. sway. The wave damping will also be affected by forward speed. By Newman (1977) the total energy in a volume Ω can be expressed by potential and kinetic energy;

$$E(t) = \rho \iiint_{\Omega} (\frac{1}{2} V^2 + gz) d\tau \tag{2.11}$$

with $d\tau$ as a symbol for volume integral. By solving the linear and dynamic boundary value problem, and assuming

$$U_n = \frac{\delta \phi}{\delta n}, U_n = 0 \tag{2.12}$$

on the body surface and far field, respectively. The time derivative of equation (2.11) can be written in terms of linear motion as;

$$\int_{SB} (p - p_0) U_n ds = \dot{\theta}(A_{44}\ddot{\theta} + B_{44}\dot{\theta} + C_{44}\theta - \rho g V) \tag{2.13}$$

with $(p - p_0)$ as the pressure changes on the body.

By representing the velocity potential as the outgoing waves, and the average energy in one period of oscillation is constant due periodic motion, the wave making damping follows;

$$B_{44} = \rho \big(\frac{A_4}{\theta}\big)^2 \frac{g^2}{\omega^3} \tag{2.14}$$

where A_4 is the radiated wave amplitude. It follows that the wave making damping is proportional to the square power of radiated waves.

2.4.2 Eddy making damping

The eddy making damping, B_E is a viscous phenomena, and is highly dependent on the ship geometry. It is common to calculate B_E for a cross-section of the ship, and then integrate over the length. Physically, it is connected to flow separation from sharp edges on the naked ship hull, and will be different for typically full ships with sharp corners compared to a more rounded hull form. At the bow and stern, there will be typically high damping factors due the sharp edges. Bilge keel damping will be separated from the eddy making damping as it is a dominating component, however it is a type of eddy damping.

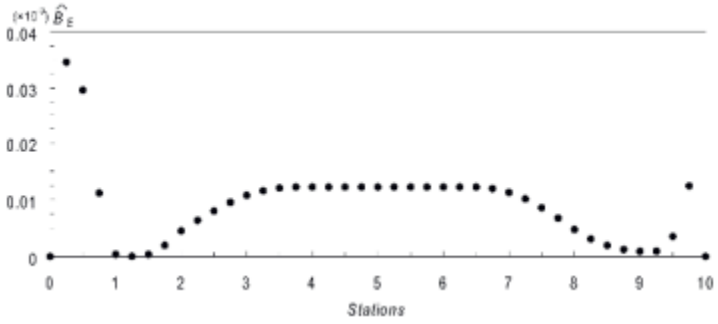

Figure 2.7: Distribution of eddy making damping coefficients for a ship, Kawahara [7]

ITTC procedures presents the empirically estimated eddy making damping for a cross section, by Ikeda as [5]:

$$B_E = \frac{4}{3\pi}\rho d^4 \omega \theta C_R \tag{2.15}$$

It shows that the eddy making damping is proportional to the roll amplitude θ and the frequency. The term C_R is given by:

$$C_R = \left[\left(1 - f_1\frac{R}{d}\right)\left(1 - \frac{\overline{OG}}{d}\right) + f_2\left(\frac{B}{2d} - f_1\frac{R}{d}\right)^2\right] C_P \left(\frac{r_{max}}{d}\right)^2 \tag{2.16}$$

The eddy making damping includes several different terms, and may seem ugly at first. r_{max} is the maximum distance from centre of gravity to the hull surface, and R is the bilge radius. C_P is the pressure coefficient, and the magnitude of it is a function of γ, the ratio between maximum relative velocity and mean velocity on the hull surface. The pressure curve was empirically constructed by Ikeda (1978) through 2D experiments, following the eddy making component, B_E was obtained. Kawahara [7] proposed an updated model for the eddy making damping, but this

is much more complex, and can be found in [7].

$$C_P = 0.5(0.87e^{-\gamma} - 4e^{-0.187\gamma} + 3) \tag{2.17}$$

$$f_1 = 0.5[1 + tanh\big(20(\sigma - 0.7)\big)] \tag{2.18}$$

$$f_2 = 0.5(1 - cos\pi\sigma) - 1.5(1 - e^{-5(1-\sigma)})sin^2\pi\sigma \tag{2.19}$$

Here, σ is the cross sectional area under water. In special cases like a barge, improved methods has been carried out as the latter case tends to underestimate the eddy making damping for large B/d ratios.

2.4.3 Skin friction damping

The skin friction damping is the only damping mechanism that are strongly influenced by scale effects, ITTC procedure [10]. Ikeda performed tests on a small ship model (two meters long), and estimated the skin friction damping to account for between 5% to 10% of the total damping. Due it's connection with Reynolds number, it will typically only account for 1% to 3% for a full scale ship, and is thereby usually neglected. In the references, Katos formula for friction damping in a laminar flow field in terms of an equivalent linear damping coefficient is given;

$$B_f = \frac{4}{3\pi}\rho S r_e^3 \theta\omega C_f \tag{2.20}$$

with S as the wetted surface, r_e as effective bilge radius and C_f as the friction coefficient. C_f can be estimated by:

$$C_f = 1.328\Big[\frac{2\pi\nu}{3.22 r_e^2\theta^2\omega}\Big] \tag{2.21}$$

In the latter case, the scale effect can be shown by introducing the Reynolds number as a function of roll amplitude and frequency,

$$R_e = \frac{(r_e\theta)^2\omega}{\nu} \tag{2.22}$$

and we note that the friction coefficient is a function of R_e.

2.4.4 Lift damping

Lift damping is a phenomena related to $F_N \neq 0$, i.e. when the ship has forward speed. It occurs as a lifting moment when the pressure distribution around the hull changes, similarly as what

can be experienced with sway. It is a complex phenomena, but Ikeda (1978) proposed a simple expression for it,

$$B_L = \frac{0.15}{2}\rho U L d^3 k_N \left[1 - 2.8\frac{\overline{OG}}{d} + 4.667\left(\frac{\overline{OG}}{d}\right)^2\right] \tag{2.23}$$

where k_n is the slope constant. For increased velocities, the lift damping can become quite large [8]. The slope constant is given as;

$$k_N = 2\pi\frac{d}{L} + \kappa\left(4.1\frac{B}{L} - 0.045\right) \tag{2.24}$$

with κ as a function of the mid ship cross section, given as either 0, 0.1 or 0.3, where a high C_M will result in the largest κ. The effect of lift damping happens as a forward moving ship in roll, will no longer be symmetrical. Hence, pressure difference along the sides will produce a lifting force on the hull. The lift damping will be further discussed in the next section as we see bilge keels and rudders also will contribute to lift damping.

2.4.5 Bilge keel damping

The bilge keel damping, also referred to as appendages damping in some cases, is a contribution to the damping due to installation of damping devices. Bilge keels are by far, the most used damping device to get additional damping, and is fitted on the great majority of ships. Installation of bilge keels may contribute up to 80% of the total damping according to Kawahara [7]. An important aspect, is that the bilge keels must penetrate the boundary layer of the ship to ensure the effect. Normally, they do not protrude outside the sides of the ship, neither below the keel, to avoid damage. The bilge keel damping may further be subdivided into three sub-components. For FPSO platforms the bilge keel dimensions are often much larger with fewer constraints than for ships, as the platform will spend the majority of time moored to the seabed.

1. Bilge keel damping, normal force component - B_{BKN}
2. Bilge keel damping, hull pressure component - B_{BKS}
3. Bilge keel damping, wave making component - B_{BKW}

Both the normal force and hull pressure components are functionally dependant on the Keulegan-Carpenter number (KC), [23].

Figure 2.8: Bilge keels on a cargo ship

B_{BKN}, Normal forces on bilge keels

The normal force acting on a bilge keel is expressed in terms of an equivalent linear damping [10];

$$B_{BKN} = \frac{8}{3\pi}\rho r^3 b_{BK}\theta\omega f^2\left(22.5\frac{b_{BK}}{r\pi\theta f} + 2.4\right) \tag{2.25}$$

where b_{BK} is the bilge keel width, l_{BK} the bilge keel length and r the distance from centre of roll to bilge keel. f is a correction factor for the velocity at the bilge keels, given as a function of the cross sectional area coefficient σ:

$$f = 1 + 0.3e^{-160(1-\sigma)} \tag{2.26}$$

The normal force component can be related to a drag component, as a result of they are oscillating in a fluid. It is frequency & amplitude dependant, and is identified nonlinear as the drag force is a function of the square velocity.

B_{BKS}, pressure differences

The presence of bilge keels will cause pressure changes on the hull surface when oscillating as the flow separates. As for the normal force component, this term is also considered nonlinear, and is given on the form;

$$B_{BKS} = \frac{4}{3\pi}\rho r^2 d^2\omega\theta f^2 I \tag{2.27}$$

with I as a moment lever,

$$I = \frac{1}{d^2}\int C_{P1} l_{BK} ds \tag{2.28}$$

C_P denotes the pressure coefficient on the hull surface due the presence of the bilge keels, and varies from the front and back side of the bilge keel. Their maximums are given as:

$$C_P^+ = 1.2 \tag{2.29}$$

$$C_P^- = -\frac{22.5 b_{BK}}{r f \pi \theta} - 1.2 \tag{2.30}$$

B_{BKN}, Wave making

The bilge keel wave making damping is a phenomena related to interaction with free surface. As Bassler et al. [23] states, it is difficult to calculate. This is partially due the phase difference between the bilge keel wave making, and the global ship wave making. It might contribute to additive damping, but may also subtract the total roll damping. Often, the wave making damping from bilge keels are also neglected, as the contribution often is small compared to the other damping components for small roll amplitudes. This is the case for $b_{BK} = B/60$ to $B/80$. For larger roll amplitudes, or ships with larger bilge keels the effect may be of importance. An proposed model for the wave making damping contribution at $F_N = 0$ is given in [23] where the bilge keel is considered as pulsating source with frequency ω and source strength C_{BK}.

$$B_{BKW} \sim C_{BK}(b_{BK}) e^{\left(-\frac{\omega^2}{g} d_{BK}(\theta)\right)} \tag{2.31}$$

where d_{BK} is a function describing the length from the free surface to the bilge keel.

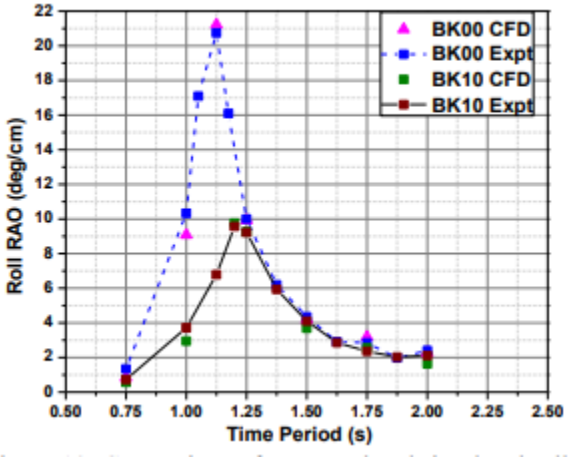

Figure 2.9: Effect of bilge keels, roll RAO [12]

To illustrate the effect of bilge keels Mohsin et. al [12] performed numerical and experimental test on a cross section with and without bilge keels, as seen in figure 2.9.

2.5 Bilge keels and KC-Number

A further investigation in the Bilge Keel damping will be discussed in the following section, as the upcoming case study will be about the effect of bilge keels and KC number.

By recalling the Morrison equation, which is widely used in the maritime industry,

$$dF = \rho\pi\frac{D^2}{4}C_M a + \frac{\rho}{2}C_D D|u|u \tag{2.32}$$

you will have two contributing terms which gives the total forces acting on a body. The first term, which is proportional with accelerated fluid particles is denoted as the inertia force, whereas the second term is proportional with the velocity squared (signed) u and gives the drag force. In terms of bilge keel damping, we are interested in the drag force. The D is the area of the cross section perpendicular to the flow direction, C_D is the drag coefficient. This implies that the bilge keel damping will take the form $B_{BK}|u|u$. As discussed in the previous section, the bilge keel damping can be divided into three different contributions.

The normal force component, B_{BKN} arises due to vorticities shed from the bilge keels, that changes the pressure on the hull and the bilge keels. This normal force will cause a moment about the rolling axis r, and can be described as a drag force on the form presented in Morrison equation. By expressing the cross section area perpendicular to the flow as the bilge keel area and the flow velocity as the relative velocity at the bilge keels due to roll motion, and substitute it in the Morrison equation, we get one step closer to the bilge keel damping presented in equation 2.25.

The Keulegan Carpenter number (KC-number), also referred to as the period number number, is an expression for the ratio between drag and inertia forces in a fluid flow. For low KC numbers, inertia forces are dominating and for large KC numbers, the drag force will be dominant. The KC number is expressed as;

$$KC = \frac{u_{max}T}{D} \tag{2.33}$$

where u_{max} is the maximum fluid velocity at the bilge keel, given as $u_{max} = fr\omega\theta$. The period T is expressed in terms of frequency which gives $T = \frac{2\pi}{\omega}$ and the relation for D is projected area $2b_{bk}$. Then, the KC number can now be expressed as;

$$KC = \frac{fr\theta\pi}{b_{bk}} \tag{2.34}$$

Based on experimental data and the given relations, the bilge keel damping B_{BKN} presented in

2.25 can be expressed in terms of the KC number as;

$$B_{BKN} = \frac{8}{3\pi}\rho r^3 b_{BK}\theta\omega f^2\left(\frac{22.5}{KC} + 2.4\right) \tag{2.35}$$

From this, one can see that the B_{BKN} damping component corresponds to $B_{44,2}$ in equation 2.7.

For the hull pressure component, B_{BKS} presented in equation 2.27 one can also express the damping in terms of the KC number. The damping component is represented by a pressure integrand, I. It was found that the pressure distribution in front of the bilge keel, or the positive coefficient C_P^+ can be set as 1.2 empirically [10]. The negative coefficient C_P^- however do depend on the KC number and can formally be expressed as:

$$C_P^= \frac{-22.5}{KC} - 1.2 \tag{2.36}$$

.

The KC number will indicate if the flow around a body will separate and shed vortices or not. For rounded bodies at low KC numbers, there will be no flow separation according to Faltinsen [1]. In the case of a flat plate, which is a valid approximation for bilge keels, a separation point will always be present at the edge, hence one could also expect flow separation to occur. This implies that even for small KC numbers ($KC < 10$) flow separation will be relevant in context of roll motions of ships with bilge keels. It is also clear that the corresponding KC number 2.34 is only amplitude dependant, as the period does not have any influence in this context.

Chapter 3

Theory

Computational fluid dynamics (CFD) is a strong and efficient tool in numerical methods to analyze and solve fluid problems. It was intentionally developed for use in the aeronautics, but has grown to become an essential tool in several design and engineering disciplines.

3.1 Governing equations

In naval hydrodynamics, a practice of dividing the fluid governing equations in two methods, namely Navier-Stokes methods and the potential flow methods can be done according to Faltinsen and Timokha. Combinations of these methods are also available, so-called hybrid methods which takes advantages of both methods, e.g. using potential flow theory for handling the free surface effects and then Navier-Stokes is used in the fluid domain.

3.1.1 Navier-Stokes

The Navier-Stokes equation (NS) is referred to as the cornerstone in fluid mechanics. It is an unsteady, non-linear, second order PDE, which can describe the physical phenomena from air pollution, weather forecasts to car design, in addition to naval problems.

For an incompressible, isothermal fluid the Navier Stokes equation reads:

$$\rho \frac{D\boldsymbol{V}}{Dt} = -\nabla p + \rho g + \mu \nabla^2 \boldsymbol{V} \tag{3.1}$$

By assuming incompressible, ρ is constant, and the isothermal condition eliminates the need for a differential energy equation, saying that the local variations in temperature are small. The latter assumption also leads to constant dynamic and kinematic viscosity.
The NS equation consists of four unknowns, with three velocity components (x, y and z-component in Cartesian coordinates), as well one pressure component. Since the NS equation is a vector

equation, only representing three different equations, there is a need of a fourth equation to solve the problem.

By introducing the conservation of mass, the continuity equation, we get a fourth equation which helps solving the problem.

$$\nabla \boldsymbol{u} = 0 \tag{3.2}$$

The continuity equation states that for incompressible flows, net flow across a control volume is zero.

3.1.2 Finite Volume Method

The finite volume method - FVM, is a common discretization technique in CFD, and also the one applied in OpenFOAM. From the governing equations, by neglecting the body force term one can write the NS equation in the form of:

$$\underbrace{\frac{\delta \boldsymbol{u}}{\delta t}}_{\text{temporal term}} + \underbrace{\nabla \cdot (\boldsymbol{u}\boldsymbol{u})}_{\text{convection term}} - \underbrace{\nabla \cdot (\nu \nabla \boldsymbol{u})}_{\text{diffusion term}} = \underbrace{\frac{\nabla p}{\rho}}_{\text{source term}} \tag{3.3}$$

The governing equations are transformed into their integral form by applying a volume integration over the flow domain D, then utilizing the Gauss theorem to transform the volume integral of the convection and diffusion terms to a surface integral. Dividing the flow domain into n number of control volumes, the volume and surface integrals are transformed into discrete ones and applying temporal and spatial discretization schemes on the integral terms lead to a set of equations that form the finite volume method. The set of equations is then numerically integrated through the use of integration points. For a thorough description of the finite volume method, one can refer to [33].

3.1.3 Volume of Fluid

In OpenFOAM, the volume of fluid method is used in case of multiphase flow. To capture the boundary between the two fluids, another scalar, α is introduced. This scalar varies between 0 and 1 that represents the amount of fluid in the control volume. α is defined by the transport equation reading:

$$\frac{\delta \alpha}{\delta t} + \nabla \cdot (\boldsymbol{u}\alpha) = 0 \tag{3.4}$$

In the control volume, the density and viscosity is defined by fraction of the respectively prop-

erties for the fluids in the form

$$\mu = \alpha\mu_1 + (1-\alpha)\mu_2 \tag{3.5}$$

3.1.4 Concerns in CFD

Stability

Stability in CFD concerns the error propagation of a numerical scheme. For a stable scheme, one say that the error is damped out. The variables of u, Δx, Δy and Δt are parameters that will affect the stability of a numerical scheme, and are the including terms in the stability criteria named Courant number, or CFL (Courant Fredrichs-Levi) number. The Courant number is defined as;

$$C = u_x\frac{\Delta t}{\Delta x} + u_y\frac{\Delta t}{\Delta y} < C_{max} \tag{3.6}$$

where the criterion C_{max} is specified by the user. It's recommended value depends on implicit or explicit methods, which for explicit solvers is typically set to 1. The criterion states that there should be no flow through more than one cell for each time step, such that no information is lost.

3.2 OpenFOAM

3.2.1 General

OpenFOAM is an open source numerical toolbox applicable for many types of CFD simulations. A reason for it's popularity is that it is free, but also that the user have full control over all parts of the simulation. A drawback is that it requires a lot of time to get the full potential out of it. It is neither a GUI software, which is not as user friendly as commercial CFD software. With OpenFOAM there comes a lot of tutorials that covers many problems in the fluid dynamics, that in most cases sets up the base for further simulations. For the current work, the tutorial "floatingObject" was used to set the basis, and then necessary adjustments and additional scripts were added. This is the common procedure when using OpenFOAM.

3.2.2 Pre-processing

As mentioned, in order to be able to solve the mathematical equations describing the flow, one have to divide the computational domain into a finite number of sub domains, which are primitive blocks often referred to as cells. The collection of these sub domains, is called a mesh or grid. In general, pre-processing when it comes to CFD may be the difference between success

or failure. It can be a time consuming process, and is often the part of the study where most of the time is consumed. In this work, a lot of time have been used to create, and study the effect of different meshing techniques and how this discrete representation of the body will influence the parameters investigated. There are several methods for creating meshes when doing simulations in OpenFOAM. Either one can use one of OpenFOAM's built-in meshing tools, such as blockMesh or snappyHexMesh. It is also possible to generate a mesh with commercial CFD software or numerical tools such as python. This work has been carried out by utilizing the two OpenFOAM meshing tools blockMesh and snappyHexMesh. To simulate the case of a moving body, there are also different techniques to handle the mesh motion. The work by Piehl [34] discuss the advantages and drawbacks between the different methods, and are briefly presented in the following text.

Rigid mesh

The rigid mesh is an easy to make mesh. With this method, the whole mesh is moved according to the body motion. A drawback with this method is that the boundary fields become complex as they are not stationary, and that a large part of domain may be exposed to multiphase flow, implying a large refinement region.

Overset mesh

This method takes the advantage of two meshes, where a small, overset mesh rotates according to the body as a rigid mesh, while a background mesh is stationary. The flow fields are then interpolated between the two meshes. This method may face some difficulties with preservation of the continuity condition, but is assumed to be a good method in ship motions.

Sliding interface mesh

This method is much like the overset method. The difference is that the background mesh does not span over the whole domain, so there is no overlapping with this method. Instead, the two meshes are aligned with the other mesh and share a boundary interface. A drawback with this method is that a combination of motions such as heave-roll may cause trouble.

Morphing mesh

With the mesh morphing method, only cells near the body is moving with the body. This method is computational expensive, but provides good results. This is because an interpolation of the whole flow field is needed between each time step. Also, special care must be taken with respect to cell distortion near the body.

The work in this paper have been performed with the mesh morphing method. The overset method, which is promising according to many, including DNV-GL, is only valid for a different version of OpenFOAM then the one used in this work. The decisive factor, and reason for not investigating this was due to time limitations.

The blockMesh utility have been used in the cases without bilge keels, and is the simplest meshing tool that comes with OpenFOAM. It's principle is to decompose the domain into three dimensional, hexahedral blocks. The blocks can have edges specified as arcs, splines or straight lines. Each block is again defined by a set of eight vertices, specified with coordinates. The blockMesh utility can also be combined with a script to make rather complex geometries as well.

SnappyHexMesh is the second mesh utility used, and for the cases with bilge keels, blockMesh was not appropriate to use. SnappyHexMesh is a three dimensional meshing tool, creating hexahedral and split-hexahedral meshes automatically to a pre-defined surface in either STL or OBJ format. In the current work, these geometry files have been made in SolidWorks. The procedure is to create a simple background mesh with blockMesh that defines the overall domain. Then, an iterative process of refining a starting mesh to the surface will run, until the surface is fully captured by cells.

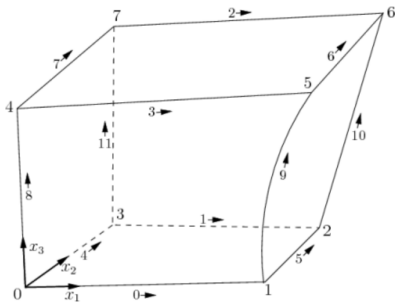

Figure 3.1: Hexahedral block, used for creating mesh with blockMesh

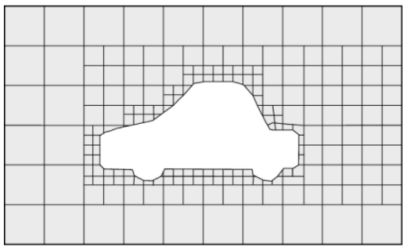

Figure 3.2: SnappyHexMesh illustration where hexahedral and split-hexahedral cells conforming the body

Figure 3.3: Meshing methods from OpenFOAM [35]

SnappyHexMesh can be a bit tricky, and demands that the user knows how to use the tool. Since it is a tool for three dimensional cases, it was necessary in this case to utilize an extra configuration in order to do 2D simulations. After the mesh generation process, the mesh is extruded to create a 2D mesh with only a single cell-layer in the z-direction. Thus, 3D effects of the flow

are eliminated. This procedure was done with the extrudeMesh dictionary which can be seen in 3.4.

3.2.3 Solver

An advantage, and the reason for choosing OpenFOAM as the software for these studies, is that the user can have full control and determine how the problem should be solved, and one avoid the "black box" problem where the results come out without any information about how they are obtained. For the current work, the interDyMFoam solver has been used, which is a solver for two fluids satisfying the conditions stated in the Finite Volume method. The solver is using a VOF (volume of fluid) phase-fraction based interface capturing approach, with optional mesh motion and mesh topology changes including adaptive re-meshing. The mesh is deformed according to the body motion [49].

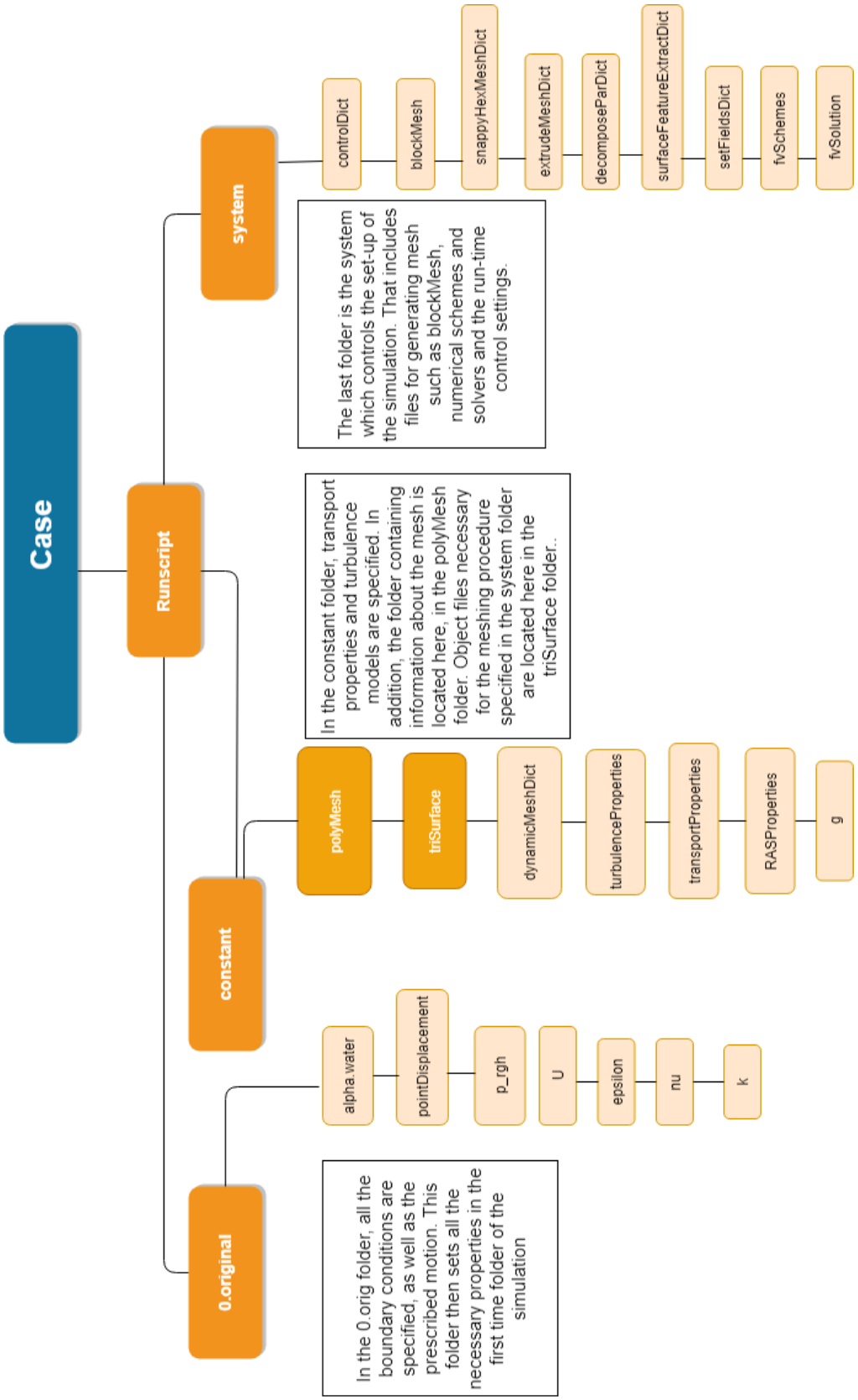

Figure 3.4: The topology of the OpenFOAM case

The set-up for the case is shown in figure 3.4. This case is based on the floatingObject tutorial, and modified according to the specific case. For the forced oscillation simulations, the motion solver used is "angularOscillatingDisplacement". The specific motion solver is set in the dynamicMesh dictionary, with the properties in the pointDisplacement file. For the free decay test a solver named "sixDoFRigidBodyMotion" was applied with some constraints so that only motion about the x-axis was permitted.

3.2.4 Post-processing

Post processing of the results from OpenFOAM are obtained from the GUI application ParaView that is compatible with OpenFOAM and is used for visualization of the simulations. All figures of the flow features are retrieved from paraView. For the roll damping estimation and time history plots of the forces, MATLAB was used. In the controlDict file the user have the opportunity to specify functions that read the desired results to a file, which then can be exported. The dynamic pressure was applied to calculate the hydrodynamic forces acting on the body.

3.3 Estimation of the roll damping

In order to obtain the roll damping coefficient one could perform both free decay tests and forced roll experiments. For the forced simulations, OpenFOAM calculates the forces which are written to a .DAT file. These files can further be analyzed with MATLAB. For the free decay test different strategies are utilized.

3.3.1 Forced roll simulations

From the forced roll simulations, the dynamic pressure is used to calculate the hydrodynamic moment acting on the body. The damping coefficients are then obtained similarly as explained in Yeung [26].

From potential flow theory, the hydrodynamic moment for an uncoupled motion can be written as;

$$M(t) = -A_{44}\ddot{\theta} - B_{44}\dot{\theta} - C_{44}\theta \tag{3.7}$$

where θ represents the roll amplitude given as:

$$\theta = \theta_0 sin(\omega t) \tag{3.8}$$

θ_0 is the maximum roll angle. Following, $\ddot{\theta}$ and $\dot{\theta}$ represents the angular acceleration and angular velocity in roll, respectively. As the roll angle is expressed as a sine function, the hydrodynamic

coefficients at $t = t_0$ can be found separately by extracting the Fourier coefficient of the primary frequency over a period T, expressed by the moment[26].

$$B_{44} = \frac{-1}{\theta \pi n} \int_{t_0}^{t_0+nT} M(t) cos(\omega t) dt \tag{3.9}$$

n is the number of integrated periods and $M(t)$ the instantaneous moment. The added mass, related to the acceleration can by obtained by:

$$A_{44} = \frac{1}{\omega \theta \pi n} \int_{t_0}^{t_0+nT} M(t) sin(\omega t) dt \tag{3.10}$$

In order to compare the results with previous studies, the roll damping and angular frequency have been non-dimensionalized according to the following relations:

$$B_{44}^* = \frac{B_{44}}{\rho \nabla B^2} \sqrt{\frac{B}{2g}} \tag{3.11}$$

$$\omega^* = \omega \sqrt{\frac{B}{2g}} \tag{3.12}$$

Since this is a 2D evaluation, the moments are given per unit length. That means the ∇ which represents the submerged volume is given as the submerged cross sectional area. The damping coefficient obtained from the forced roll simulations is representing the equivalent damping, i.e. it does not differentiate the linear and quadratic term. In order to do so, Yeung et al. [26] proposed a method where the linear damping was obtained based on the free surface elevation and the quadratic damping as a difference in the total moment and the linear damping contribution. The current work does neither include a Fourier transform on the moment signal, which means the results obtained may include other frequencies which is not in phase with the velocity.

3.3.2 Free decay test

A free decay test may also be conducted to estimate the damping coefficient for the body, and is performed in calm water. The body is subjected to an external moment giving it an initial angle, before this moment is removed causing the body to freely oscillate. The body is freely oscillating at its natural frequency, which usually can be taken as the undamped natural frequency for lightly damped systems. A system with a damping ratio of 0.1 will have less than 1% change in the undamped natural frequency. During a free decay test, the roll angle is gradually decaying, and is plotted against time which then can be used to estimate the characteristics of the body.

A normal way to describe the motion of a free decay test is described in [1].

$$\ddot{\theta} + p_1\dot{\theta} + p_2|\dot{\theta}|\dot{\theta} + p_3\theta = 0 \tag{3.13}$$

Here, p_1 and p_2 are the linear and quadratic damping terms, respectively. p_3 denotes the restoring terms, and can be calculated by known formulas. The damping terms can be found by assuming constant damping with respect to the amplitude from the following relation;

$$\frac{2}{T_m} log \frac{\theta_{n-1}}{\theta_{n+1}} = p_1 + \frac{16}{3}\frac{\theta_n}{T_m} p2 \tag{3.14}$$

where T_m is the roll period. There is one half time period between θ_n and θ_{n+1}. This is shown in figure 3.6. By plotting the left hand side of 3.14 versus $\frac{16}{3}\frac{\theta_n}{T_m}$ and then fit a straight line through these points by the least square method, one can obtain the damping coefficients p_1 and p_2, now denoted as the Faltinsen fit. The linear damping will then be the intersection point of the straight line and the y-axis, while the slope will give the quadratic damping.

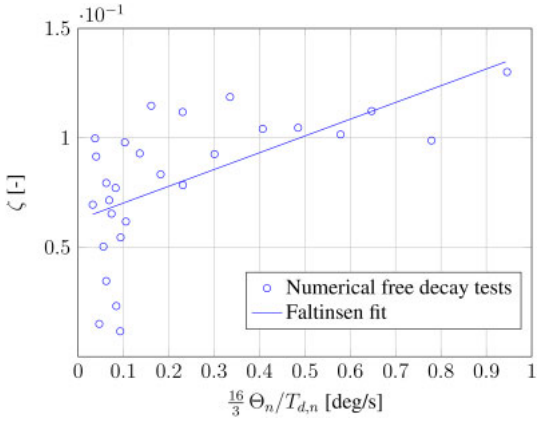

Figure 3.5: Results from a free decay test and how the Faltinsen fit is used [39].

A drawback with this method is that when the system has a strong KC dependence it is impossible to fit a straight line through the points [1]. Thus, one can not find valid damping parameters for the total decay time. To give a good estimate for p_1 and p_2 there should be no significant change in Reynolds number or KC number. The fact that a body with bilge keels will experience large variations in the velocity and amplitude between oscillations means that it could be difficult to determine the correct damping components. It was found that the quadratic damping was strongly dependent on the KC number and roll amplitude 2.35. To express the system 3.13 in a dimensional form, the equation of motion can be written as:

$$(I_4 + A_{44})\dot{\theta} + B_{44,1}(\dot{\theta}) + B_{44,2}|\dot{\theta}|\dot{\theta} + C_{44}\theta = 0 \tag{3.15}$$

It is then possible to represent the damping terms p_1 and p_2 as an equivalent damping by the relation:

$$\frac{B_{eq}}{(I_4 + A_{44})} = p_1 + \frac{8\omega}{3\pi}\theta p_2 \tag{3.16}$$

An updated method to estimate the damping components from free decay tests is the bi-linear method, which divides the decay plot into two regions, large angle region and small angle region. The idea is that a linear decrement can describe the small angle region, where the relative change between oscillation periods is small. For the large angle region, which will be the first oscillations that show a more non-linear trend, a linear model with a steeper slope can be utilized. This method has showed promising results according to [38].

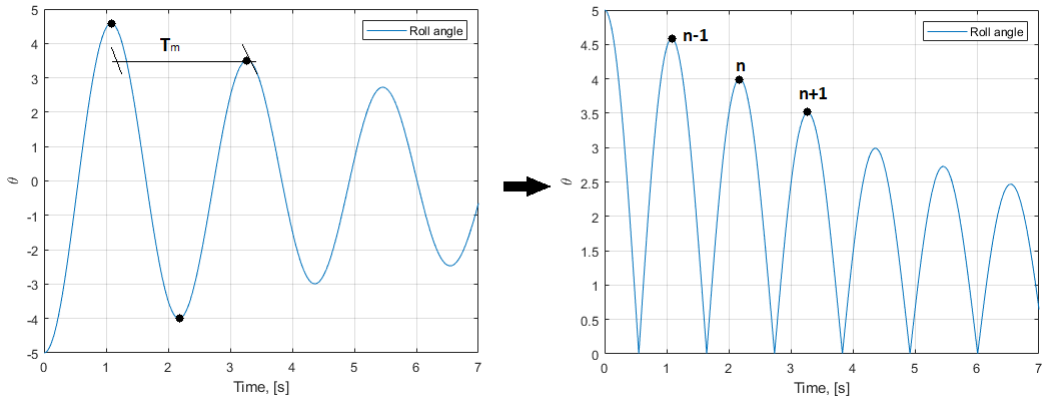

Figure 3.6: Definition of amplitudes in the free decay test calculations in terms of absolute value

3.3.3 Flow memory

Flow memory effects may be important in roll damping estimation. It has been clarified that a vortex close to a body will interact with the following development of new vorticities, and hence the fluid velocities around the body. That means memory effects in the flow can influence the prediction of roll damping coefficients. In case of free decay tests, the fluid surrounding the body is "at rest" before the decay starts. This is described by e.g. van't Veer [45], which states that special concerns must be taken for such test.

For a free decay test, a normal procedure to avoid flow memory effects is to disregard the first oscillation period, as it was found that the damping was lower when the fluid was at rest at the beginning. To eliminate this factor, one possibility is to perform a couple of forced roll motions before the actual free decay test starts, to ensure velocity fields are present in the fluid before the decay starts. However, this introduced new concerns as it was found . The findings says that damping estimation based on calm water test may not represent a realistic result where the surrounding waters rarely are calm. In case of forced roll simulations, according to vant' Veer

it usually takes two to three oscillations period for the bilge keel force to establish a constant maximum amplitude during a forced roll simulation.

For irregular motions, flow memory effects will always be present as the drag never reaches a steady state amplitude as for the forced, harmonic motions. Following one can argue that memory effects always will be present in a free decay test, and cause a certain uncertainty in the damping predictions. However, as concluded by van't Veer [45], in calm water test the effect showed not to be of importance.

Chapter 4

Validation case

In an attempt to validate the numerical solver used, OpenFOAM, it was conducted a study in the project thesis to reproduce the experiments performed by Vugts in the 1960's of an oscillating box. His study has been widely used as a reference value when it comes to damping coefficients for different box shaped bodies, and was also the basis in the project thesis. It was found that the damping coefficients obtained from OpenFOAM did not match the experimental results very well, without any further explanation. One theory is that in Vugts experiments, the box did not have perfectly sharp bilges, but a bilge diameter of 2.5 mm, which may be one reason for lower damping in the experiments compared to the numerical results. Another problem may have been the meshing technique, which later will show to have an important impact on the results.

An important aspect when it comes to CFD and it's accuracy is to examine the effect of the grid, and the element size. Type of grid is of importance as the numerical calculations strongly depend on the distribution of points around the body, and a poor grid may cause bad results. In the study of roll, the flow features of importance are connected with flow separation around the sharp corners, which requires a grid that is capable of capture the flow in the region of the bilges. In addition, with a moving grid the deformation will also be of importance. In the present work, different types of grids have been studied and compared against each other to see how the effect of grids impact the parameters of , and to validate the numerical code. For each type of grid, a sensitivity study, also referred to as a mesh convergence study, has been performed to ensure that the accuracy of the results are satisfying.

A systematic study to investigate the accuracy both the numerical solver, and the different meshing strategies have been conducted. To eliminate the problems with round bilges in the Vugts experiments, it was chosen to use the experiments performed by Ikeda et al as reference, with additional data from the numerical simulations by Jaouen [18].

Table 4.1: Characteristic data for grid study

Beam	0.28 [m]
Draft	0.112 [m]
ω	2π [s^{-1}]
θ	0.107 [rad]

When it comes to numerical calculations, pre-processing may be very time consuming, and in the current work a lot of time has been used to both create, and investigate the importance of the grid. Several different techniques to generate a grid have been tested, and also a grid made by Giuseppina Colicchio has been used for comparison.

4.1 Critical damping

A simple calculation to estimate the 2D critical damping has been performed analytically.

According to Faltinsen [1], the natural period in roll can be expressed;

$$T_{n4} = 2\pi\sqrt{\frac{Mr_{44}^2 + A_{44}}{\rho g V G M_T}} \tag{4.1}$$

following which gives the natural frequency:

$$\omega_4 = 2\pi\sqrt{\frac{\rho g V G M_T}{I_4 + A_{44}}} = \sqrt{\frac{g G M_T}{r_{44}}} \tag{4.2}$$

where r_{44} is usually 0.35*B [1], and GM_T is the transverse metacentric height. Calculating the metacentric height based on the waterplane moment of inertia and displacement, the natural frequency is roughly estimated to be 2.42 s^{-1}. Calculating the restoring coefficient C_{44} then gives the relation to find $(I_4 + A_{44})$ where

$$(I_4 + A_{44}) = \frac{C_{44}}{\omega_n^2} \tag{4.3}$$

Finally, the critical damping can be expressed as

$$B_{crit} = 2(I_4 + A_{44})\omega_n \tag{4.4}$$

By non-dimensionalizing the critical damping coefficient, it is possible to evaluate the damping ratio to the system, which can be used to discuss the results. The non dimensionalized critical damping is approximated to be 0.17.

4.2 Grid types

4.2.1 H-grid

The H-grid is the simplest grid studied in this work, where the cells are distributed uniformly in the x- and y direction. With this grid, the cells in the region of the body surface has a lower Δx and Δy compared to the rest of the domain, as an incremental grading is applied to the cells in the outer region. This grid was the first one tested, and the one applied in the preparatory work during the project thesis. The idea was to have a fine resolved mesh near the body to better capture the flow field, with a more coarse mesh in the far field domain to reduce the total number of cells. However, it is clear that a disadvantage with this type of grid is that the aspect ratio between the cell regions often gets to high, and demands careful treatment by the user to avoid this.

H-grid with an inner domain

In order to have a constant cell size in the flow field close to the body, the H-grid was modified in a way so that the domain is divided into two parts. The inner domain have cells with constant size. In the outer domain the cell size is expanding to correct for the aspect ratio in the transition between the inner and outer grid. This grid was made to better capture the flow field with a fine mesh in the area of interest compared to the initial H-grid. In the outer domain the grading was applied to reduce total number of cells, and by that computational time.

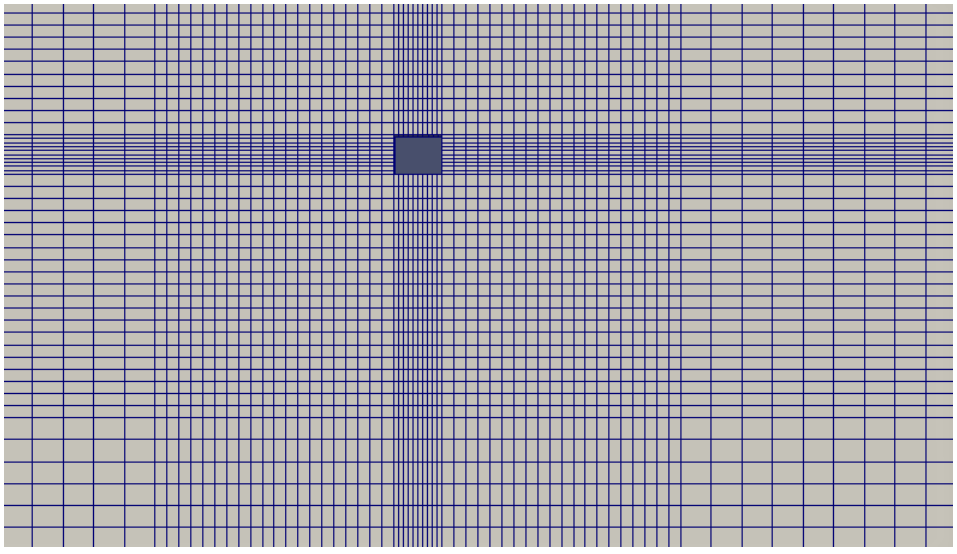

Figure 4.1: H-grid

4.2.2 O-type grid

Two different O-grids have been investigated in this study, as one was made with the OpenFOAM utility blockMesh as the previous ones. The other type was made by Giuseppina Colicchio by use of the program Pointwise. This grid can also be defined in to an inner and outer grid, where the inner grid is O-shaped around the body. The advantage of this grid is that the rotation of the mesh will be of less importance, and the flow field is assumed to be better captured around the boundaries. The main differences between the two O-grids studied, are that the free surface is not captured very well in the one made with blockMesh, as the cells are expanding in both x and y-direction away from the body. This is clearly shown in 4.2. With the VOF method, this means that the volume fraction gets low resolution in the free surface in the far field boundaries.

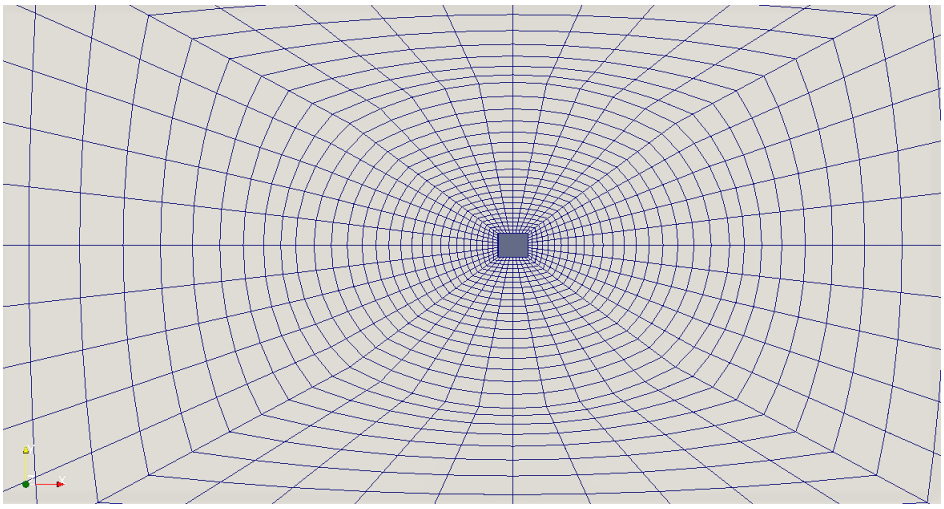

Figure 4.2: O-grid made from blockMesh (not the actual size of cells, only for illustration)

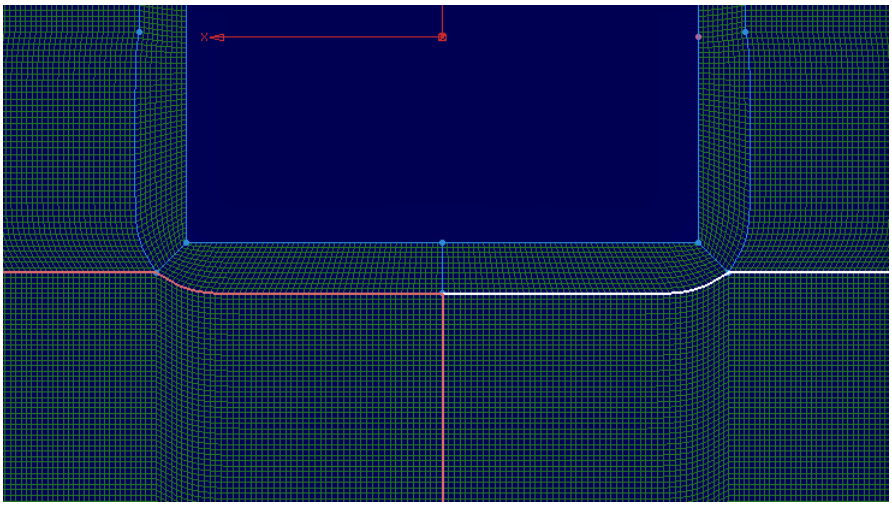

Figure 4.3: A more close-up view of the O-grid from Pointwise, made by Giuseppina Colicchio

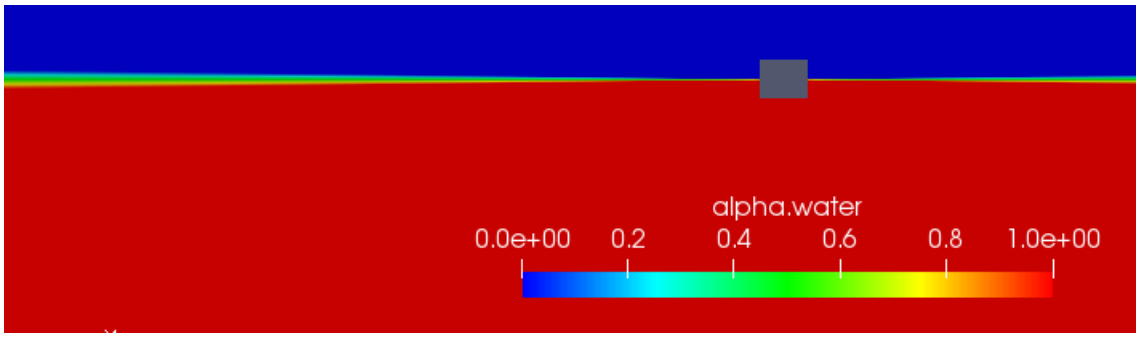

Figure 4.4: A consequence of the O-mesh in figure 4.2 is the poor capture of the free surface far from the body

4.3 Sensitivity analysis

For the detailed sensitivity analysis, three different grids assumed to be most appropriate are further studied. The sensitivity study is performed by evaluating the flow fields and damping coefficient for three different refinement levels of each grid, coarse, medium and fine. Their characteristics are presented in the following text.

- Grid 1: Of type H-grid grid explained in the previous section, and as in figure 4.1.

Table 4.2: Properties for grid 1

Refinement level	number of cells	Δx / Δy at body
0	400 000	0.005
1	770 000	0.0035
2	1 100 000	0.0023

- Grid 2: Of type O-grid made in blockMesh, see figure 4.2

Table 4.3: Properties for grid 2

Refinement level	number of cells	Δx / Δy at body
0	120 000	0.0035
1	290 000	0.0028
2	480 000	0.0018

- Grid 3: Is also an O-type grid, made by Giuseppina Colicchio with the software Pointwise. This grid has been used in similar simulations with good results, and are figuring in this report as a validated reference.

Table 4.4: Properties for grid 3

Refinement level	number of cells	Δx / Δy at body
0	460 000	0.0018
1	1 100 000	0.0009
2	4 600 000	0.00045

In the beginning, the refinement was done by increasing the total number of cells. However, to get better comparisons between the data, the values of Δx and Δy should be taken into concern, as this gives a better systematic relation between the different grids. The area of interest is the flow field near the body, and as the distance away from the body increases, the need for well refined cells gets less important. As the different meshes are made with different techniques, it was clear that even though one grid type had a higher number of total cells, it could be less cells covering the body compared to another type of grid, which is clear from the tables presented above. One important aspect is also that in order to refine the mesh provided by Giuseppina Colicchio, the built-in refinement command in OpenFOAM was used, which splits the cell in four, meaning that the Δx / Δy values are reduced by a factor of two. In the previous simulations, the refinement procedure was done by manually specifying the total number of cells in around the body, and in the whole domain as well.

The procedure of the sensitivity study has been to run each simulation for at least five seconds, and by that five periods. The characteristics are then evaluated over one time period for the moment, while the damping and added mass coefficients are calculated over a time of three periods. To reduce the sensitivity for errors in the moment history one could have averaged over a longer interval. As some of the most refined simulations run for several days, it was chosen to set a limit at five second to not spend too much time.

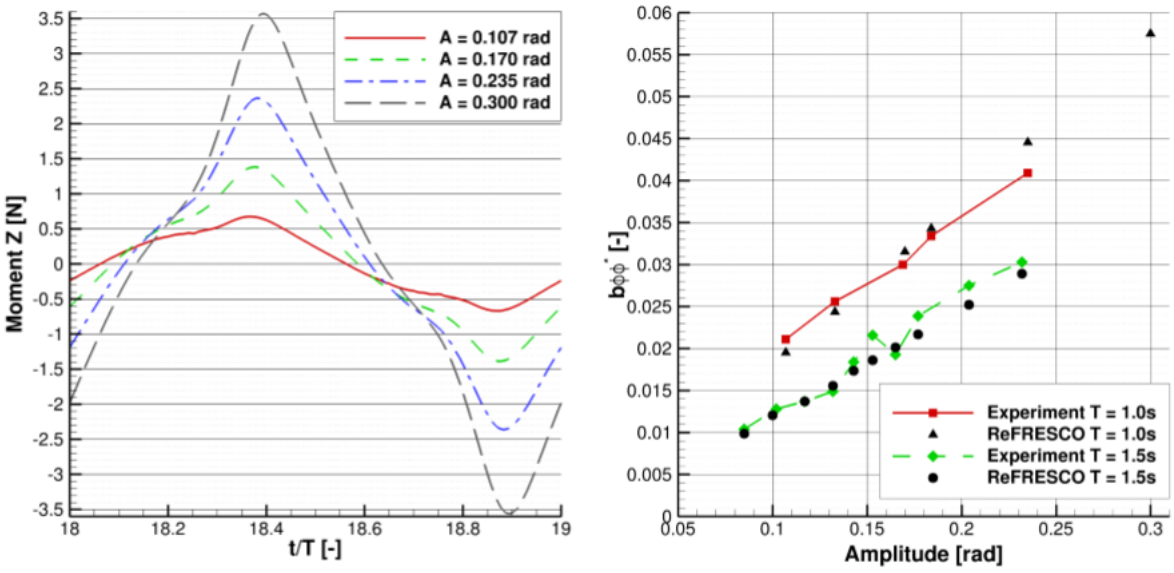

Figure 4.5: The characteristics for the study presented in the work by Jaouen [18] where the red lines mark the results for this test case parameters.

4.3.1 Results of damping convergence

In order to determine if the results of the simulations has converged or not, the non dimensionalized damping coefficient was evaluated for three refinement levels.

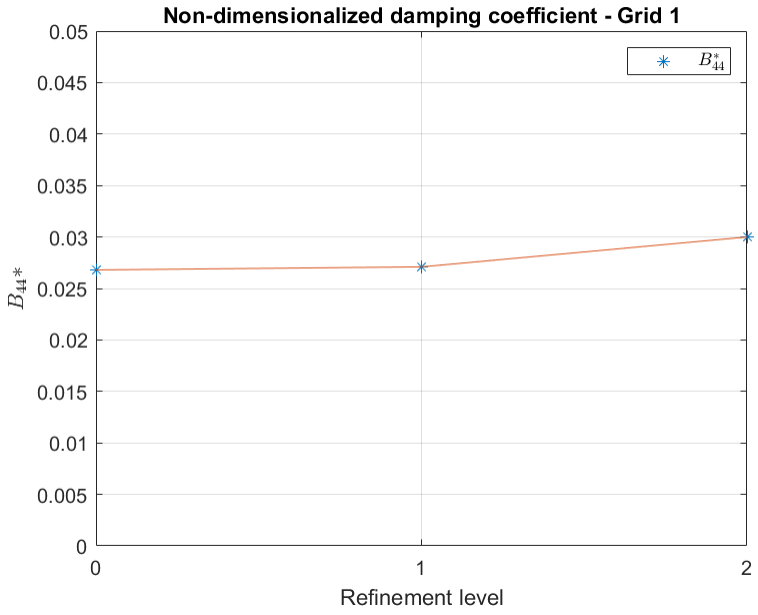

Figure 4.6: Study of non dimensionalized damping coefficient

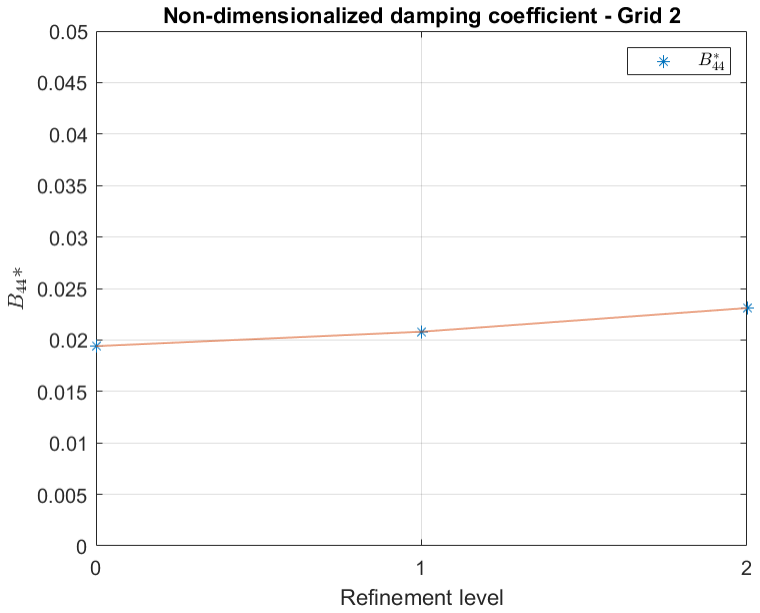

Figure 4.7: Study of non dimensionalized damping coefficient

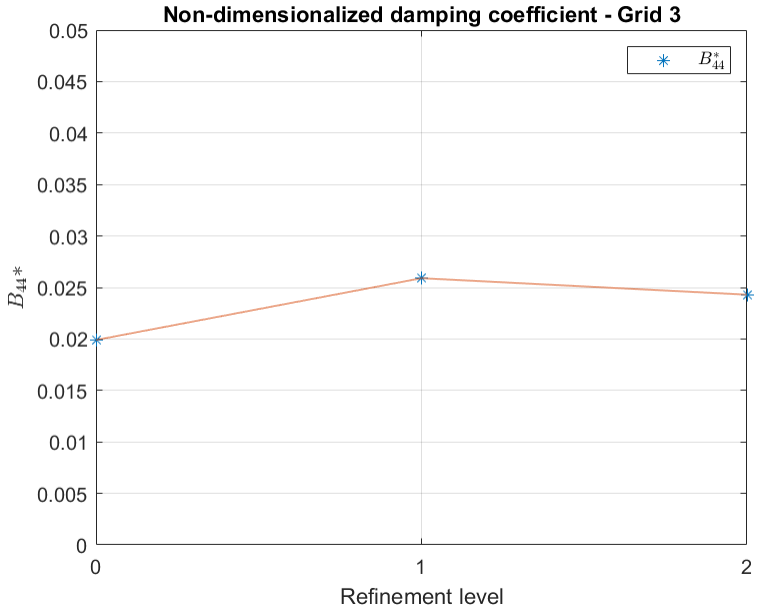

Figure 4.8: Study of non dimensional damping coefficient

Based on the results obtained by Ikeda and Jaouen, as shown in figure 4.5, one can see that the non dimensionalized damping coefficient should be somewhere around 0.02. By looking at the results presented in the figures above, there is quite a large gap between grid 1, and the two O-type grids. Grid one, which was developed after a long process of failing and testing, still overestimates the damping compared to the reference value, and the two other grids tested. For

both grid 2 and 3 the damping coefficient estimated seem to be good. However, for grid 1 and 2 that both are made with OpenFOAM, there is a trend of an increase in the damping coefficient when the grid is refined. Even though the data presented here only shows three different grids with three levels of refinement, this trend was studied further with several refinement levels, and other types of grid (all H-grids) where all show the same behaviour. For grid 3, which is the only grid not made with one of the built-in options from OpenFOAM, one could argue for an oscillatory behaviour of the convergence. However, the changes from the first refinement to the second are significant lower compared to the first, and it can also be justified to say that the results have converged. Further refinements of this grid would result in a total amount of cells of over 16 millions cells, which is too costly with respect to computational resources, and also could lead to other types of errors resulting in less accurate results.

The reason for the changes in the damping can be explained by looking at the moment history for the different grids. The damping, which is calculated by integrating the moment history will be changed if there is a change in the phase of the moments according to 3.9.

In the following figures, the moments are plotted over one time period for all three refinement levels, including the reference plot obtained by Jaouen [18].

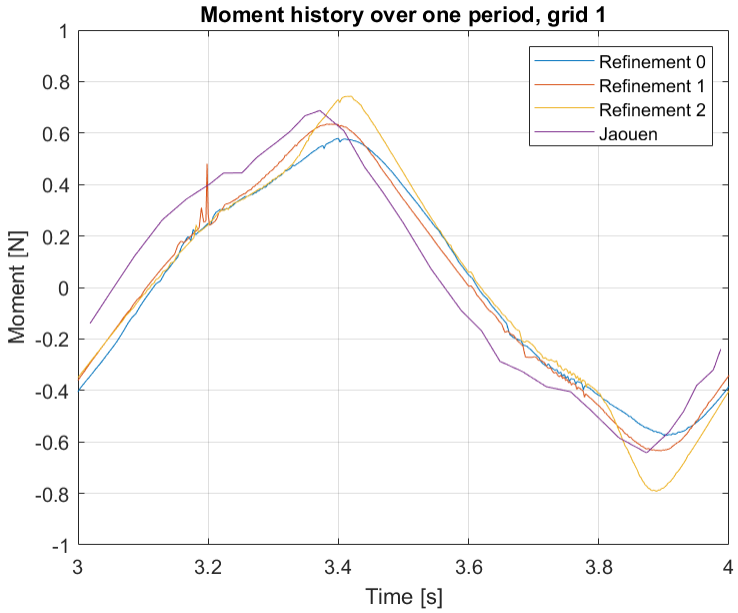

Figure 4.9: Moment history over one period, grid 1

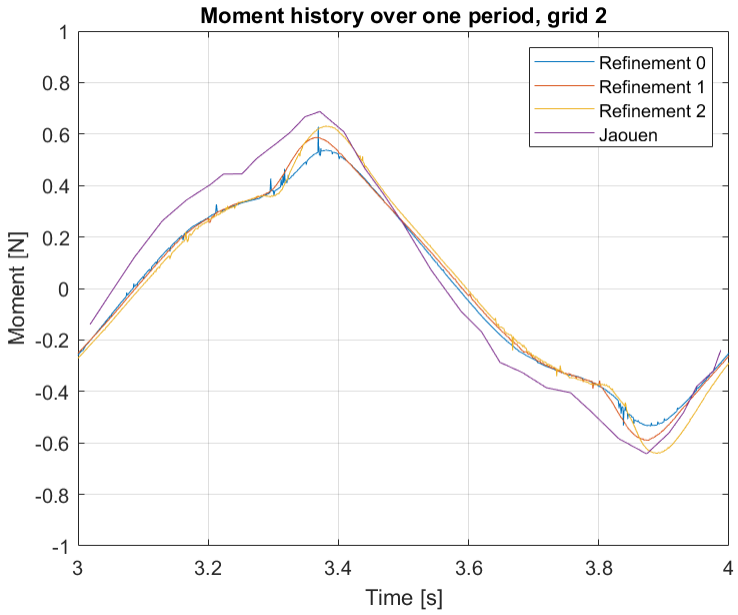

Figure 4.10: Moment history over one period, grid 2

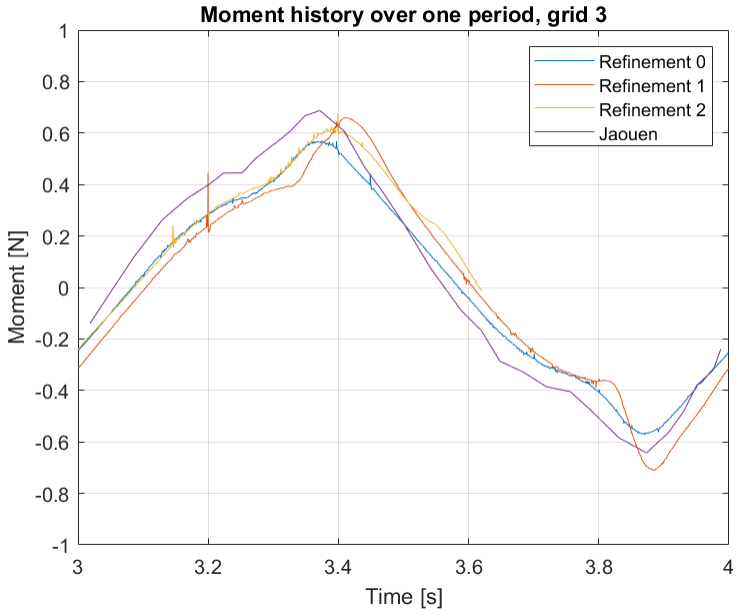

Figure 4.11: Moment history over one period, grid 3

These plots show that for the refinement steps, there is a slightly change in the phase of the moment. By considering that the damping will increase as the phase difference between the roll motion and the roll moment gets larger, and highest damping will occur when these two are 90 degrees out phase. It also shows that the finer mesh captures higher peaks. The fact that the comparison plot by Jaouen [17] was digitized it's accuracy is not 100 %, but still gives a good

representation.

4.3.2 Flow fields

In order to identify the reason behind the damping and moment behaviour, the flow fields of the different grids have been investigated in ParaVIEW. The damping coefficient is estimated by the moments calculated in OpenFOAM, which again are a result of the velocity and pressure fields around the body. By evaluating plots such as the vorticity, one could try to identify the origin for the forces obtained, and to see how the different meshing techniques captures the flow near the bilges.

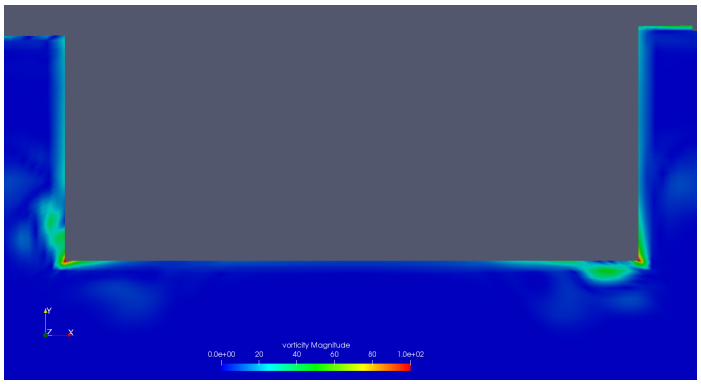

(a) t = 3 s

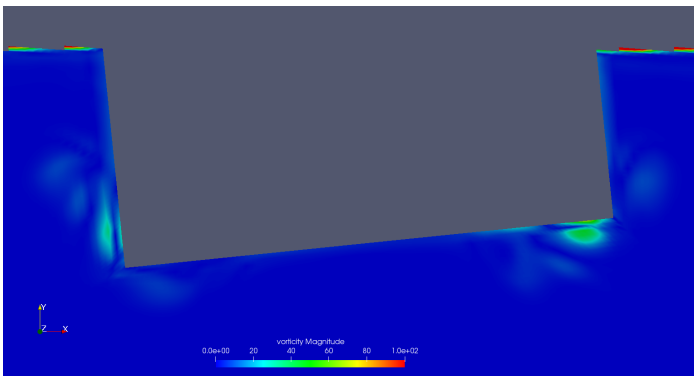

(b) t = 3.2 s

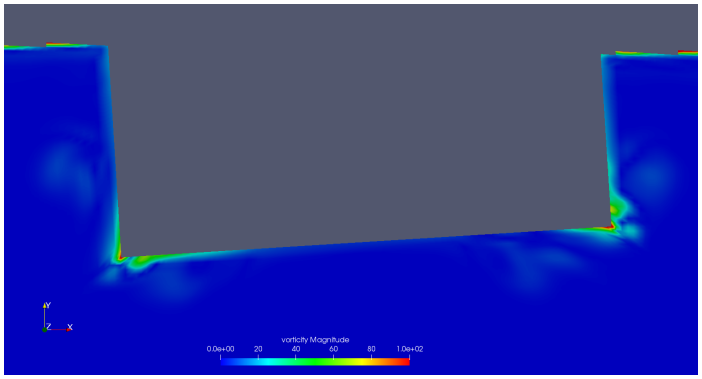

(c) t = 3.4 s

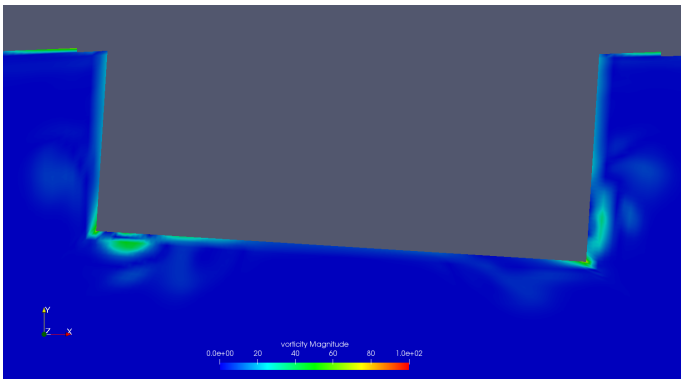

(d) t = 3.6 s

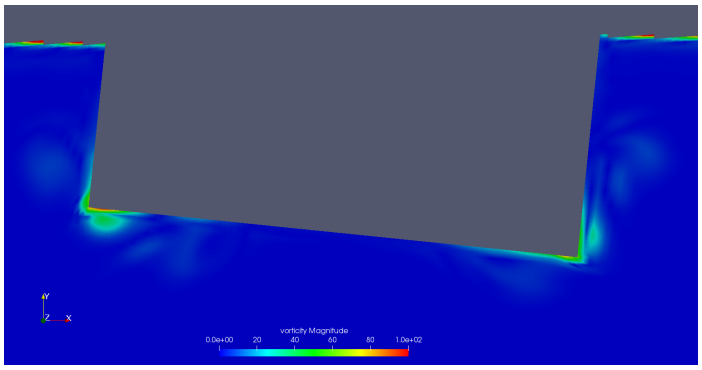

(e) t = 3.8 s

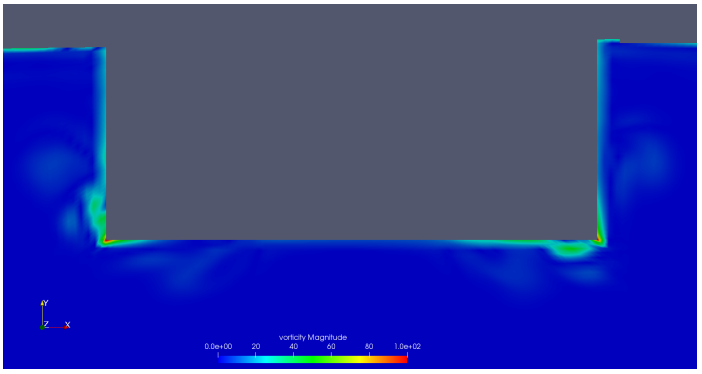

(f) t = 4 s

Figure 4.12: Vorticity plots for O-grid during one period

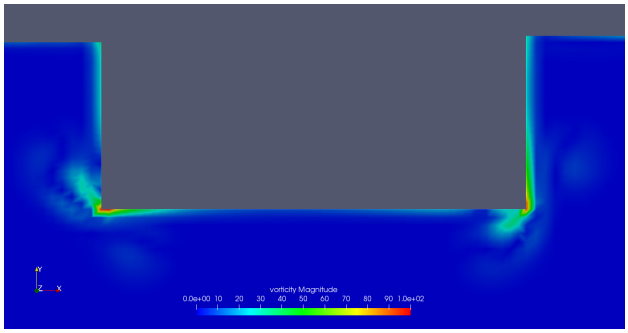

(a) t = 3 s

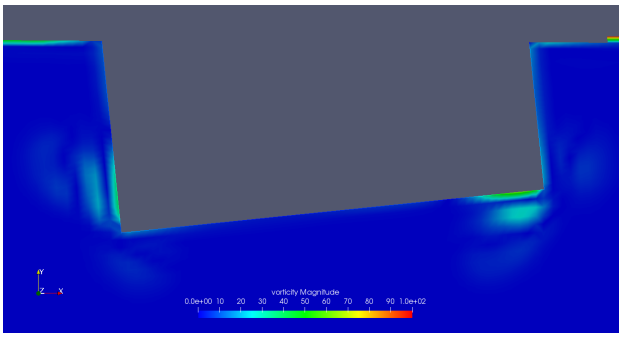

(b) t = 3.2 s

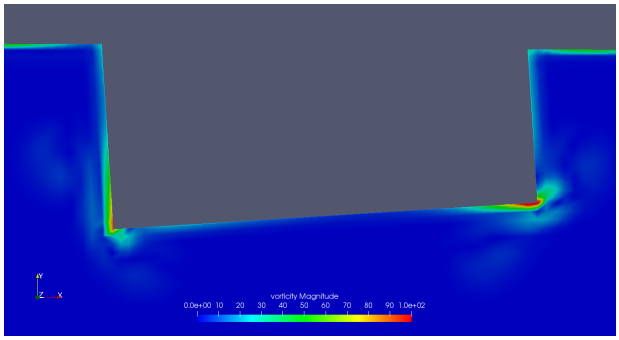

(c) t = 3.4 s

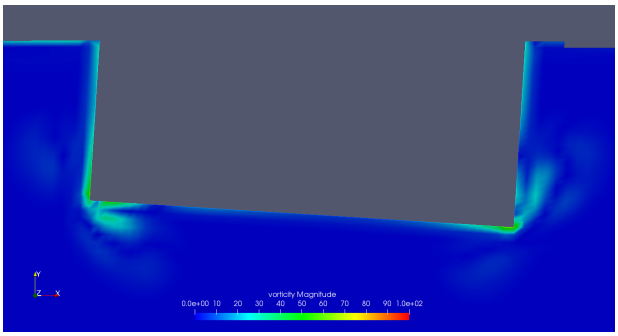

(d) t = 3.6 s

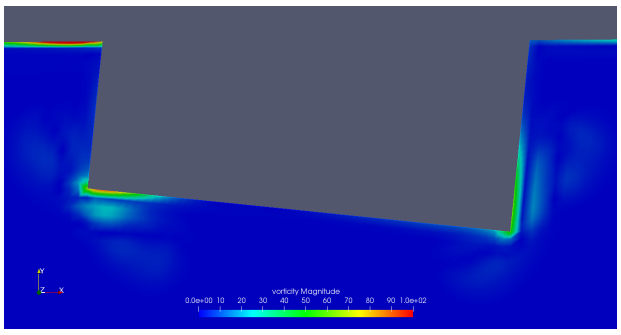

(e) t = 3.8 s

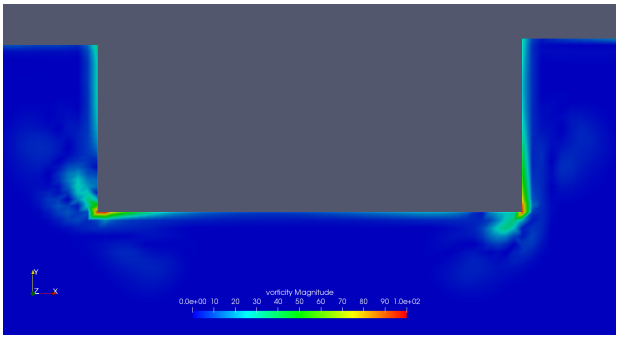

(f) t = 4 s

Figure 4.13: Vorticity plots for H-grid during one period

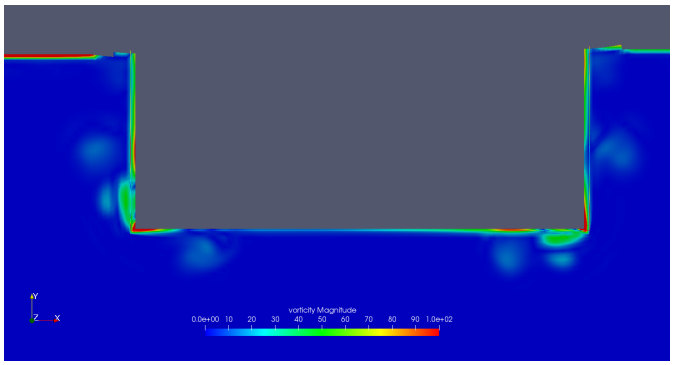

(a) t = 3 s

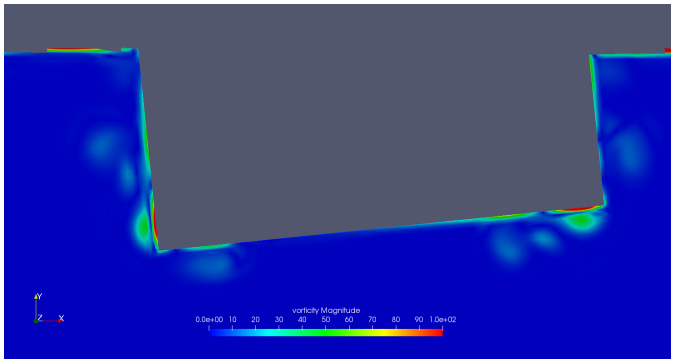

(b) t = 3.2 s

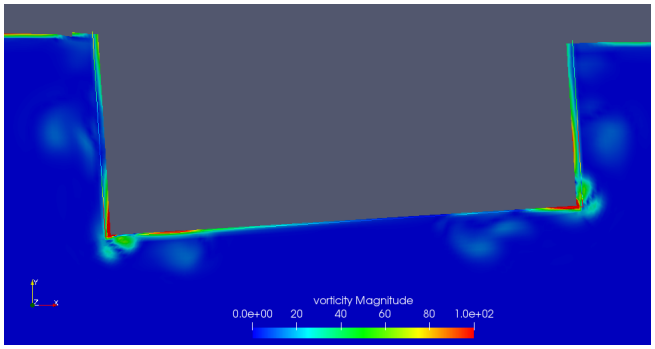

(c) t = 3.4 s

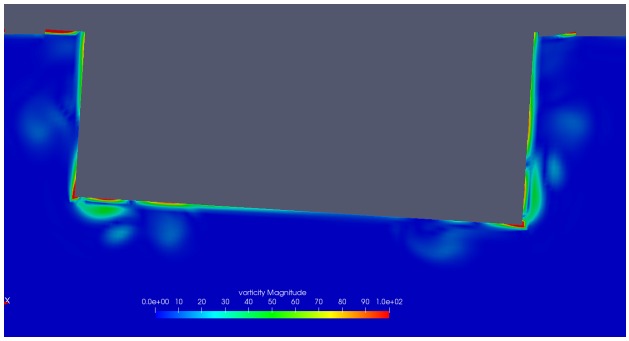

(d) t = 3.6 s

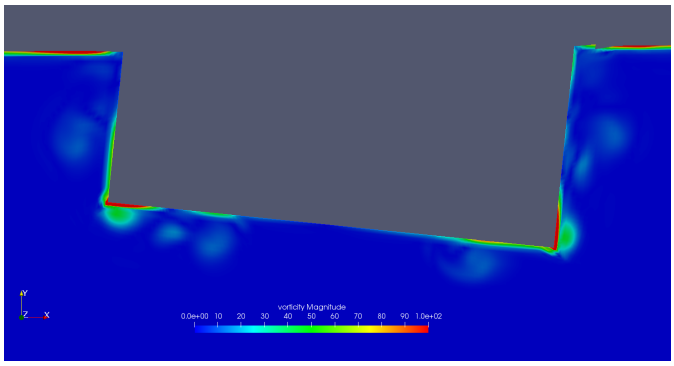

(e) t = 3.8 s

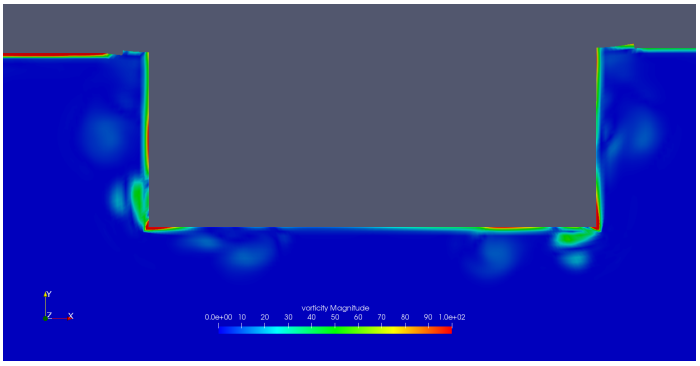

(f) t = 4 s

Figure 4.14: Vorticity plots for O-grid made by Giuseppina during one period

From the vorticity plots, one could look closer to what happens during some of the phases in the oscillation period. By evaluating two times steps, at 3.4 seconds where there is a peak in the moment, and after and 3.8 seconds one can address the differences with the different mesh techniques.

- T = 3.4 sec
  At time-step three after 3.4 seconds, there is a maximum in the moment as seen from e.g. figure 4.11. The cross section has started rotate clock-wise with visible vortices shed from the body. From the previous time step it is clear that the vortices have changed, and by

looking at the left bilge a new vortex is being formed under the hull. Comparing results from the H-grid and the O-grid at this time step one can see markedly differences in the flow behaviour. In figure 4.16 and 4.15 the results are enlarged and marked out for the vorticities shed. The results show that the O grid is capable of capture the flow with more details compared to the H-grid. Where the O-grid has five distinct vorticities at each bilge, the H-grid seem to capture only four vorticities. The captured vorticities also seem to be of a lower magnitude, and they all seem to be more smeared out a bit. This might be due to the sharp corners where the singularity will appear is be covered with one cell, whereas the O-grid curves around the corner, leading to a more dense coverage of the edge. In addition, the location of the vorticities is also different in the two grids. For the H-grid, the vorticities 4 and 5 are located further away from the keel then the corresponding vorticities 5 and 6 in the O-grid. Considering that the section at this time is rolling clockwise, it will mean the vorticity located under the hull at the right will influence the flow around the hull different for the two grids.

- T = 3.8 sec
  At the fifth time step, reading 3.8 seconds the same trend is present as for the case at 3.4 sec. Also at this stage of the oscillation, the grid seem to be unable to capture all the vorticities and the ones that are present are not aligned in the way one could expect. At the left side, one could expect significant vorticities under the hull as the motion just changed phase, which is clearly showed in (e), figure 4.14. From figure 4.13 is only one distinct vortex, as the second one seem to die out further down. Also at the right side one can see how the grid fails to capture and distinguish the vorticities.

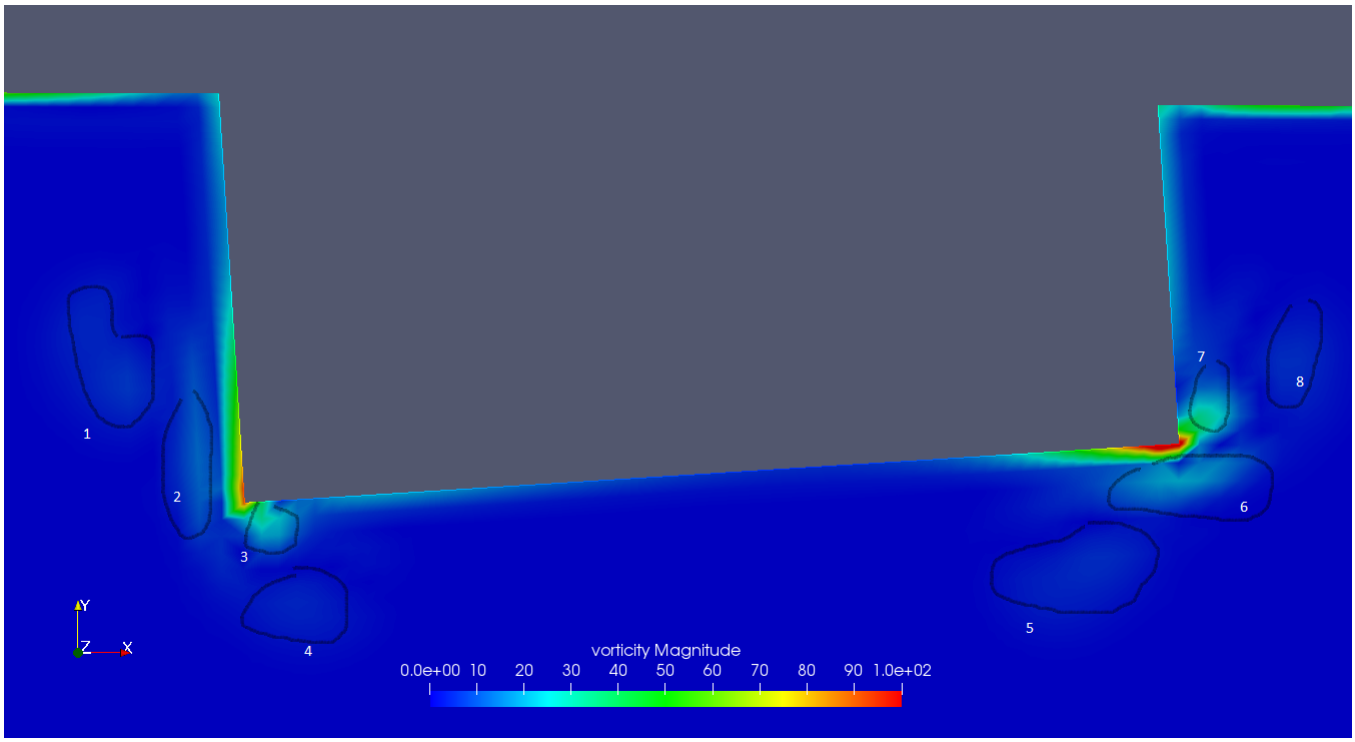

Figure 4.15: Detailed vorticity plot for the H-grid at T = 3.4 s.

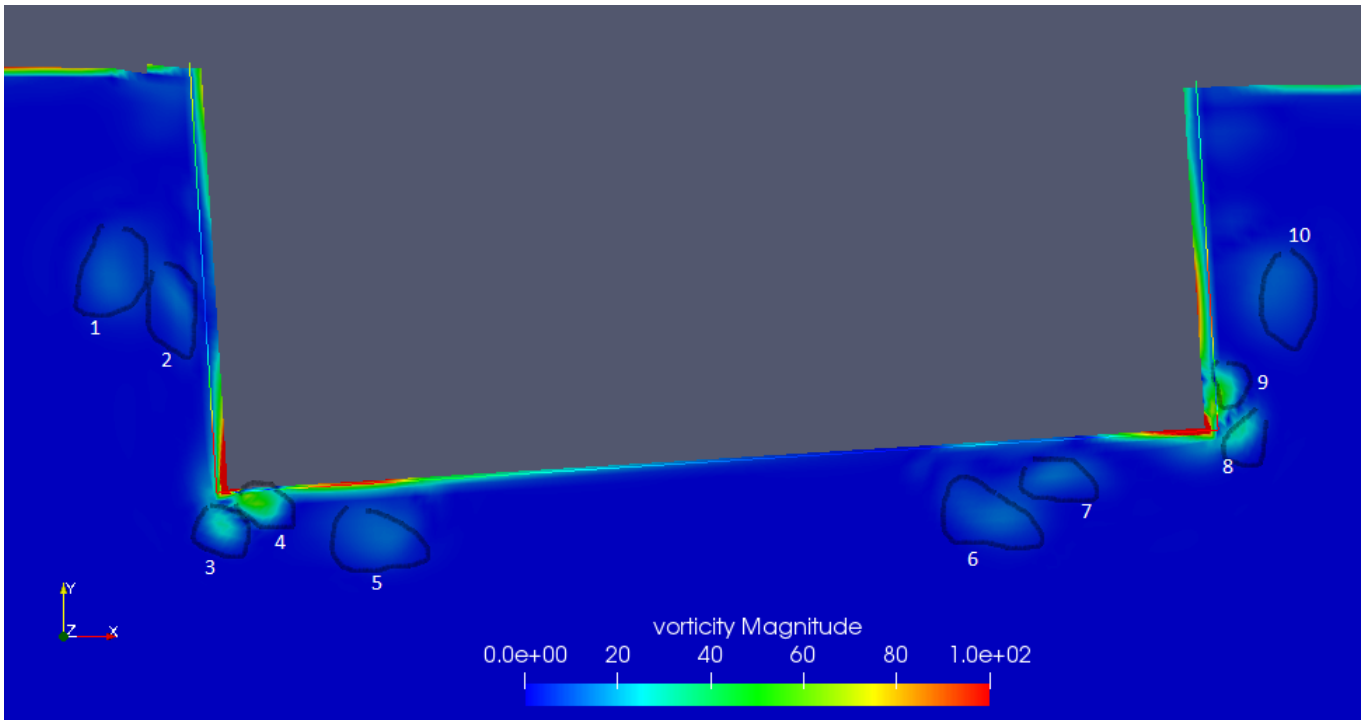

Figure 4.16: Detailed vorticity plot for the O-grid at T = 3.4 s.

For figures with a brighter contrast, see figure 6 and 4 in appendix A. There the vorticity

orientation about the z-axis, which differ in positive and negative vorticities.

4.4 Main findings

The present study reveals that one must take special care when simulating cases of a rolling box without bilge keels. It was found in the previous work done in the project thesis, that OpenFOAM tend to overestimate the damping coefficients in the terms of roll motion according to experiments done by Vugts. To eliminate the uncertainties connected with rounded bilges in Vugts experiments, the work done by Ikeda et. al. was further studied to investigate more precise results. The main findings in this study is that with an O-grid, the damping coefficients obtained only have small deviations from the reference values. This type of grid also show a better convergence behaviour compared to the H-grid such as grid 1 4.1.

What differs the two grid types from each other are mainly how the boundaries are treated. The damping is dominated by what happens near the bilges, where there will be vortexes shed from the sharp corner. At the corner, there will be a singularity, and the main difference between the grids is in fact how this single point is treated, see figure 4.17. With the O-grid that curves around the corner, and has no cells diagonal to the edge seem to be the solution in order to represent the flow field in with higher accuracy and is able to capture more details. As discussed in the time step analysis, the fact that the H-grid does not seem to capture the vorticities, neither the strength or position as the O-grid, this will effect the fluid velocity and hence the forces around the body. By taking a look at the moment history for the different grids presented in figure 4.9 and 4.11, H-grid and O-grid respectively, it also shows that the the peaks have a different shape, and that they have a slightly different phase. For the H-grid, the maximum moment is just after 3.4 seconds, where the maximum moment for the O-grid seem to be located a little bit earlier, in terms of a few hundreds of a second. Both of the two O-grids also seem to behave like the experiment measured by Jaouen et al.[18], with a sudden change in the slope around the peaks.

It is clear that the damping coefficients found are small relatively to the critical damping, roughly estimated to be around 10% of the critical damping. Even though these are simplified calculations, the order of magnitude is a good estimate. As a consequence, the calculated damping is very sensitive to the flow features and the forces for damping ratios this small.
Although the O-grid made in OpenFOAM with blockMesh does not capture the free surface as good as two other grids, the damping component is dominated by the flow at the bilges which can explain why it still gives good results.

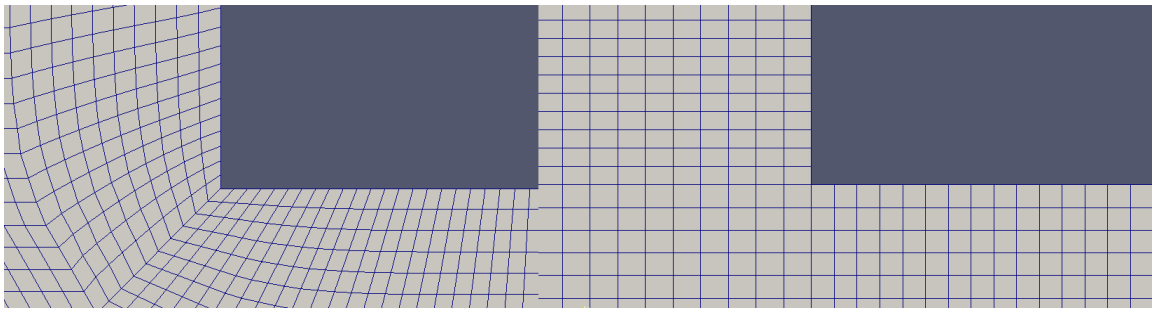

Figure 4.17: Detailed mesh distribution at the bilge, with O-grid to the left and H-grid to the right

These findings can help to explain the different values calculated for the damping coefficient.

Furthermore, it was discovered a study by a group of scientists from MIT and University of Genoa that also had been using OpenFOAM to estimate the damping and added mass for oscillating cylinders, with Vugts experiments as a reference. This work is the same as the case study conducted during the project thesis, where the damping coefficient estimated was approximately 80% larger than the reference value. Nevertheless, that seem to be consistent with the results from the MIT scientist scientist [40], at a non dimensional frequency at 0.8. This can be seen in figure 4.18. In the project work, a H-grid similar to grid 1, as seen in 4.1 was used. However, little information or discussion about the overestimated damping is presented in their work, neither information about their meshing technique. This finding was contributing for going through a systematic study mesh study and discover the reason for the deviations between the numerical and experimental results.

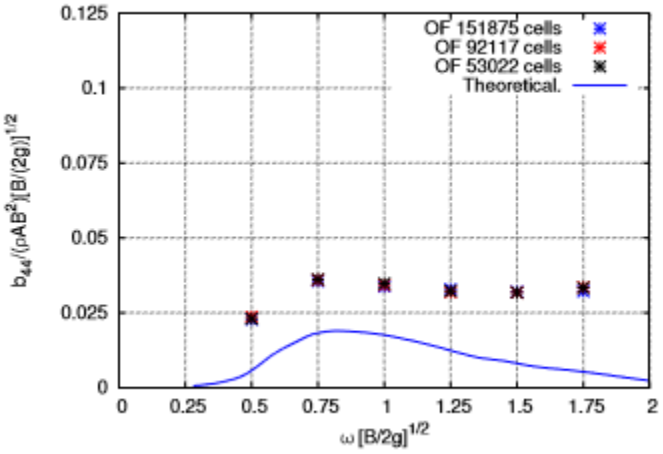

Figure 4.18: Results obtained by the MIT scientist on the Vugts experiment of a rolling box [40]

An interesting observation is that their results seem to be independent of the refinement levels, which means that their grid seem stable. How they have performed the refinement study is unclear, only that the total amount of cells was increased from approximately 150.000 cells for the coarse grid to 530.000 cells for the fine grid, which gives more or less the same results. A convergence like this was not obtained in the present study. One reason might be that the refinement level in their work was not as high as in this work, where the $\Delta x/y$ values are reduced by a factor of two. This means that the total number of cells for each refinement has increased with a factor of 4. That means the refinement is more sensitive to schematic errors.

A limitation with this work must be mentioned, as the compared grids are not directly comparable. This is because the total cell count, and $\Delta x/y$ should be same when comparing the different grids to each other. Due to the different meshing techniques, this was difficult to obtain. One could for instance notice that the most refined mesh for grid 1 has the same $\Delta x/y$ at the body as the coarse mesh for grid 3. This is a drawback, and should be considered for future studies. As a consequence, a final conclusion based on these studies should not be drawn. Illustrations in the flow field analysis are presented with refinement level 0 for the O-grid (grid 3), and refinement level 1 for the H-grid (grid 1). The corresponding damping coefficients for these two grids are 0.020 for the O-grid and 0.027 for the H-grid.

Chapter 5

Case study

In the case study, a section of a FPSO is investigated with and without bilge keels, to find the effect of KC number on the roll damping. Both free decay tests and forced motions should be applied in the simulations, and then compare the parameters of interest such as the roll damping. Rather than scaling an existing FPSO platform, this work is based on the previous experiments and simulations obtained by [41], [42], such that the results can be directly verified. This was done in accordance with the supervisors. As specified in the task, the forced roll motions should be examined at the natural frequency of the cross section. In order to do so, the free decay tests had to be done first to find the cross section's natural period in roll. When the natural period was found, a new grid convergence study was performed in order to obtain the optimal grid for the rest of the simulations. As it became clear that the free decay tests were not that simple to conduct, it was done a preliminary study in order to obtain the natural period, such that the forced roll simulations could be done as further investigation of the free decay was necessary. In table 5.2 the natural frequency for the three different cross sections have been provided after studying the time evolution of the roll angle, further discussed in 5.3.
Four different cross sections are studied at three different amplitudes, 5, 7.5 and 10 degrees.

5.1 Geometry

For the current work, a cross section representing a FPSO was chosen based on previous studies, such that the results are possible to verify. The model was then made in SolidWorks as a 3D object, and exported to OpenFOAM where the meshing procedure was by the snappyHexMesh utility.

Table 5.1: Cross-section characteristics

Parameter	value	unit
B	0.8	[m]
D	0.25	[m]
L_{BK}	0 - 2 -4-6	[cm]
α	45	[deg]

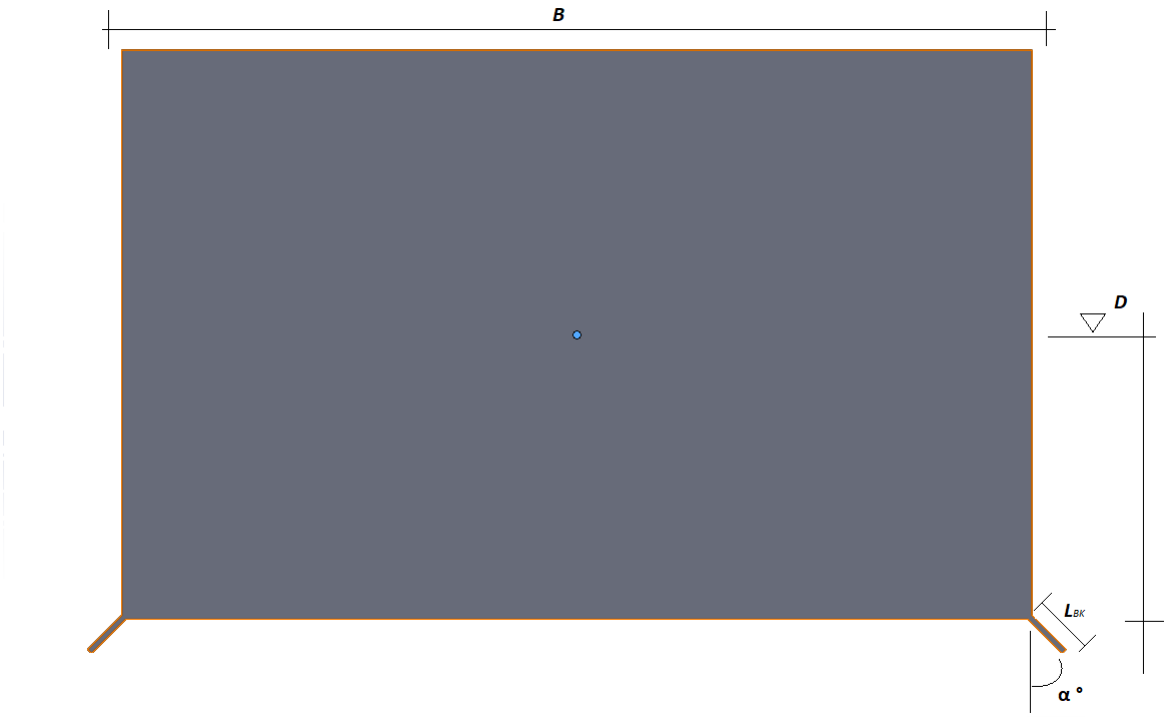

Figure 5.1: Cross section of FPSO hull

Table 5.2: Characteristics of the different sections investigated

Section name	Bilge keel width L_{BK} [m]	b_{bk}/B [%]	$\omega_n[\frac{rad}{s}]$	ω_n^* [-]	Critical damping B^*_{crit}[-]
BK0	0	-	2.91	0.59	0.19
BK2	0.02	2.5	2.72	0.55	0.20
BK4	0.04	5	2.51	0.51	0.22
BK6	0.06	6.25	2.28	0.46	0.24

The center of roll is located at the free surface. In figure 5.2 the domain set-up is shown.

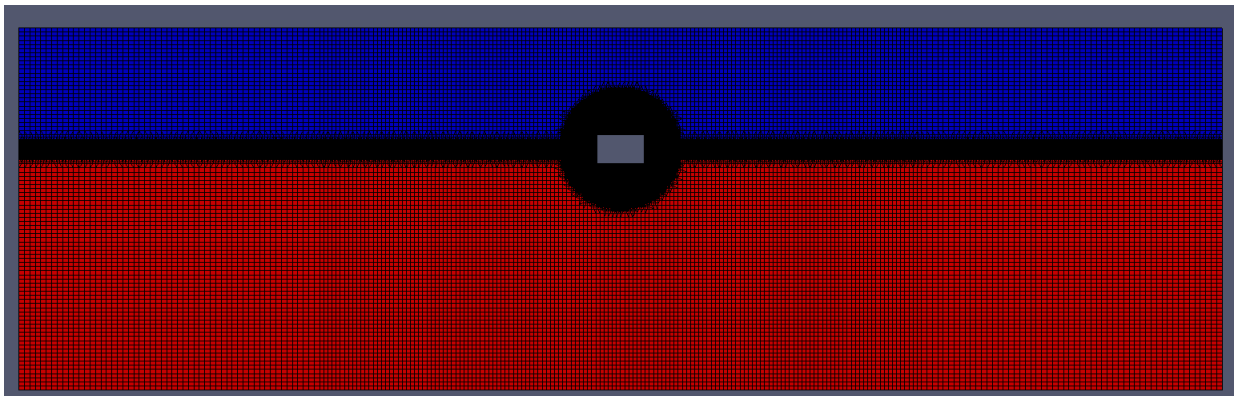

Figure 5.2: Computational domain, red indicates water and blue air.

The domain span over $25 * B$, with a water depth of $16 * D$.

5.1.1 Test case

The conducted study was chosen so that some of the results could be compared to previous experiments. The amplitudes are chosen within the range of what are the possible roll angles that FPSO platforms can experience. It should be noted that a roll angle of ten degrees however is a rare occurrence, and more chosen as an extreme value. Thiagarajan and Braddock [43] states that in special areas roll excitation can reach 15°. Further, the simulations are performed in laminar conditions, as the damping is assumed to be dominated by the flow separation. If time allows, simulations with a turbulence model and full scale simulations will be performed for comparison of the non-dimensionalized damping coefficient. The effect of bilge keel size is also investigated. As the drag force is linearly dependant to the projected area of the bilge keel, it is assumed that the size of bilge keels will increase the damping linearly. Based on the previous work and this assumption, the three different bilge keel lengths are chosen such that this should be easy to detect. According to Pettersen [32]bilge keels normally have the dimensions 1-3% of the ships beam. Similar to [43], this study has investigated larger than usual bilge keels, as the bilge keels studied range from 2.5-6.25 % of the beam. For the simulations three different time-steps were considered. A fixed time step of $\Delta T = \frac{1}{1000}$ was chosen after the variations in terms of damping were not significant by evaluating three time steps. This is consistent with the findings by Jaouen [17], which concluded that the influence of time step is small, but is recommended to be at least $\Delta T = \frac{1}{800}$.

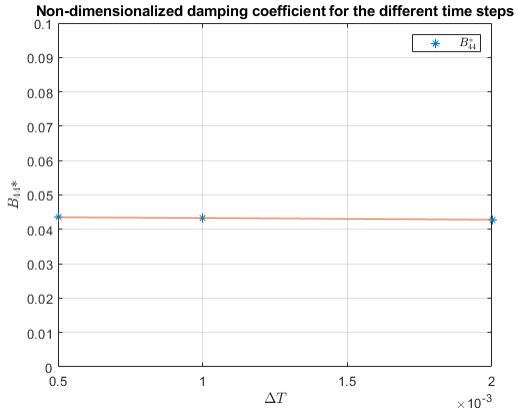

Figure 5.3: Time step sensitivity

All simulations in the work presented have been run in parallel on the supercomputer Vilje at NTNU. As this is a 2D case, with a limited amount of cells, the computational set-up has been decomposed to one node with 16 processors.

5.1.2 Mesh convergence

From the findings in 4, a good mesh is an important factor in order to get accurate results. For the cross sections with a bilge keel, the damping contribution is assumed to be strongly connected with flow separation from the bilge keels, and that the singularity problem connected with sharp bilges will be of less importance. Following, a new sensitivity study was performed at an roll angle of 5 ° on the cross section. The results from the mesh sensitivity study are presented in table 5.3

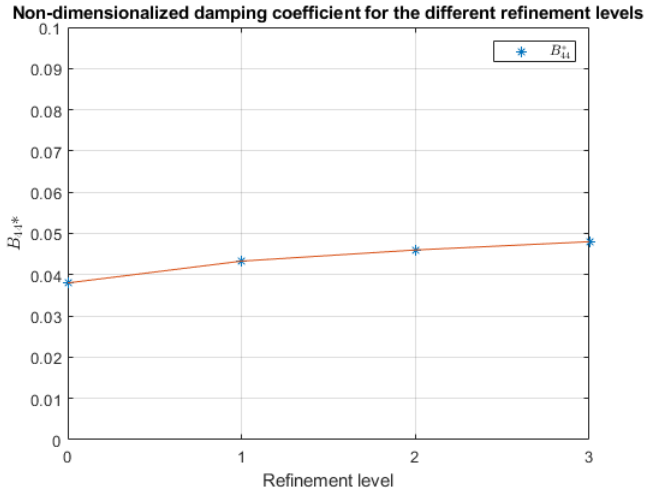

Figure 5.4: Convergence study of the damping

As the meshing procedure of the cross section fitted with bilge keels is done with snappyHexMesh and not blockMesh, the sensitivity study is not as easy to control. With the snappyHexMesh utility, there is a large set of parameters the user must control which can be quite complicated in the beginning. The meshing procedure is automatic, and the user specifications only sets a minimum or maximum criteria, so you actually do not have full control over the final mesh. Again, a sensitivity study is performed with three different refinement levels of the mesh, and compared against one mesh made by Giuseppina Colicchio with Pointwise. With snappyHexMesh, the refinement study has not been focusing on the element size but rather how the grid is covering the critical areas around the bilge keels.

By evaluating the moment plot and the damping coefficient, the most appropriate grid was chosen based on the reference grid, and similar numerical studies as found in [44].

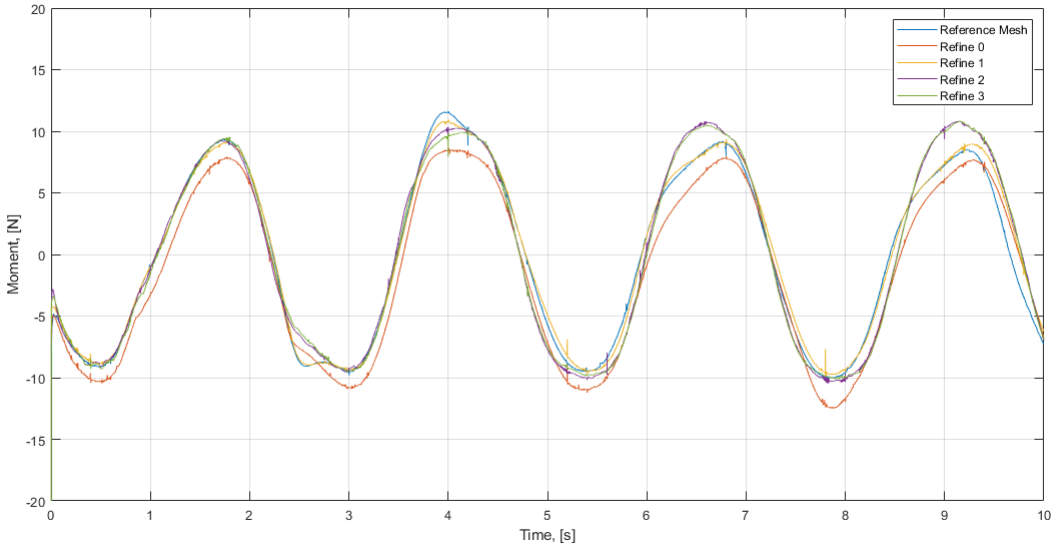

Figure 5.5: Moment history from mesh refinement study. The Reference mesh is made by Giuseppina Colicchio in Pointwise

Table 5.3: Mesh convergence - damping

Refinement level	B^*_{44}
Refine 0	0.04
Refine 1	0.043
Refine 2	0.046
Refine 3	0.048
Reference mesh	0.045

It is worth noticing that the sensitivity study only was performed for 10 seconds, and three oscillation periods. A better estimation would be to let the simulations run longer so that the results are averaged over more periods. As no ramp-up function is used, transient effects may occur in the beginning. However, the solution and time history of the moment looks to be stable, and the very first oscillation is not included in the results. Another effect is that the reflected waves may disturb and affect the flow after a while if the domain span is not large. For the O-grid made in Pointwise, the domain size is 6.8 meters. That means reflected waves will reach back to the body after 8.4 seconds by the relation of the group velocity for deep waters,

$$C_g = \frac{\omega}{2k} \tag{5.1}$$

with k as the wave number. Considering time steps after 8.4 seconds with this grid there is possible that the results are influenced by the reflected waves. To avoid effects like this, one should make sure that the domain is big enough so there will be no reflection during the desired time-window for the simulation. There are also possible to include numerical damping devices to damp the waves at the boundaries.

After the first refinement, there is approximately a 5% change in the damping coefficients, which is considered acceptable. It was concluded that the best grid is identified as "Refinement 1". Both the moment history and damping are corresponding well with the reference grid. It could be discussed if this was the better grid by comparing with the results by Na et. al. [41], as it seems to underestimate the damping with approximately 10 %. The last refinement, "Refine 4", seem to get a closer match of the damping when comparing to Na et. al. but it does not seem to behave similar as the reference grid with respect to the moment seen in figure 5.5. Uncertainties regarding the mesh quality as well defends the decision, and as discussed in the detailed grid study, valuable information can be interpreted from the force history.

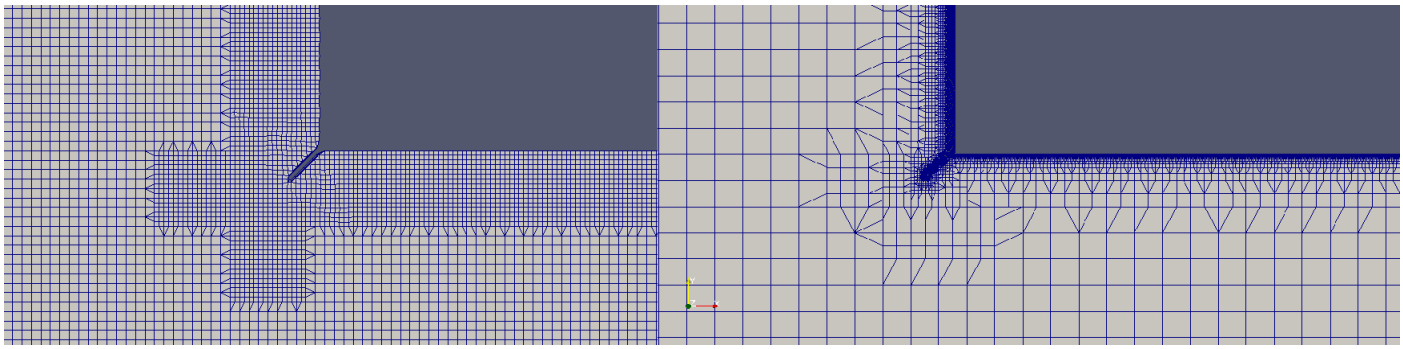

Figure 5.6: Coverage of the bilge keel. Mesh to the left identified as most optimal as the vortex street is mostly covered by equal cells.

This mesh study was performed by comparing the damping coefficient against the work by Avalos and Wanderley [44] that did a study on the same geometry. They also used an unstructured grid, made in gmsh. The results from their work can be seen in figure 6.1, and their damping coefficient show less than 5% deviation compared to the current studies.

5.2 Forced Roll motions

The forced roll simulations have been performed at the natural frequency for each section as described in the task. The hydrodynamic forces are written to a file such that the damping coefficients can be evaluated according to 3.9.

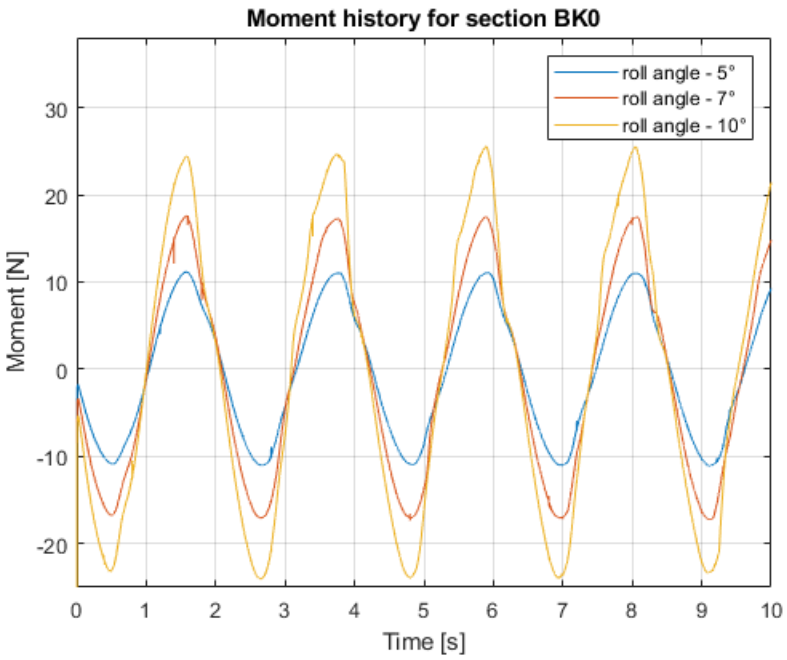

Figure 5.7: Moment data for section BK0 at three different roll angles

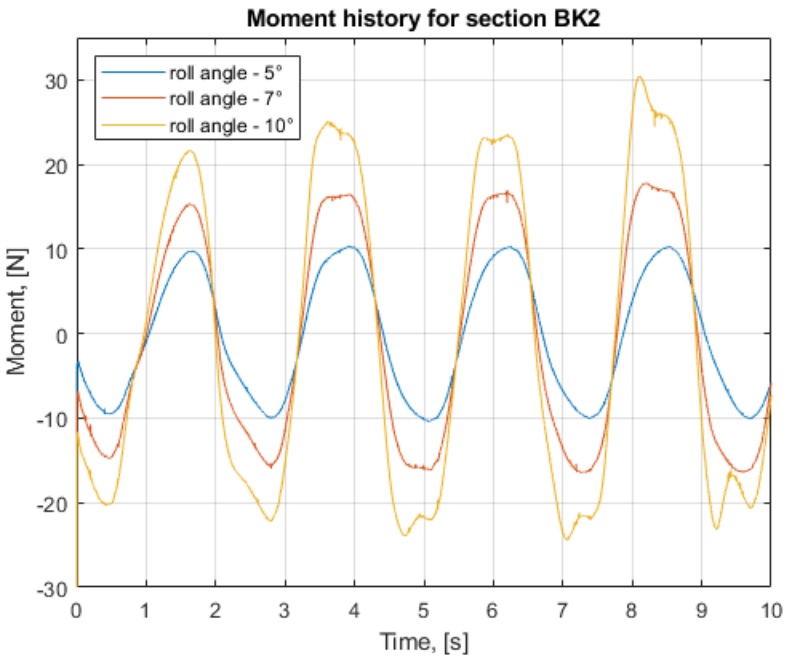

Figure 5.8: Moment data for section BK2 at three different roll angles

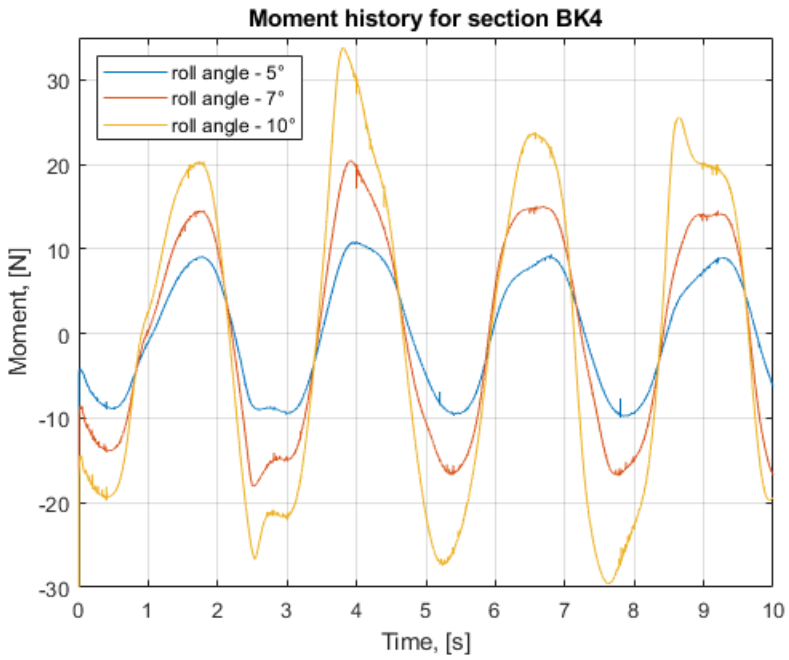

Figure 5.9: Moment data for section BK4 at three different roll angles

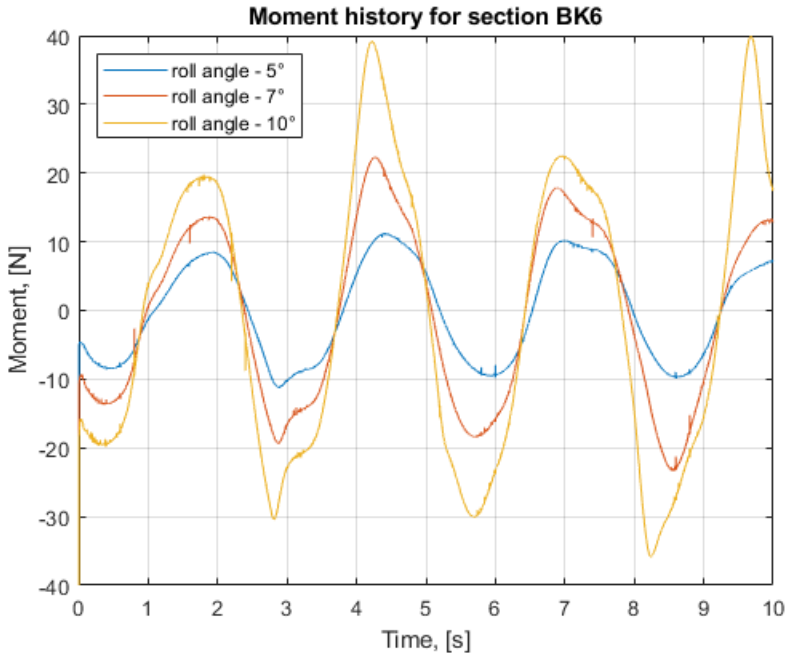

Figure 5.10: Moment data for section BK6 at three different roll angles

With the moments obtained, the damping coefficient is estimated by integrating over the last three periods. In table 5.4 the damping coefficients for all four sections at the three different roll angles are presented.

Table 5.4: Non-dimensional damping coefficients for sections at all roll angles

Roll angle θ	Section name	Damping B^*_{44} [-]
5°	BK0	0.011
	BK2	0.035
	BK4	0.043
	BK6	0.055
7.5°	BK0	0.017
	BK2	0.055
	BK4	0.061
	BK6	0.079
10°	BK0	0.022
	BK2	0.066
	BK4	0.08
	BK6	0.1

5.3 Free decay simulation

Simulating a free decay test in OpenFOAM can be performed with different methods. In the current work, two methods were tested as it was the importance of mesh quality turned out to be of a significant importance. The first decay tests were performed where the cross section was created with an heeling angle equal to the desired angle for the decay test. Then, the meshing procedure was run to create a mesh around the body. The drawback with this method is that the final mesh will not be symmetric. It turned out that the importance of a symmetric mesh influenced the result to a greater extent than what was expected.

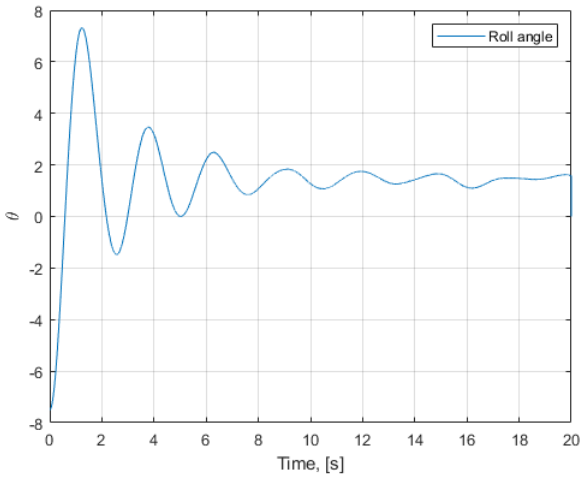

Figure 5.11: Time history of the roll angle in the first decay simulations

In figure 5.11 it is clear that the roll oscillations are about a mean position of almost 2°. That implies the freely floating body floats with an heeling angle of two degrees, something that does not make sense as the body is perfectly symmetric about the y-axis. With an error like that, it was difficult to determine if the further analysis would be correct so new simulations had to be performed.

The solution to this problem was to force the body to rotate from it's initial position of 0° with a prescribed motion, just as in the forced roll simulations. Then, one could calculate at which time step the body will have it's maximum angle, and make sure that this angle corresponds to the desired angle for the free decay test. By extracting the data in the polyMesh folder, you have a distorted, but uniform mesh of the body with the wanted initial angle ready to be used for the decay test. By utilizing this method, it was clear that the problems with equilibrium position was eliminated. Another possible method, not further investigated in this work is to give the freely floating body a moment during a short time period in order to rotate it.

After performing a free decay test, one could find the natural period to the system by evaluating how long time it takes between two successful peaks. Then, the natural frequency is given:

$$\omega_n = \frac{2\pi}{T_n - T_{n-1}} \tag{5.2}$$

As the forced oscillations was to be performed at the sections natural frequency, the case study was a bit of an iteration process. As the sensitivity study was done with forced motions, a free decay simulation had to be performed at the beginning to give a brief estimate of the natural frequency. Then, this process was repeated to ensure accurate results, and that the decay test was performed with a suitable grid. The following plots show the decay history for the four

different FPSO-sections with an initial roll angle of $\theta = 5°$.

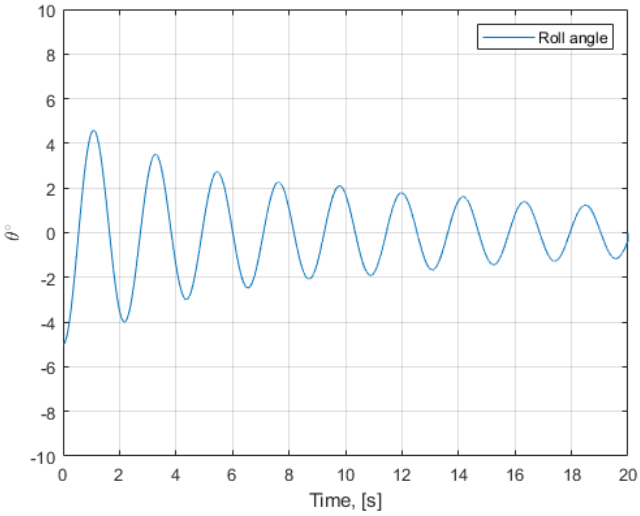

(a) BK0

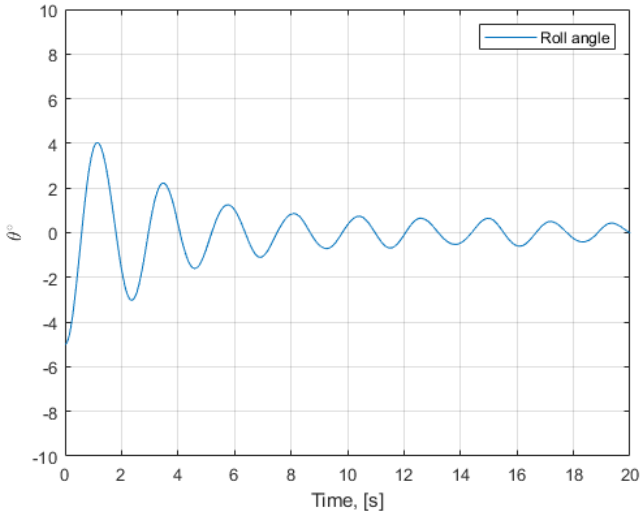

(b) BK2

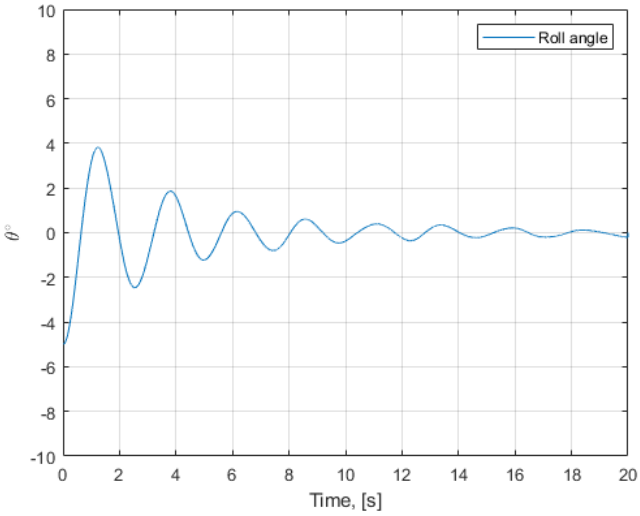

(c) BK4

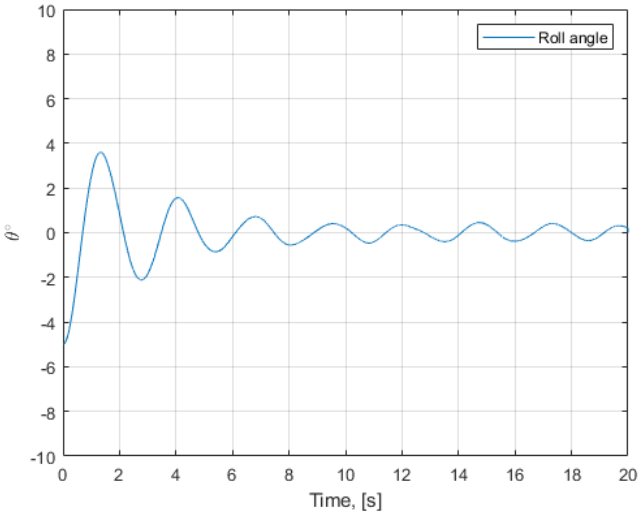

(d) BK6

Figure 5.12: Roll decay simulation for all sections at $\theta = 5$ °

The roll decay simulations for $\theta = 5°$ and $\theta = 10°$ can be found in the Appendix.

According to the relations presented in chapter 3.3.2, the results and corresponding damping coefficients could be obtained through the least squares method. However, as the damping is known to be dependant on the KC number it is stated that fitting a straight line through the sampling points is difficult. Based on this, the damping terms found are strongly dependant on the chosen decay period and number of peaks included in the calculations. For the following results, the damping coefficients p_1 and p_2 were found by evaluating the absolute value for the

peaks of four successful oscillation periods, illustrated below.

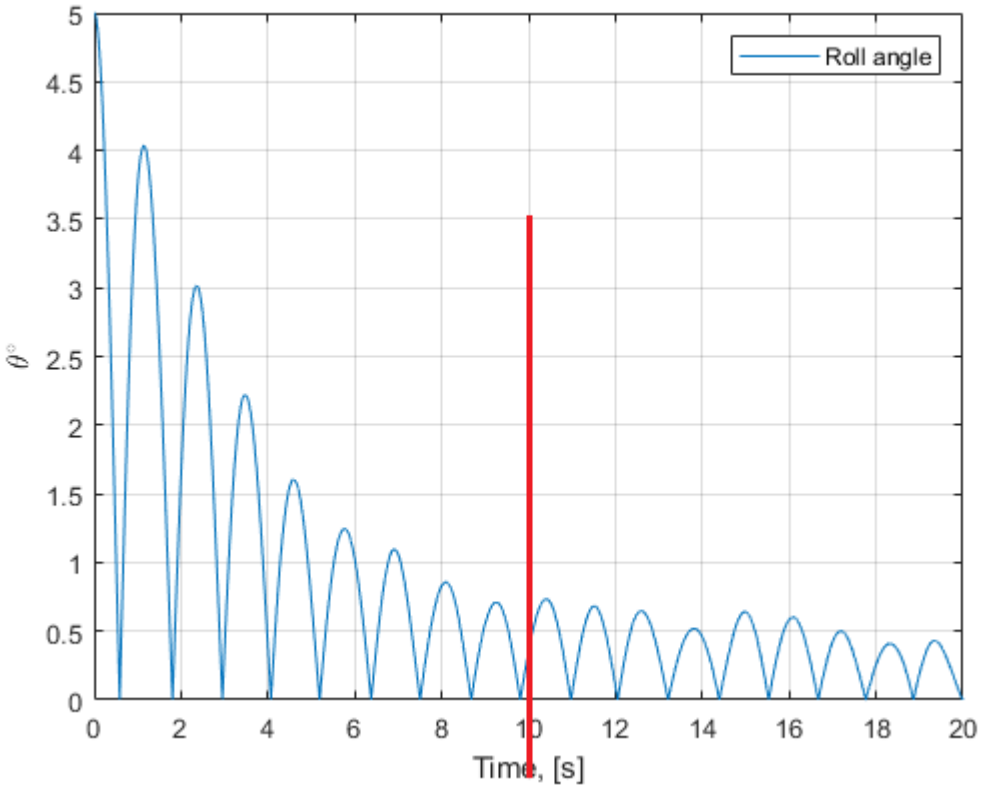

Figure 5.13: Representation of the roll angles used for the damping analysis, only the peaks to the left of the marker are included.

Solving equation 3.14 and fitting a straight line will then provide results as shown in figure 5.14

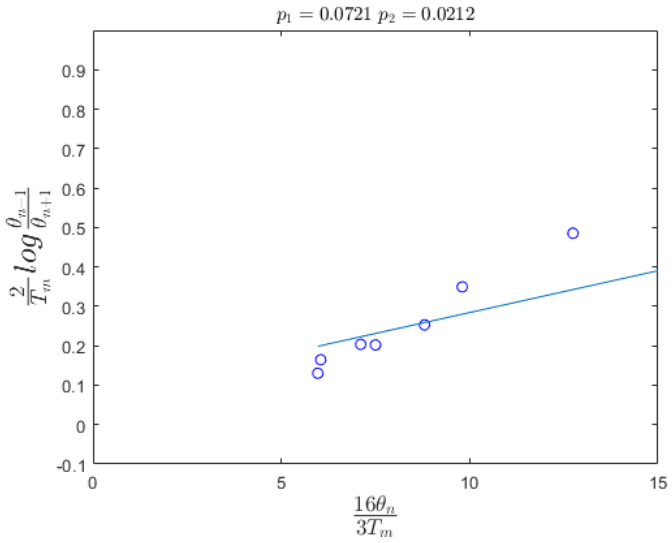

(a) BK0

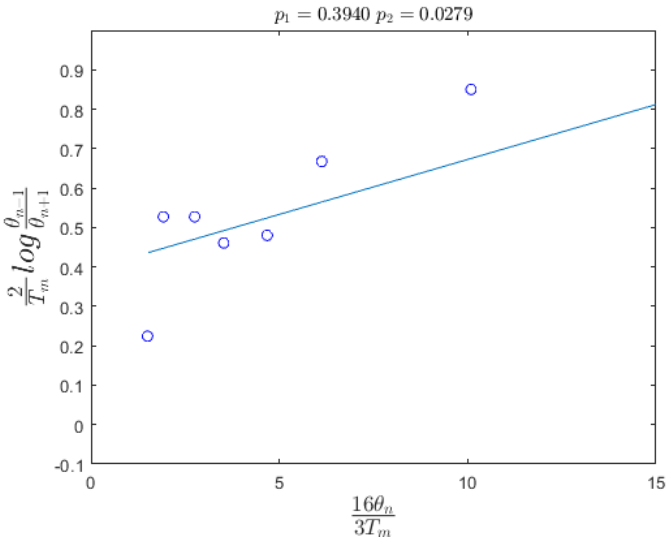

(b) BK2

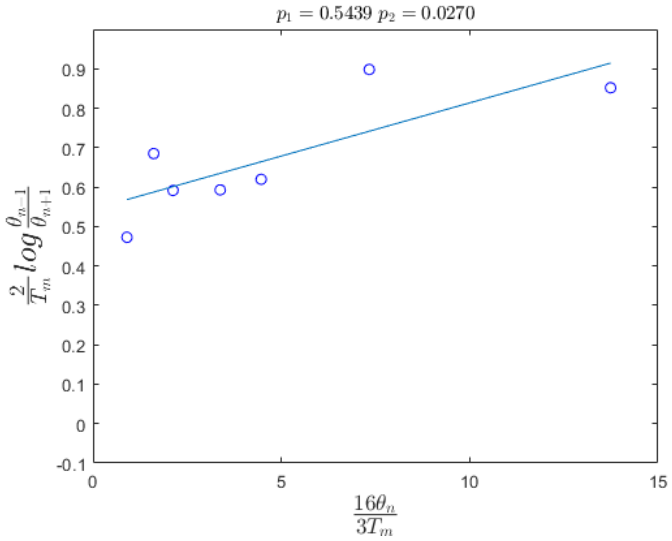

(c) BK4

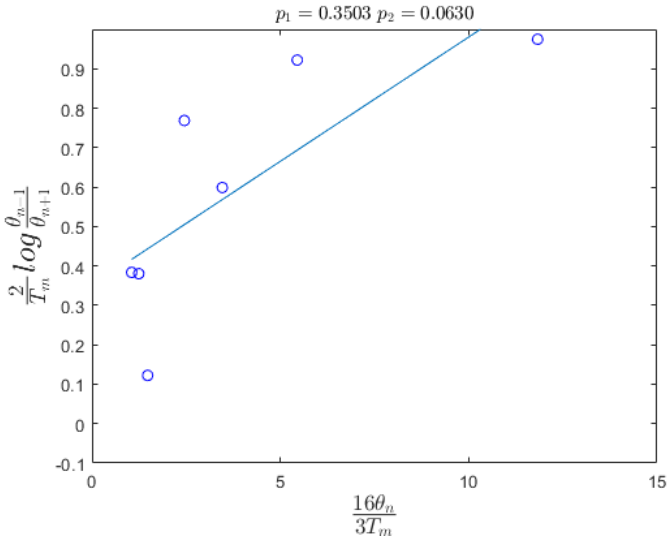

(d) BK6

Figure 5.14: The Faltinsen approach to estimate the damping coefficient p_1 and p_2. Results for all sections at initial roll angle of 10°

The values for p_1 and p_2 are dimensionless. The obtained results for all free decay simulations are presented in table 5.5 below.

Table 5.5: Linear and quadratic damping components according to Faltinsen ([1]

Roll angle θ	Section	p_1	p_2
5°	BK0	0.11	0.012
	BK2	0.36	0.018
	BK4	0.38	0.030
	BK6	0.32	0.060
7.5°	BK0	0.072	0.019
	BK2	0.24	0.038
	BK4	0.59	0.013
	BK6	0.29	0.068
10°	BK0	0.072	0.021
	BK2	0.39	0.27
	BK4	0.54	0.27
	BK6	0.35	0.063

5.3.1 Analytic approximation

Once the damping terms have been established, 4th Runge-Kutta method may be applied to solve equation 3.13 in order to see if the obtained damping terms are able to reproduce the time series from the simulations. This would give valuable insight if it is sufficient with only a linear and quadratic damping term, or that maybe higher order damping terms is needed to find the damping coefficient. Recall the equation of motion that was introduced in chapter 3.3.2 as;

$$(I_{44} + A_{44})\ddot{\theta} + B_1\dot{\theta} + B_2\dot{\theta}|\dot{\theta}| + C_{44}\theta = 0$$

and the relation 3.16, the results from decay test and Faltinsen fit are multiplied with $(I_4 + A_{44})$ in order to find an analytic approximation of the free decay simulations. This is because B_1 and B_2 are the dimensionalized constants of p_1 and p_2, with dimensions $[\frac{kgm^2}{s}]$ and $[kgm^2]$ respectively.

The term $(I_4 + A_{44})$ which is the roll moment of inertia and added mass moment of inertia may be found based on the following relation,

$$(I_4 + A_{44}) = \frac{C_{44}}{\omega_n^2} \tag{5.3}$$

and that the natural frequencies for the different sections are known. The restoring term,

C_{44} can be found from;

$$C_{44} = \rho g \nabla G M_T$$

where GM_T is the transverse metacentric height.

$$GM_T = KB + BM - KG$$

KB is the distance from the keel to buoyancy center, which is half the draft. KG is distance from keel to center of gravity and BM is the distance from buoyancy center to metacenter.

For the analytic approximation of the decay test, the restoring coefficient C_{44} is assumed to be constant. The bilge keels are assumed only to increase the added mass moment A_{44}. This assumption is confirmed in [12]. Based on the restoring coefficient and the natural frequency, the corresponding added mass and inertia term is found.

Table 5.6: Properties for the added mass and moment of inertia for the different sections

Section	$(I_4 + A_{44})[kgm^2]$
BK0	2.0
BK2	2.3
BK4	2.7
BK6	3.3

It should be mentioned that each of the terms have not been found, only the resulting, effective moment of inertia $(I_4 + A_{44})$. As a consequence, in the MATLAB routine found in Appendix A that approximates the free decay test, the values set for each parameter I_4 A_{44} is not their actual value, but the sum is correct.

By multiplying the obtained p1 and p2 values with these results we get the dimensionalized damping coefficients B_1 and B_2 from equation 5.3.1. The equation of motion 5.3.1 can now be solved by use 4th order Runge-Kutte method numerically. It is also possible to express B_1 and B_2 in terms of an equivalent damping by utilizing equation 2.9. Once these coefficients are obtained, an analytic solution for the decay test can be approximated.

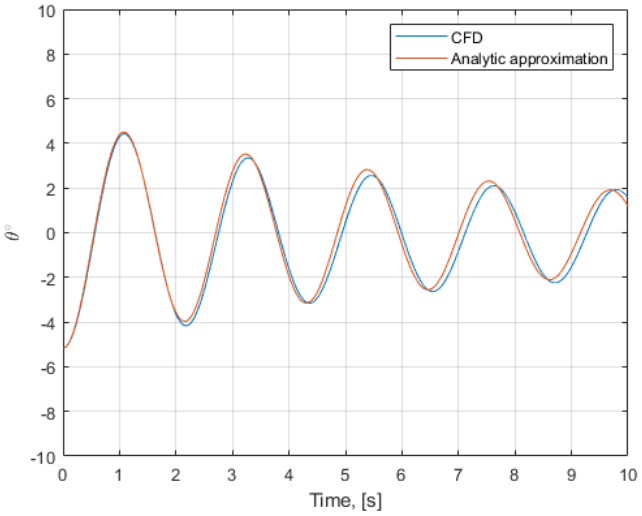

(a) BK0

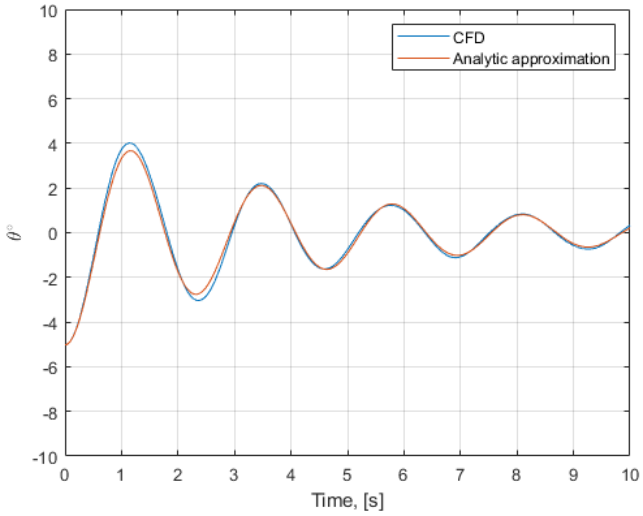

(b) BK2

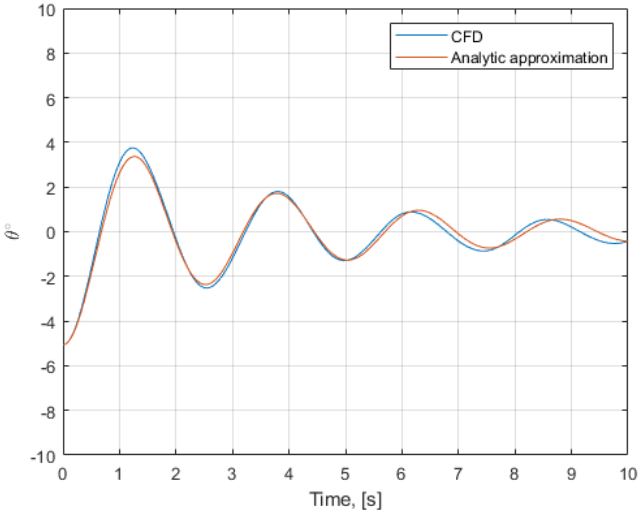

(c) BK4

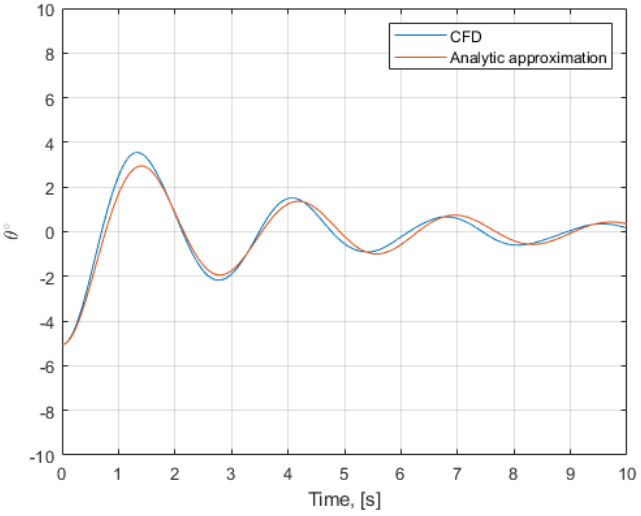

(d) BK6

Figure 5.15: Analytic approximation of the free decay test at $\theta = 5°$

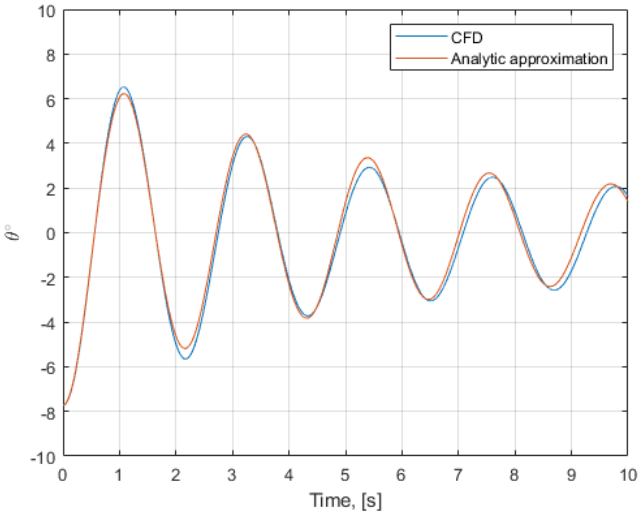

(a) BK0

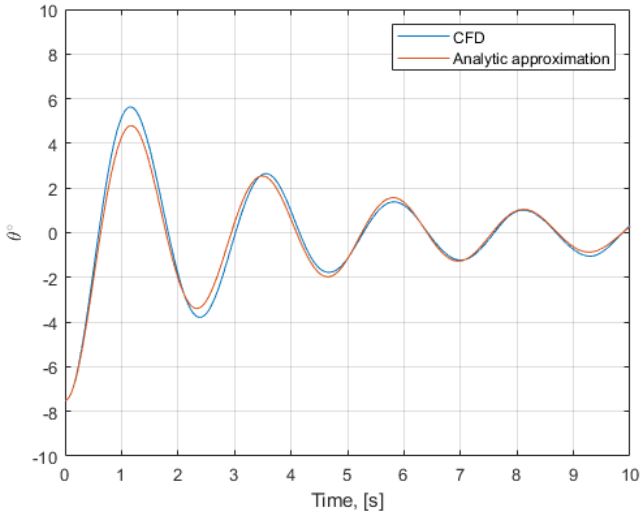

(b) BK2

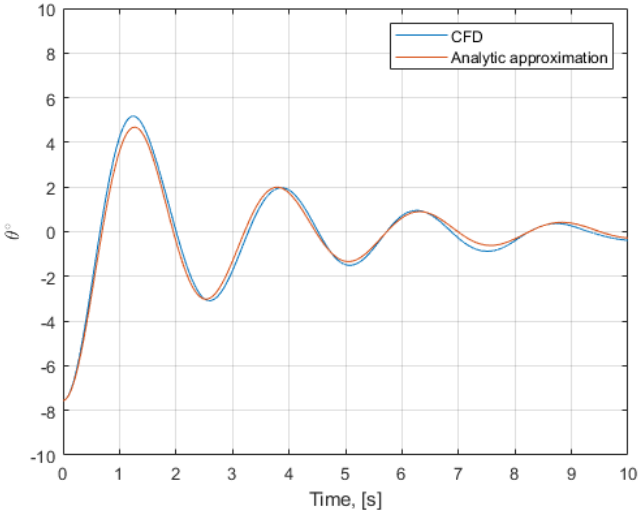

(c) BK4

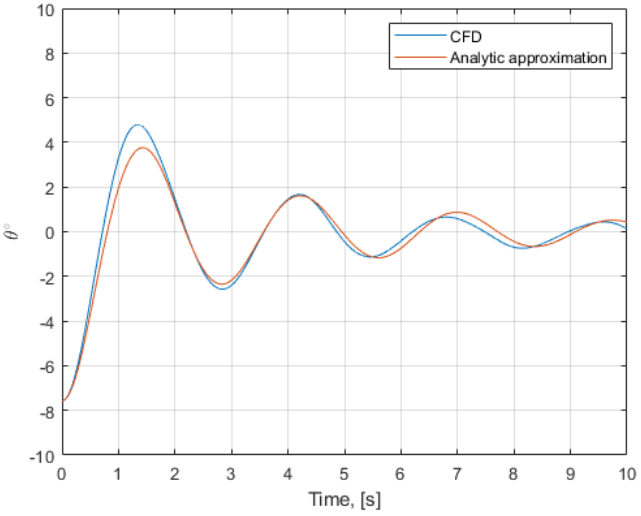

(d) BK6

Figure 5.16: Analytic approximation of the free decay test at $\theta = 7.5°$

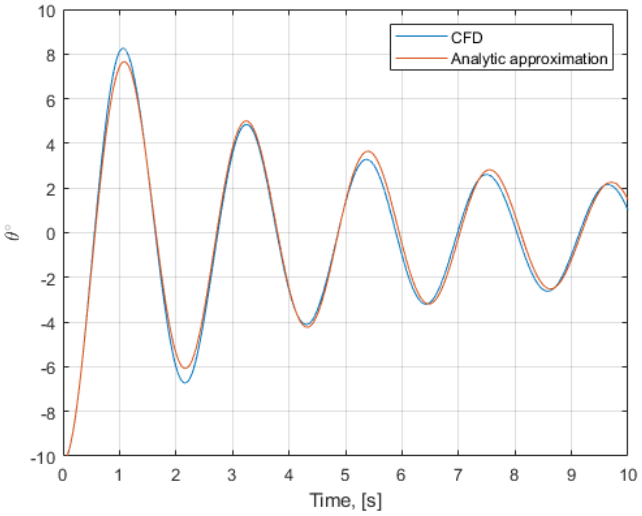

(a) BK0

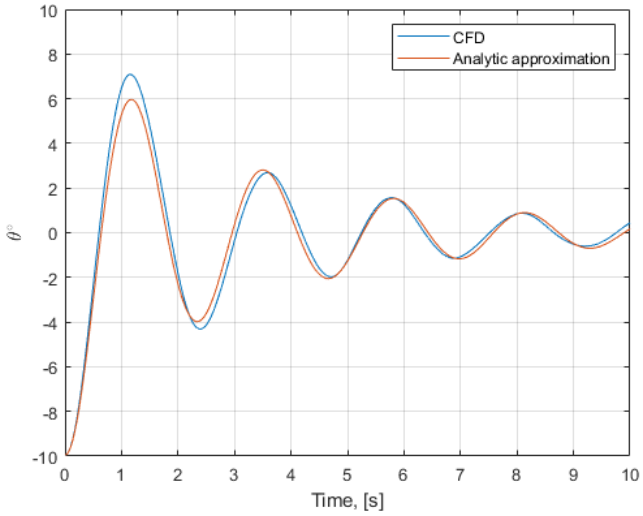

(b) BK2

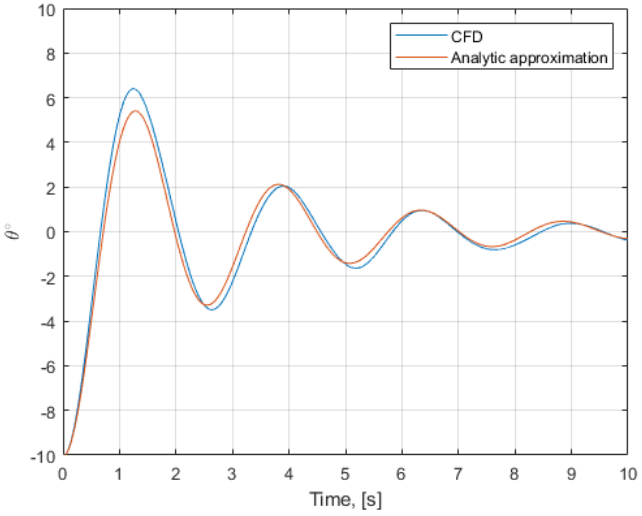

(c) BK4

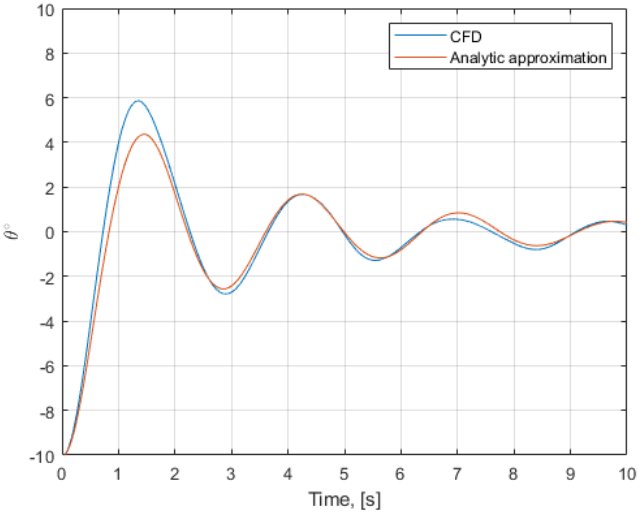

(d) BK6

Figure 5.17: Analytic approximation of the free decay test at $\theta = 10°$

The damping coefficients estimated with the Faltinsen fit seem reasonable, and the analytic solution for the free decay motion is acceptable. It appears that the damping is slightly over-damped in some cases.

Chapter 6

Results and Discussion

6.1 Forced simulations

The forced simulations show that the bilge keels increases the hydrodynamic moment on the sections. However, this is more evident for large roll angles.

The damping ratio that express the ratio between the damping and critical damping which was defined in section 4.1 can be used to define the damping provided by the bilge keels. It is given by the fraction:

$$\zeta = \frac{B^*_{44}}{B^*_{crit}} \tag{6.1}$$

An important aspect with the damping ratio, is that a system with a low damping ratio will be more sensible with respect to changes in the flow field.

Table 6.1: Damping ratio for the different sections at $\theta = 5°$

Section	ζ [-]
BK0	0.058
BK2	0.18
BK4	0.20
BK6	0.23

As seen, the damping ratio for the hull without bilge keels, has a damping ratio significantly lower than the sections with bilge keels. It is clear that the damping ratio corresponds well with the results from
Even though the damping ratios for the sections fitted with bilge keels are significant larger than for the case without bilge keels, the mesh quality will nevertheless be of importance. Comparing the obtained results with the experimental results by Na et al. in terms of non dimensional

damping coefficient [41] show some deviations.

Table 6.2: Comparison of non dimensional damping coefficient, current studies vs. Na et al. [41]

Section	B^*_{44} - current studies	B^*_{44} - Na et al. [41]
BK2	0.035	0.03
BK4	0.043	0.051

From table 6.2 it is clear that the damping estimated is not matching the results by Na et al. too good. For the smallest bilge keel configuration the damping coefficient is overestimated by 16%. For the bilge keel which was used in the mesh sensitivity analysis, BK4 the damping is on the other hand underestimated by 15%. Also the reference mesh made in Pointwise underestimates the damping by 12 %. This shows that more attention should be given to the meshing procedure. As the intentional bilge keel configurations was BK4 and BK6, the mesh found for these two sections may not be applicable to the smallest bilge keel configuration BK2. Since the present study has investigated the roll damping at resonance, one reason may be that inaccuracies in the natural frequencies may be present.

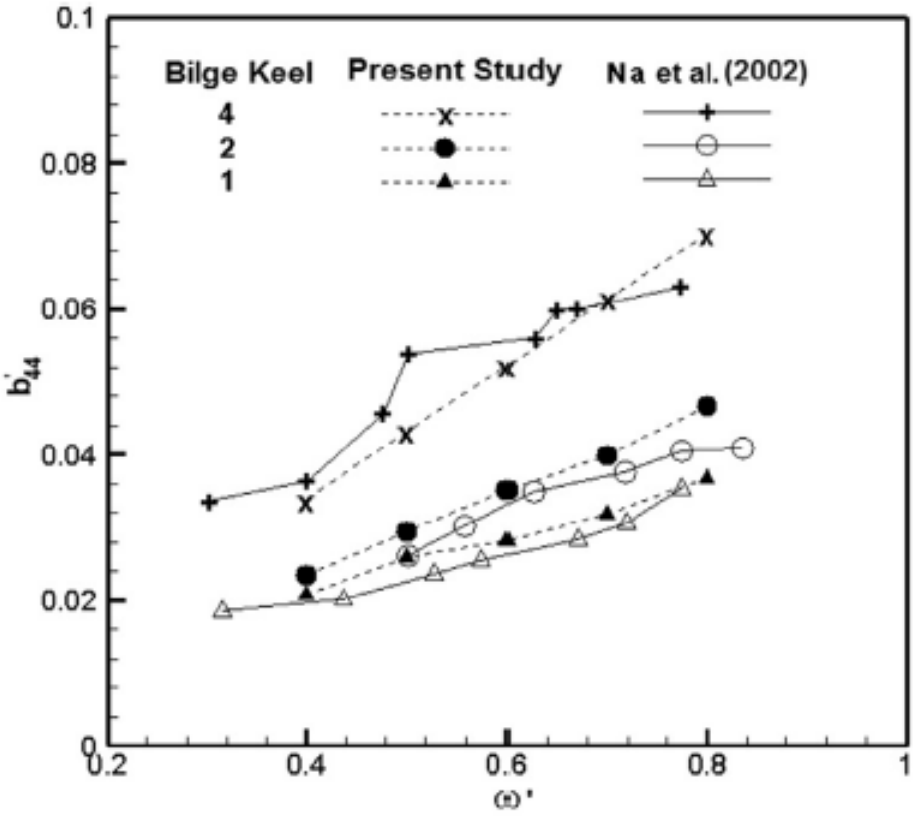

Figure 6.1: Experimental results by Na et al. and the numerical results by Avalos and Wanderley [44]

It is also difficult to read precisely the results from the graph. Bilge model 2 and 4 corresponds to section BK2 and BK4 respectively. Specially BK4 one can see a steep change around the resonance frequency which is 0.5. On the other hand, the results by Avalos and Wanderley [44] which was used as a comparison in the mesh sensitivity study, show similar results as the current study. That means there might be some uncertainties in the experimental results as well.

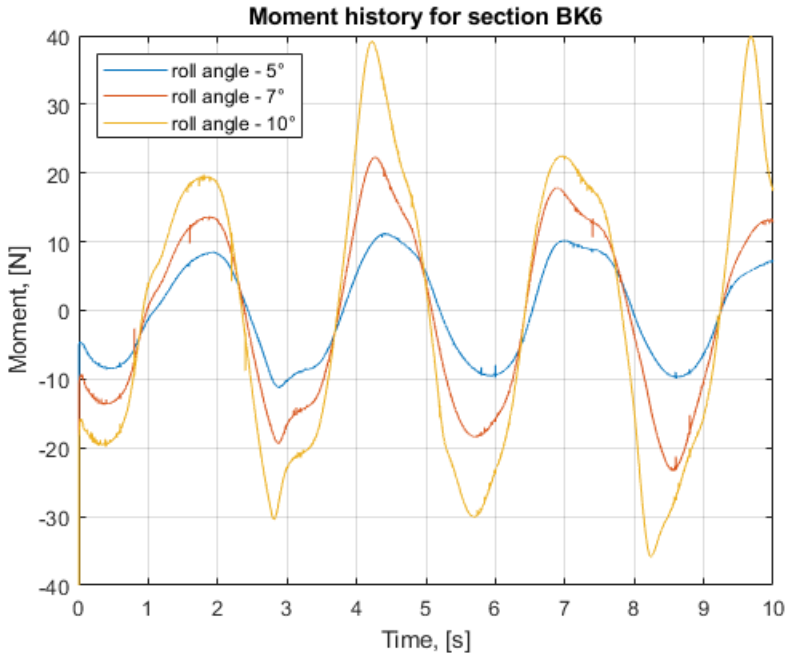

Figure 6.2: Moment data for section BK6 at three different roll angles

From figure 6.2 it is clear that the moment amplitudes not are constant. It may be that the variation in moment amplitudes are due to higher order frequencies. This trend becomes more clear for higher KC numbers as well as large bilge keel width. Also, this figure can illustrate how the first roll cycle is different from the following cycles in terms of forces, as the moment peak in the first cycle is lower for all KC numbers.

6.2 Free decay

The free decay simulations also illustrated the importance of a good mesh. The automatic meshing procedure with snappyHexMesh was difficult to control when the section was inclined and not horizontal. In other words, making the geometry with the wanted roll angle before importing to OpenFOAM is not to recommend. In figure 6.3 it is clear that the mesh is of a much lower quality and one can see how the free surface is captured compare to a symmetric mesh.

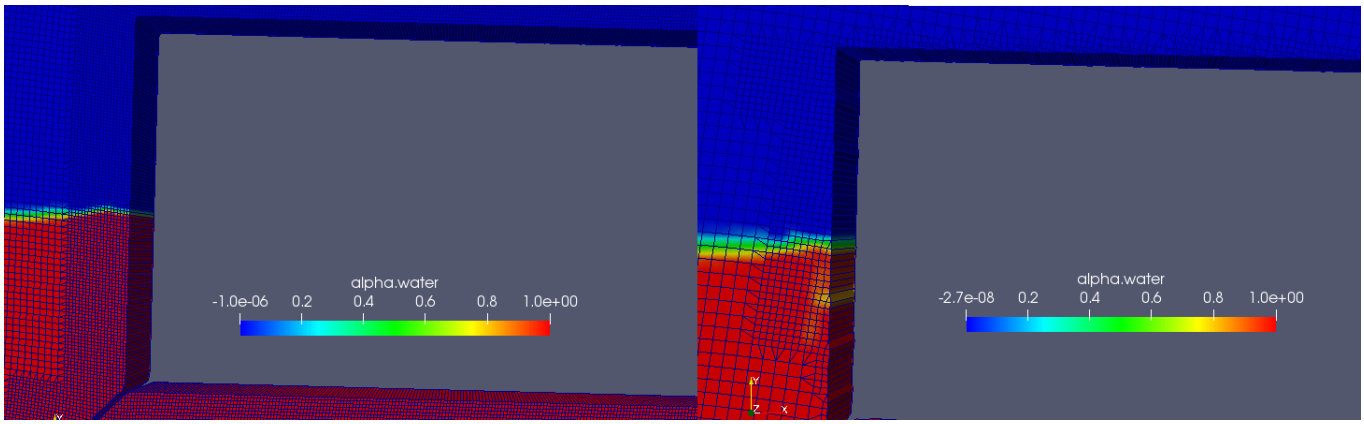

Figure 6.3: Mesh resolution at the free surface. Mesh on the left is the method used with a symmetric mesh. To the right is the asymmetric mesh.

This happened despite more strict requirements in terms of mesh quality, which again illustrates some of the drawback with the meshing procedure. The problem faced with the section oscillating about a mean position not equal to zero, see fig 5.11, was eliminated when a symmetric, but distorted initial mesh was used. Hence, the bad quality of the mesh is assumed to be the reason for the body not to oscillate around a mean position of 0°. An explanation may be that the pressure forces acting on the body are not captured correct as the free surface problem will cause an uneven pressure distribution.

It has been discussed that estimating roll damping coefficients are difficult from free decay tests. The results showed to be highly sensitive to the number of roll cycles included in the calculations. The current work estimates the damping coefficients from the four first oscillation periods where Thiagarajan and Braddock [43] only uses the firs three oscillation periods.

The final results showed acceptable behavior when an analytic approximation was compared with the simulations. What could be said is that the quadratic damping seem to be overestimated. When looking at the analytic approximations in figure 5.17, the first peaks are showing a lower roll magnitude compared to the simulations. This trend is more prominent for large roll angles. As the quadratic damping component is considered non linear and KC dependent, this supports the assumption on an overestimated quadratic term, as this term is dominant in the first roll cycles with large roll angles. To ensure good estimations, Fernandes and Oliveira [38] discussed new methods with both higher order polynomials and new approaches to get a better result. Neither of these are investigated in the current work.

The roll natural period found from the free decay test has quite a large shift when increasing the bilge keel width, which is shown in figure 6.4. However, by comparing with the changes in natural frequency, ω_n obtained from Gu [47], the result seem to be consistent with his results. In

his work, bilge keels with a width of $\frac{b_{bk}}{B} = 0.022$ has been investigated in different configurations, and compared to a hull without bilge keels. Equipped with bilge keels, ω_n was reduced by 10%. Current work shows a reduction of ω_n of 7% in the case of $\frac{b_{bk}}{B} = 0.025$. On the other hand, by comparing with the work from Thiagarajan and Braddock [43] it is clear that their results show a much lower reduction in ω_n when fitting the hull with bilge keels. For the case with $\frac{b_{bk}}{B} = 0.025$, their reduction of ω_n is only 1%. For the case with large bilge keels, $\frac{b_{bk}}{B} = 0.065$, ω_n reduces only with 5%. For the similar case in this work, ω_n was reduced by 20%. One reason for these large deviations in the results may be due to the fact that the model parameters are $\frac{1}{6}$ of the size in Thiagarajan and Braddock [43], while Gu [47] use an almost similar model. Further, Thiagarajan and Braddock [43] estimates the natural frequency as a function of the damped natural frequency and the damping ratio, which is not considered in this report.

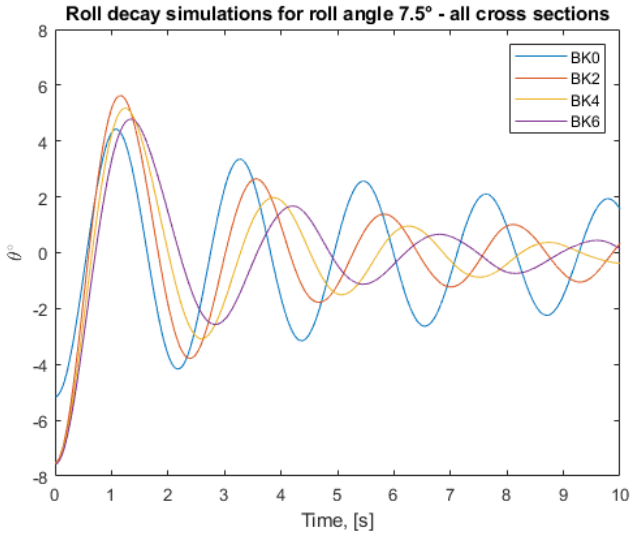

Figure 6.4: Roll decay simulation for all four sections

6.3 Comparison of Forced Motion vs Free Decay

To compare the damping obtained from simulations with analytic calculations, one must know about the restoring and inertia terms from the equation to first find $(I_4 + A_{44})$. They were found - but in order to do the comparison we must also give this term per unit length, which implies the terms are divided by the cross sectional thickness, dz, which is equal to 0.1.

In order to compare the results directly with the ones from the forced simulations, one must also convert the presented results in terms of an equivalent linear damping. This is done according to equation 6.2

$$B_{44,eq} = B_{44,1} + B_{44,2}\frac{8}{3\pi}\omega\theta \tag{6.2}$$

where $B_44,1$ and $B_44,2$ is simply the product of the $(I_4 + A_{44})$ and p_1 and p_2. θ is given in degrees. This gives:

Table 6.3: Linear and quadratic damping components with corresponding equivalent linear damping.

Roll angle θ	Section	$B_{44,1}$ $[\frac{kgm^2}{s}]$	$B_{44,2}$ $[kgm^2]$	$B_{44,eq}$ $[\frac{kgm^2}{s}]$
5°	BK0	2.2	0.24	5.3
	BK2	8.4	0.42	13.2
	BK4	10.4	0.82	19.1
	BK6	11.0	2.00	30.4
7.5°	BK0	1.5	0.39	8.7
	BK2	5.6	0.89	21.0
	BK4	16.2	0.36	22.0
	BK6	9.6	2.2	41.5
10°	BK0	1.5	0.43	11.9
	BK2	9.1	0.63	23.6
	BK4	14.8	0.55	26.5
	BK6	11.6	2.1	52.2

As these result are obtained, one can compare against the ones from the forced oscillations. By presenting the damping without dimensions we get

Table 6.4: Comparison of the non-dimensionalized damping coefficients for the two simulation cases

Roll angle θ	Section	B^*_{44} - Forced Roll	B^*_{44} - Free Decay
5°	BK0	0.011	0.0084
	BK2	0.035	0.021
	BK4	0.043	0.03
	BK6	0.055	0.048
7.5°	BK0	0.017	0.014
	BK2	0.055	0.033
	BK4	0.061	0.035
	BK6	0.079	0.066
10°	BK0	0.022	0.019
	BK2	0.066	0.037
	BK4	0.08	0.042
	BK6	0.1	0.083

As one can see, the Free decay test show a smaller damping compared to the forced roll simulations. However, to compare these results against each other may be problematic. The forced roll simulations are performed with a constant amplitude, which means that the KC number is the same through the whole cycle. For the free decay, it is clear that the amplitude changes between each roll period. That means we have a change in the KC number as well. Hence, the damping estimated from the free decay test are not experiencing the same flow field around the FPSO section as it would in case of a forced roll section. To investigate this, a forced roll simulation was performed for section BK2, at an amplitude corresponding to the mean amplitude of the first oscillation periods accounted for in the free decay test. For the initial roll angle of 7.5%, the corresponding mean roll amplitude is 4.88° if one consider the first periods of oscillations. By immediately having a quick look at table 6.4 and the damping at a forced roll motion at 5°, it is clear that this seems to be a proper comparison and with results matching quite good. From the simulation performed with a forced motion of 4.88°, the non-dimensional damping was found to be 0.033, which is the same as the free decay test at 7.5°.

6.4 Effect of bilge keel width

It was assumed that larger bilge keels would increase the damping. This is also confirmed in the figures. It is clear that the damping increases as the bilge keel width is increased, almost with an approximately linear behaviour. Thiagarajan and Braddock also found that the damping seemed to increase linearly for bilge keels with a width up to 10% of the ships beam, which confirms the findings [43].

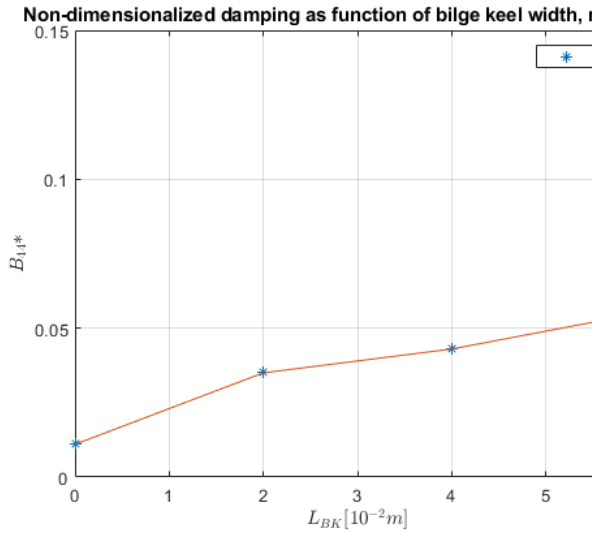

(a) $\theta = 5°$

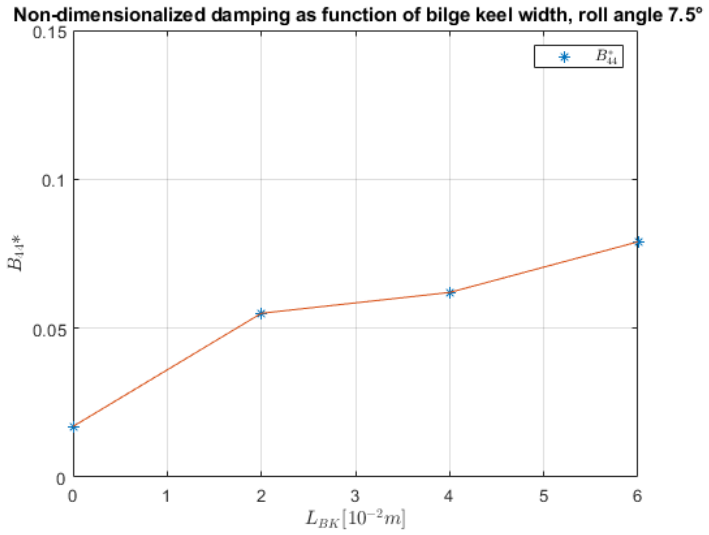

(b) $\theta = 7.5°$

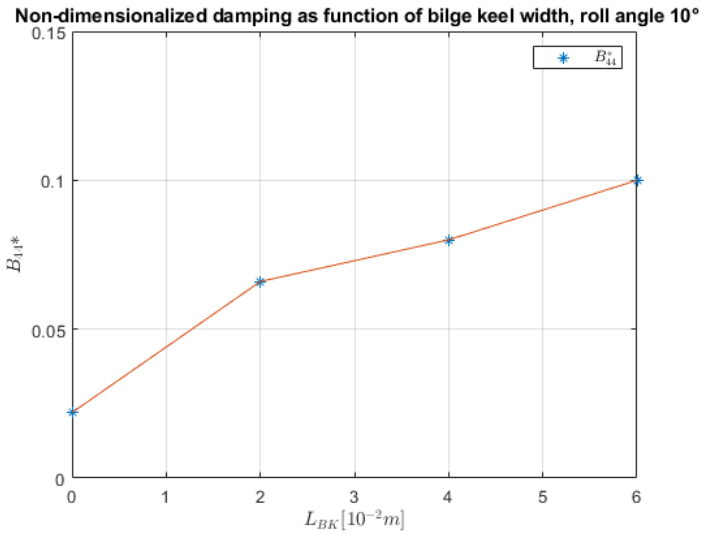

(c) $\theta = 10°$

Figure 6.5: Damping coefficient vs. bilge keel width obtained from the forced roll simulations.

In order to comment about the effectiveness of the bilge keels, the damping ratio is calculated

in table 6.5 with the smallest bilge keel width, $BK2$ as reference $L_{bk,ref}$

Table 6.5: Percentage increase of damping due to increased bilge keel width, $L_{BK,ref}$=BK2

$L_{bk}/L_{bk,ref}$	Roll angle 5° $B^*_{44}/B^*_{44,ref}$	Roll angle 7.5° $B^*_{44}/B^*_{44,ref}$	Roll angle 10° $B^*_{44}/B^*_{44,ref}$
2	23%	11%	21%
3	57%	44%	67%

Similarly can be done with $BK0$ as reference, to illustrate the damping increase due to the presence of bilge keel.

Table 6.6: Percentage increase of damping due to presence of bilge keel

Section	Roll angle $\theta = 5°$	Roll angle $\theta = 7.5°$	Roll angle $\theta = 10°$
BK2 - $\Delta B^*_{44}/B^*_{44,BK0}$	218%	224%	200%
BK4 - $\Delta B^*_{44}/B^*_{44,BK0}$	290%	269%	263%
BK6 - $\Delta B^*_{44}/B^*_{44,BK0}$	400%	365%	355%

From this one can see that the effectiveness of the bilge keels is larger at small amplitudes. This is because at a roll angle of $\theta = 10°$, even the cross section without bilge keels is able to shed distinct vorticities.

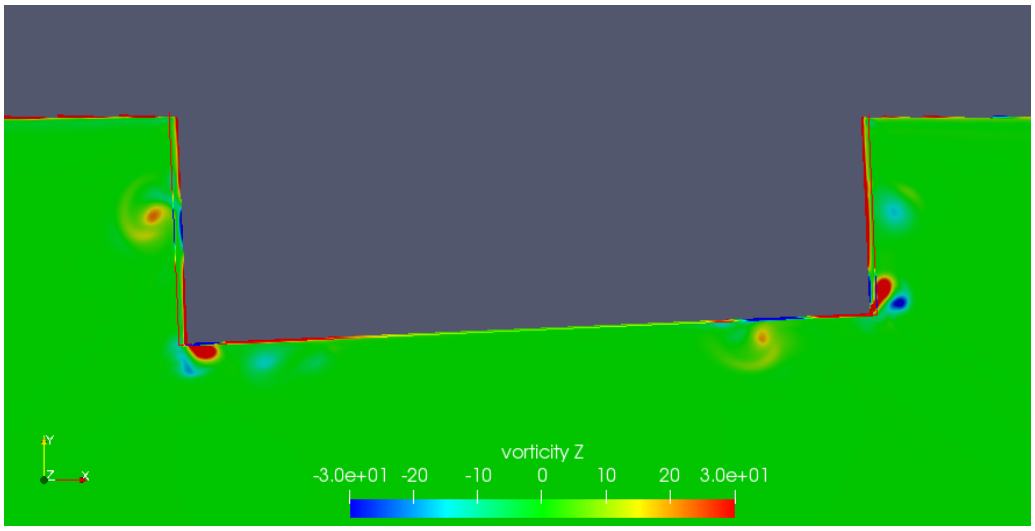

(a) BK0

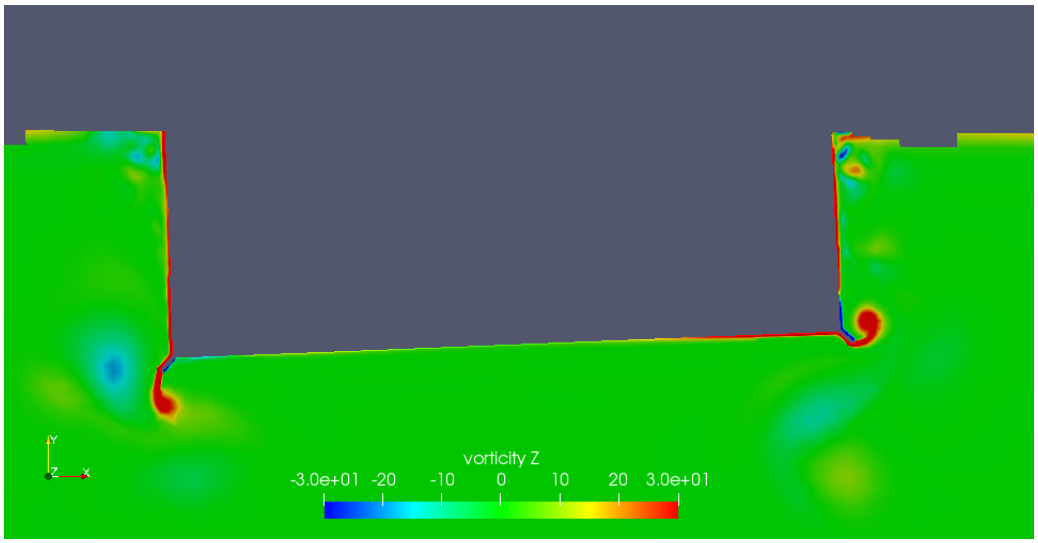

(b) BK2

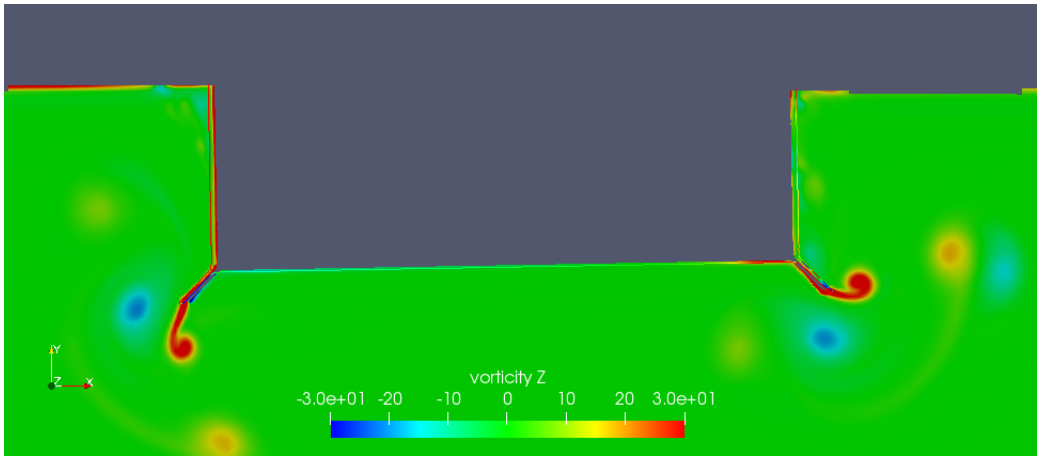

(c) BK6

Figure 6.6: Vorticity plot for different bilge keel lengths at same position, $\theta = 5°$

From the figures, it is clear that the section fitted with bilge keels provide much larger vorticities. That implies the drag force is stronger, and hence the damping is larger. With stronger vorticities, the hull pressure also changes. These two effects are the main contribution for the bilge keel damping, and the wave making damping is more difficult to illustrate from the simulations.

6.5 Effect of KC number

The KC number was previously defined as:

$$KC = \frac{f r \theta \pi}{b_{bk}}$$

For a specific cross section, it means that the only parameter that changes the KC number is the roll amplitude θ. Hence, the KC number can be expressed as a function of θ as seen in the figures in 6.7.

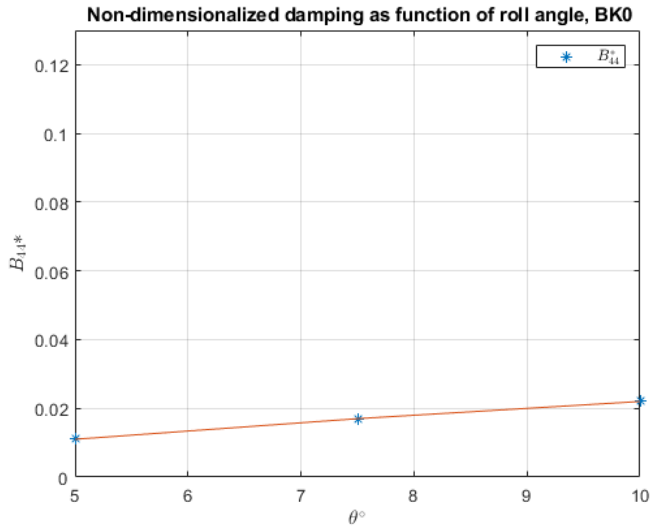

(a) BK0

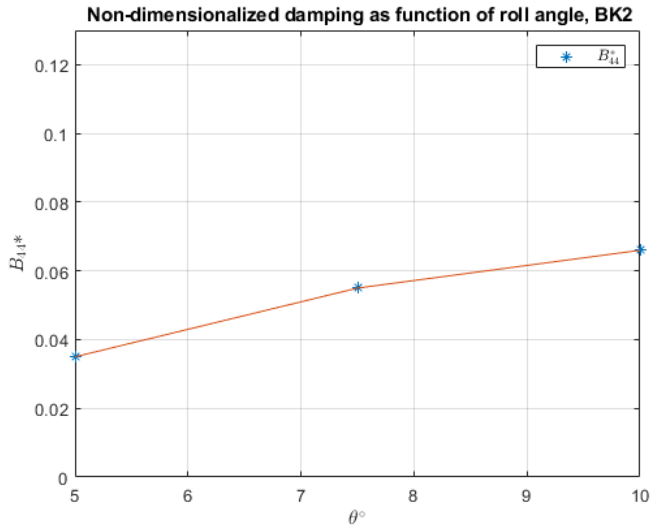

(b) BK2

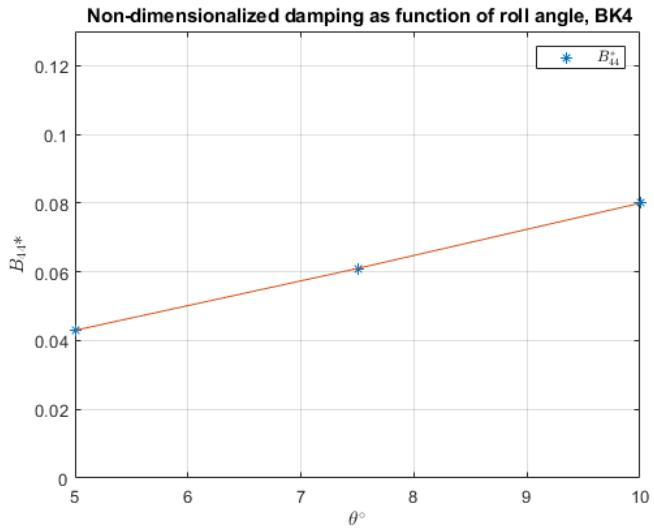

(c) BK4

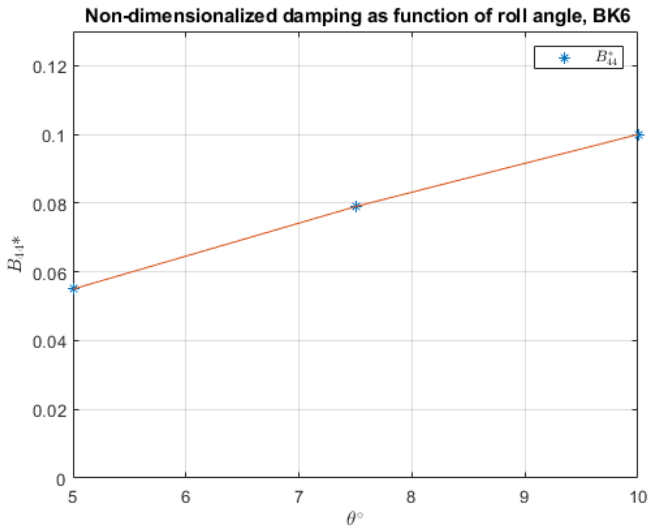

(d) BK6

Figure 6.7: Damping coefficient vs. roll angle obtained from the forced roll simulations.

It is clear the damping coefficients found show a strong dependence on the roll angle and by that the KC number.

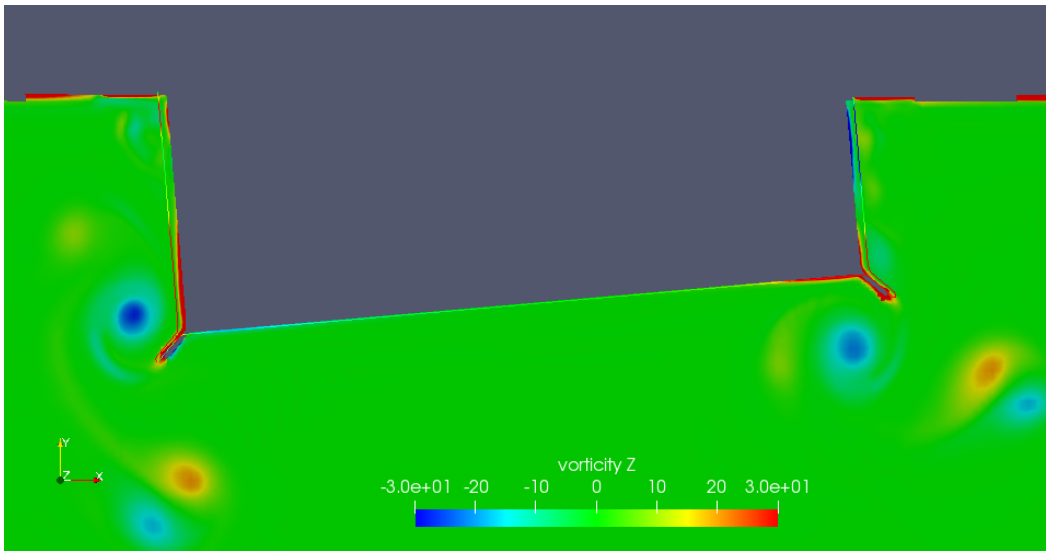

(a) $\theta = 5°$

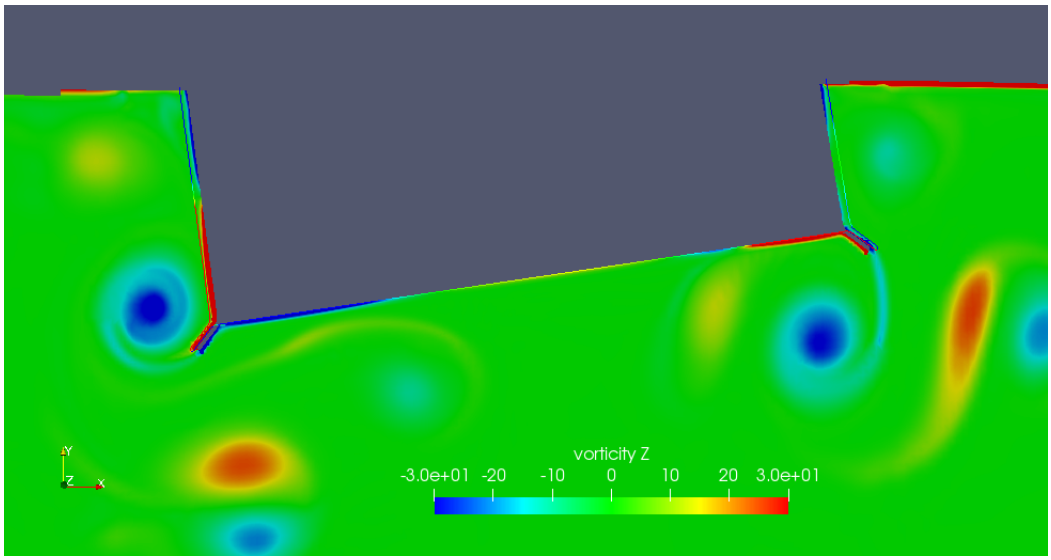

(b) $\theta = 10°$

Figure 6.8: Vorticity plot at t=5.4 seconds for two different roll angles, section BK4

In figure 6.8, two plots are carried out at the same time step for section BK4 to show the effect of the KC number in terms of roll angle. The blue fields are negative vorticities, contributing to damping as the sections are rotating counter clockwise. The blue fields will provide a low pressure region, and the damping will increase as this region becomes larger and with stronger vorticities. In terms of the normal force component, the larger angle means larger KC number and velocity, and hence the normal force acting on the bilge keels will also be larger at high KC numbers. These findings are consistent with how the bilge keel damping was defined, where both the normal force and pressure coefficient was KC dependent.

Table 6.7: Percentage increase of damping due to increase in KC number, $KC_0 = 5°$.

KC/KC_0	BK0	BK2	BK4	BK6
1.5	55%	57%	42%	44%
2	100%	89%	86%	82%

By looking in table 6.7, the increase in damping due to increase in KC number is presented. It shows that the damping is very much connected to the KC number as assumed.

6.6 Main findings

It has been discovered that the numerical simulations for rolling of ship-shaped cross sections are sensitive to the grid strategy. This was clear after the validation study, but it showed that also for the case with bilge keels, the grid has a prominent effect on the results. In the case of bilge keels where there will be strong flow separation phenomena, it is important with a mesh that is able to capture the vortex street region. Hence, large changes in the mesh around the bilge keels should be avoided.

The bilge keel damping can contribute with up to 80% of the total damping according to Kawahara [7], which seems to be reasonable in the case for larger than usual bilge keels for FPSO platforms. In the case of BK6, it is clear that the bilge keel contribution actually make up 80% precisely in the case of roll angle θ =10°. The linear trend for large bilge keels seem to continue for increasing bilge keel width. As concluded by Thiagarajan and Braddock [43], this is true as long as the shed vorticities are able to interact with the hull, which may not happen when the bilge keels become too large.

From simulations it is clear that the bilge keel damping is strongly connected with KC number. The free decay test showed that for the sections fitted with bilge keels, the quadratic term $B_{44,2}$ is the largest contribution to the equivalent damping term. An exception is for section $BK4$, which actually gets the largest contribution from the linear damping component $B_{44,1}$. This is assumed to be due to a bad sampling from the decay test, and that the Faltinsen fit approach do struggle sometimes with the damping estimation for non linear behaviour. By looking at table 6.3, it is again clear that 80% of the equivalent damping component is due to the quadratic, non linear damping contribution when looking at section BK6.
As all simulations are run with laminar flow conditions, one could introduce a turbulence model to see how this would affect the results.

Chapter 7

Conclusion and further work

This work has carried out a systematic investigation of the roll damping components and how numerical tools may be applied in order to predict the roll damping coefficient. For estimation of roll damping with OpenFOAM, much attention is needed on the grid refinement process and choice of grid strategy is very important. If this is not carefully considered, results showed a that the damping could be overestimated by up to 40% for some cases.

It was found that for a FPSO platform the bilge keels are often larger than compared for ships, which improves the roll motion stability. It has been found that roll damping near resonance is strongly connected to viscous effects. It has been shown that the viscous damping is dependent on the KC number which is a function of the roll amplitude for one specific geometry, as the generated vorticities are stronger. Thus, non linear effects dominates the roll damping for FPSO-platforms fitted with bilge keels. It is also found that for relatively large angles the additional damping comes from a stronger vortex formation and pressure changes around the hull compared with a hull without bilge keels. The roll damping also seem to linearly increase with the bilge keel width. In terms of predicting the roll damping, forced roll simulations are to prefer as the amplitude is held constant. It has been discussed that flow memory effects also are of importance, such that the obtained results may not be realistic in full scale, as the roll motion usually is excited by incoming waves.

Future recommendations

As for all numerical methods, the importance of discretization is crucial, which has further been confirmed during this work. As a recommendation for further work, a systematic sensitivity analysis should be performed with a strategic plan where the different investigated grids should have the same properties. That is for both cells, but most importantly the size of the cells in critical regions such as the bilges. It could also be interesting to compare how different CFD

solvers solves the same discretized problem.

In terms of roll damping of FPSO platforms, future work could include more realistic scenarios and see how this will affect the roll damping mechanisms. This could be done by introducing incoming waves, with frequency close to resonance. The coupled motion in sway-roll could also be interesting to investigate. As FPSO platforms are moored, analysis including the mooring lines as springs should also be included. For this case, a spread mooring system would be to prefer, as a turret moored platform is less likely to be exposed to beam sea waves as it can be weathervaned.

Full scale simulations should also be considered, to investigate possible scale effects that might be present, as both Reynolds number, Froude number and KC number will be changed.

Bibliography

[1] Faltinsen, Odd M., *Sea loads on ships and offshore structures*, 1990, Cambridge University Press

[2] Yunus A. Cengel, John M. Cimbala 2014. *Fluid Mechanics - third edition* McGrawHill Education p. 900-902

[3] N., Tuck, E. and Faltinsen, O. (1971), *Ship motions and sea loads, in: Transactions-Society of Naval Architects and Marine Engineers.* Society of Naval Architects and Marine Engineers, New York

[4] Vugts, JH (1968). *The Hydrodynamic Coefficients for Swaying, Heaving and Rolling Cylinders in a Free Surface,* Rept No 194, Laboratorium voor Scheepsboukunde, Technische Hogeschool Delft, The Netherlands.

[5] Y Ikeda, Y. Himeno, and N. Tanaka. *Components of Roll Damping of Ship at Forward Speed.* JSNA japan, 143, 1978.

[6] Himeno, Y. *Prediction of Ship Roll Damping-A State of the Art* DTIC Document, Ann Arbor 1981

[7] Kawahara, Y., Maekawa, K. and Ikeda, Y. (2012), "A simple prediction formula of roll damping of conventional cargo ships on the basis of Ikeda's method and its limitation", J. Ship. Ocean Eng., 2, 201-210.

[8] Chakrabarti, S. *Empirical calculation of roll damping for ships and barges* 2000, Technical note OceanEngineering 28

[9] Taylan, M. *Effect of forward speed on ship rolling and stability* Mathematical and computational Applications, 2004

[10] ITTC - Recommended procedures *Numerical Estimation of Roll Damping* International Towing Tank Conference 2011, revision 00

[11] Taylan, M. *Nonlinear roll motion of ships in beam waves* Article, 1996

[12] Mohsin, I. Nallayarasu, S. Bhattacharay, S.K *Experimental and CFD simulation of roll motion of ship with bilge keel* International conference on Computational and Experimental Marine Hydrodynamics, MARHY, 2014

[13] Oliveira, A. Fernandes, A.*The roll damping assessment via decay model testing (new ideas about an old subject)*Journal of Marine Science application, 2009

[14] Molin, B. (2004), "On the frictional damping in roll of ship sections", Int. Shipbuild. Prog.

[15] Falzarano, J.Somayajula, A. Seah, R.*An overview of the prediction methods for roll damping of ships* Oceans System Engineering vol.5 no.2, 2015

[16] Ikeda, Y. *Prediction Methods of Roll Damping of Ships and Their Application to Determine Optimum Stabilization Devices* Marine Technology, vol.41, no.2, 2004

[17] Jaouen, F. Koop, A. Vaz, G.*Predicting Roll Added Mass and Damping of a Ship Hull Section Using CFD* conference paper, OMAE, 2011

[18] Jaouen, F. Koop, A. Vaz, G. Crepier, P. *RANS PREDICTIONS OF ROLL VISCOUS DAMPING OF SHIP HULL SECTIONS* International Conference on Computational Methods in Marine Engineering - MARINE 2011

[19] Greco, M. Colicchio1, G. Lugni, C. *Assessment study of a Domain-Decomposition strategy for marine applications* IWWWFB27, 2012

[20] Yu, Y. *Prediction of Flows around Ship-shaped Hull Sections in Roll Using an Unsteady Navier-Stokes Solver* Thesis, doctor of philosophy, Uni. at Texas at Austin, 2008

[21] Yu, Y. Kinnas, S. *Roll and heave response of hull sections of variable shapes in waves* OMAE 2010

[22] Haddara, M.R. Leung, S.K*Experimental investigation of the lift component of roll damping* Ocean Engng, Vol. 21, No 2, 1994

[23] Bassler, C. Reed, A. *An analysis of the bilge keel roll damping component model*

[24] Council, J. Boulama, K. *URANS Investigation of Ship Roll Motion Damping Using Bilge Keels* Contract report, Department of Mechanical Engineering, Royal Military College of Canada, 2016

[25] Spieler, T. *Roll damping of an FPSO: towards a CFD investigation of the problem*, unpublished student work, Master Thesis 2012

[26] Yeung, R.W Liao, S-W. Roddier, D. *Hydrodynamic Coefficients of Rolling Rectangular Cylinders* International journal of Offshore and Polar Eng. vol 8, 1998

[27] Kristiansen, T. Faltinsen, O.M *Gap resonance analyzed by a new domain-decomposition method combining potential and viscous flow DRAFT* Ocean Research, vol. 34, pp. 198–208, 2012.

[28] Kristiansen, T., Ommani, B. Faltinsen, O.M *Simplified CFD modeling for bilge keel force and hull pressure distribution on a rotating cylinder* ASME 33rd International Conference on Ocean, Offshore and Arctic Engineering, 2014

[29] Querard, A.B.G, Temarel, P. Turnock, S.R *The hydrodynamics of ship-like sections in heave, sway, and roll motions predicted using an unsteady Reynoldsaveraged Navier–Stokes method* University of Southampton, 2008

[30] Ikeda, Y., Himeno, Y., and Tanaka, N., 1978. "Report no. 405: *A prediction method for ship roll damping*

[31] Ikeda, Y., Himeno, Y., and Tanaka, N.,. *Report no. 403: On eddy making component of roll damping force on naked hull* Journal of the Kansai Society of Naval Architects(142). 1977

[32] Pettersen, B. *Marine Technology 3- Hydrodynamics* Department of Marine Technology, 2007

[33] Moukalled, F., Mangani, L., Darwish, M., 2016. *The FiniteVolume Method in Computational Fluid Dynamics*

[34] Piehl, H.P., 2016. Doctoral thesis University of Duisburg-Essen*Ship Roll Damping Analysis*

[35] CFD Direct - OpenFOAM suppurt site*https://cfd.direct/openfoam/user-guide/v4-blockmesh/*

[36] Ledoux, A., Molin, B., de Jouette, C., Coudray, T. *FPSO Roll Damping Prediction from CFD and 2D and 3D Model Tests Investigations* Proceedings of the 14th international Offshore and Polar Engineering Conference, 2004

[37] Zeraatgar, H., Asgahri, M. *A Study of the Roll Motion by Means of a Free Decay Test* Journal of Offshore Mechanics and Arctic Engineering , 2010

[38] Antonio C. FERNANDES, et al. *The roll damping assessment via decay model testing (new ideas about an old subject* Journal of Marine Science, 2009

[39] Asmuth, H., Henry, A., Schmitt, P., Elsaesser, B.. *Determination of non-linear damping coefficients of bottom-hingedoscillating wave surge converters using numerical free decay tests* Renew 2014 1st International Conference on Renewable Energies Offshore

[40] Bonfiglio, L., Brizzolara, S., Chryssostomidis, C. *Added Mass and Damping of Oscillating Bodies: a fully viscous numerical approach* Recent Advances in Fluid Mechanics, Heat Mass Transfer and Biology , 2012

[41] Na, H.J., Lee, W.C., Shin, H.S., Park,K.I *A Design of Bilge Keels for Harsh Environment FPSOs* Proceedings of The Twelfth (2002) International Offshore and Polar Engineering Conference Kitakyushu, Japan, 2002

[42] Tan, J.H., Teng.Y.J., Kim, J.W., Sinha, S.K. *CFD Simulation of Roll Damping of a New-Build Barge-Shaped FPSO Vessel with Bilge Keels* Offshore Technology Conference Asia, Kuala Lumpur 2018

[43] Thiagarajan, P.K., Braddock, C.E. *Influence of Bilge Keel Width on the Roll Damping of FPSO* Journal of Offshore Mechanics and Arctic Engineering, 2010

[44] Avalos, O.G.G., Wanderley, B.V.J *Numerical study of forced roll oscilaltion of FPSO with bilge keel* Article in Ocean Engineering 147, 2018

[45] van't Veer, R., Schut, X.B., Huijsmans, R.H.M.*Bilge keel loads and hull pressures created by bilge keels fitted to a rotating cylinder* Article in Applied Ocean Research 53, 2015

[46] Avalos, O.G.G., Wanderley, B.V.J, Fernandes, c.A., Oliveira, C.A *Roll damping decay of a FPSO with bilge keel* Article in Ocean Engineering 87, 2014

[47] Gu, Y., Day, S., Boulougouris, E. *A Study on the Effects of Bilge Keels on Roll Damping Coefficient* Proceedings of the 12th. International Conference on the Stability of Ships and Ocean Vehicles, 2015

[48] Bluewater Energy Services, Netherlands *https://www.bluewater.com/fleet-operations/our-fpso-fleet/bleo-holm/* - picture downloaded 10.02.2019

[49] Devolder, B., Schmitt, P., Rauwoens P., Elsaesser, B., Troch, P.*A Review of the Implicit Motion Solver Algorithm in OpenFOAM® to Simulate a Heaving Buoy*

Appendices

.1 Appendix A - MATLAB routines

Code 1: Damping coefficient calculations

```
time = T5;
mom = momtot5;

amp=0.0873; % 0.0873 0.131 0.175 (5 -7.5 & 10 deg)


%%%%characteristics for calculations
b=0.8;
d=0.25;
omega=2.72;
period=2.31;
n=3;


mcos=zeros(length(time));
msin=zeros(length(time));
for i = 1:length(time)
    mcos(i)= mom(i)*cos(omega*time(i));
    msin(i)= mom(i)*sin(omega*time(i));
%read values for time and moment
end
%run script

y_int = cumtrapz(time, mcos);   %%%%%%%%%% periods 2.15 - 2.31 - 2.5 - 2.75
intDamp = y_int(find(time <= 10, 1, 'last')) - y_int(find(time <= ...
    (10-period*n), 1, 'last'));

% x_int = cumtrapz(time, msin);
% intAdd = x_int(find(time <= 10, 1, 'last')) - x_int(find(time <= 2.47, ...
    1, 'last')); %endre integrasjonsperiode, 2.51



damp=(-1/(amp*pi*n))*intDamp %damping coeff
nondamp=(damp/(998.2*b^3*d))*sqrt(b/19.62) %non.dim dampingcoeff
% add=(1/(amp*pi*omega*n))*intAdd; %add.mass coeff
% nonadd=(add/(998.2*b^3*d)) %non.dim add.mass coeff (998.2*0.4^3*0.2)
```

Code 2: Analytic approximation for the free decay test

```
clear all;


%%%%%%%%%%%%%%%  Read Data   %%%%%%%%%%%%%%%%

filename='rollhistorybk2deg7.xlsx';
M = xlsread(filename,1);
time_s=M(:,1);
roll_exp=M(:,2)-mean(M(:,2));

q0 = [roll_exp(1);0];         % Initial Condition (vector)
h=0.02;                    % Time step
t = 0:h:14; .
%--------------------------------------------------------------------
I44=2;                %Only the sum of I44+A44 that matters, not correct
A44=.33;              %values for each one
C44=17.3;             %Restoring coefficient assumed constant
%--------------------------------------------------------------------
p1=0.072;  %damping values obtained from the Faltinsen fit
p2=0.021;
%--------------------------------------------------------------------
%dimensionalized damping coefficients
B44=p1*(I44+A44);
B44q=p2*(I44+A44);

qstar = zeros(2,length(t));  % Preallocate array (good coding practice)

Tr=2*pi*((I44+A44)/(C44))^0.5;

qstar(:,1) = q0;
for i=1:(length(t)-1)


k11=qstar(2,i);
k12=-C44/(I44+A44)*qstar(1,i)-B44/(I44+A44)*qstar(2,i)-B44q/(I44+A44)...
    *qstar(2,i)*abs(qstar(2,i));


q1=qstar(1,i)+h/2*k11;
q2=qstar(2,i)+h/2*k12;


k21=q2;
k22=-C44/(I44+A44)*q1-B44/(I44+A44)*q2-B44q/(I44+A44)*q2*abs(q2);
```

```
45
46
47 qstar(1,i+1)=qstar(1,i)+h*k21;
48 qstar(2,i+1)=qstar(2,i)+h*k22;
49
50
51
52 end
53
54 plot(time_s,roll_exp,t,qstar(1,:));        % ystar = first row of qstar
55 legend('CFD','Analytic approximation')
56 xlim([0 10])
57 xlabel ('Time, [s]')
58 ylabel('$\theta ^\circ$',  'interpreter','latex')
59 ylim([-10 10])
60 grid on
```

Code 3: Code for estimating the damping coefficients from the Free decay test

```
1   [pks,loc]   = findpeaks(roll_ang);    % same function in wafo, be careful
2
3  % must first run the script importEuler to establish needed data
4
5     loct(1:2:2*length(loc)-1) = loc;
6     pkst(1:2:2*length(loc)-1) = pks;
7     % Find pos of trough values
8
9     [pks,loc]   = findpeaks(-roll_ang);
10
11    loct(2:2:2*length(loc)) = loc;
12    pkst(2:2:2*length(loc)) =-pks;
13
14    initial_angle=7.5;%%%%%%%%%%%%%%%%%%%%%%%%%%%%%%%%%%%%%%%%%%%%%%%%%%%%%%%%
15
16
17     % Find linear and nonlinear damping coefficient
18    t = Time(loct);
19    r = zeros(1,length(pkst)+1);
20    for i =2:length(r)
21
22    r(i)=pkst(i-1);
23
24    end
25    r(1)=initial_angle;  %%%%% iniital roll amplitude
```

```
26
27      for i=1:length(t)-2
28          TT(i)=t(i+2)-t(i);
29      end
30
31  %     plot(Time,roll_ang)
32  %     hold on
33  %
34  %     plot(Time(loct),pkst,'k^')
35  %     hold on
36      Tm=mean(TT);
37
38       r2=abs(r) ;
39
40
41   end_val=length(t)-10;%subtract number of cycles at the end with this value
42
43       yy=zeros(1,end_val);
44       xx=zeros(1,end_val);
45      for i=2:end_val+1
46          yy(i-1)=2/Tm*log(r2(i-1)/r2(i+1));
47          xx(i-1)=16*r2(i)/(3*Tm);
48      end
49
50      P=polyfit(xx(1:end_val),yy(1:end_val),1); P1=P(2); P2=P(1);
51      output=polyval(P,xx(1:end_val)); %solving eq on p.252 in SeaLoads
52
53
54   fig = figure(2);
55   plot(xx(1:end_val),yy(1:end_val),'bo',xx(1:end_val),output(1:end_val))
56   title(['$p_1 =',num2str(P1,'%7.4f'),'$','  $p_2 =',num2str(P2,'%7.4f'),...
57       '$'],'Interpreter','latex','Color','k')
58  xlabel('$\frac{16 \theta_n}{3 T_m}$','Interpreter','latex','Fontname',...
59      'Times','fontsize',18);
60  ylabel('$\frac{2}{T_m}log\frac{\theta_{n-1}}{\theta_{n+1}}$',...
61      'Interpreter','latex','Fontname','Times','fontsize',18)
62  ylim([-0.1 1])
63     xlim([0 15])
```

.2 Appendix B - Grid sensitivity

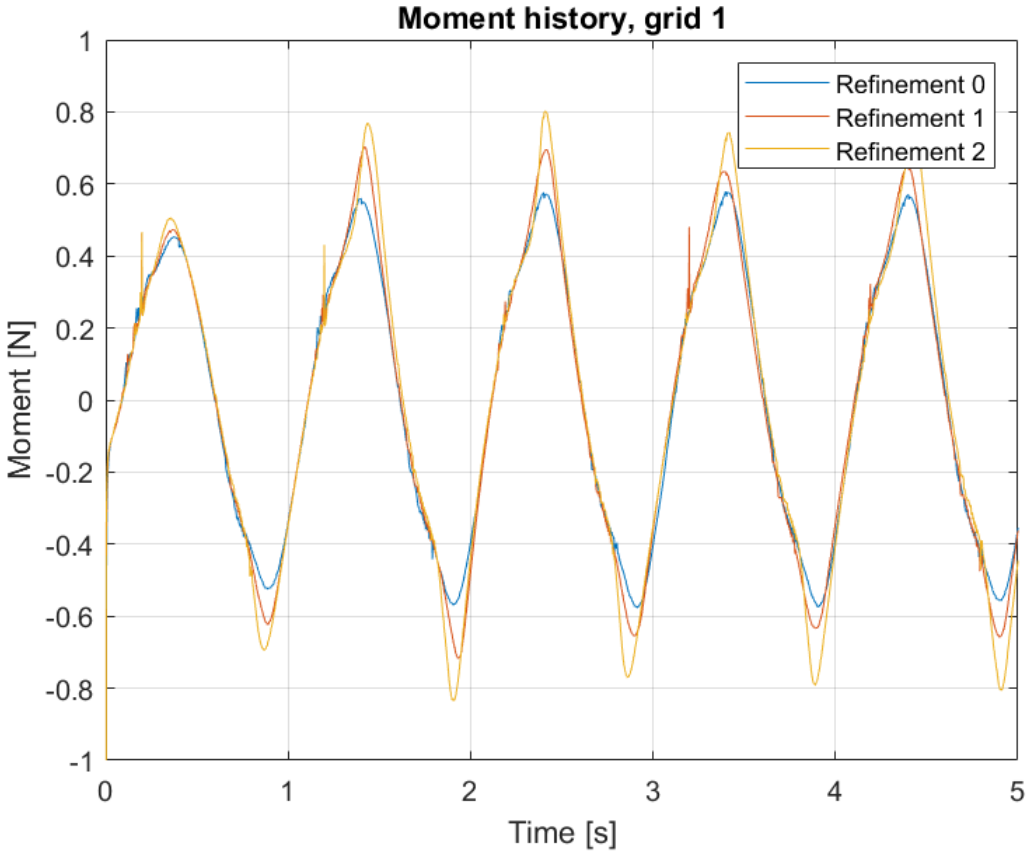

Figure 1: Moment history grid 1

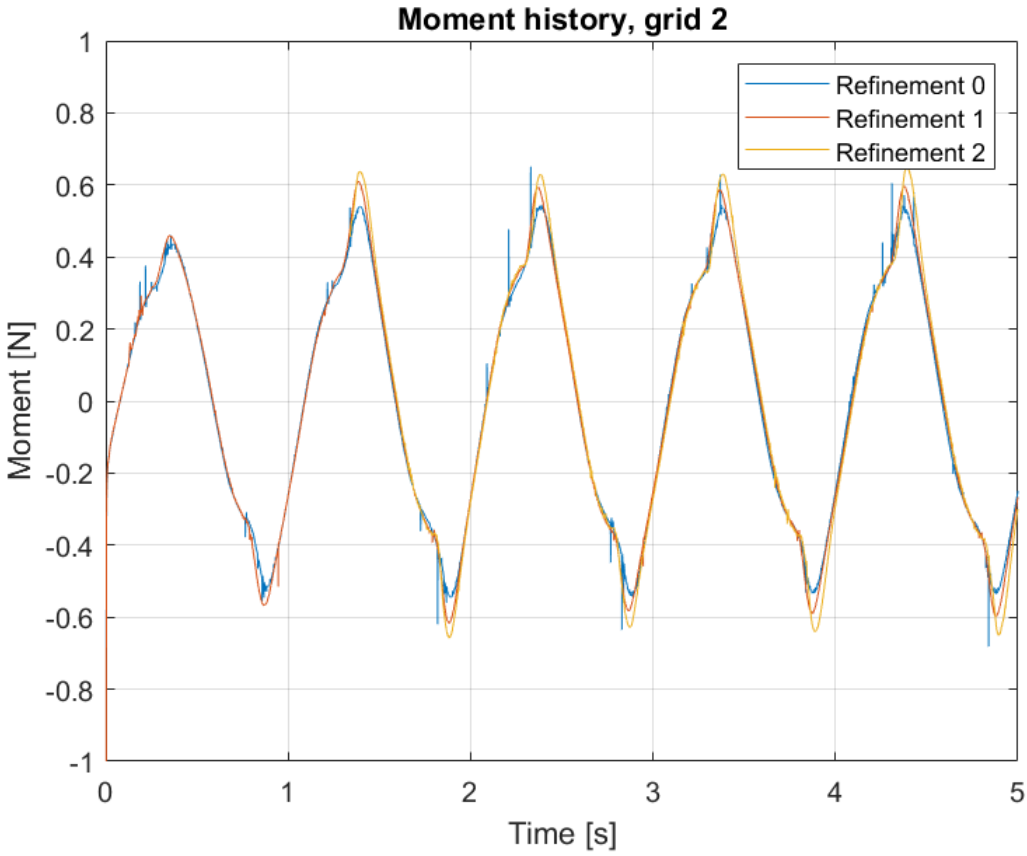

Figure 2: Moment history grid 2

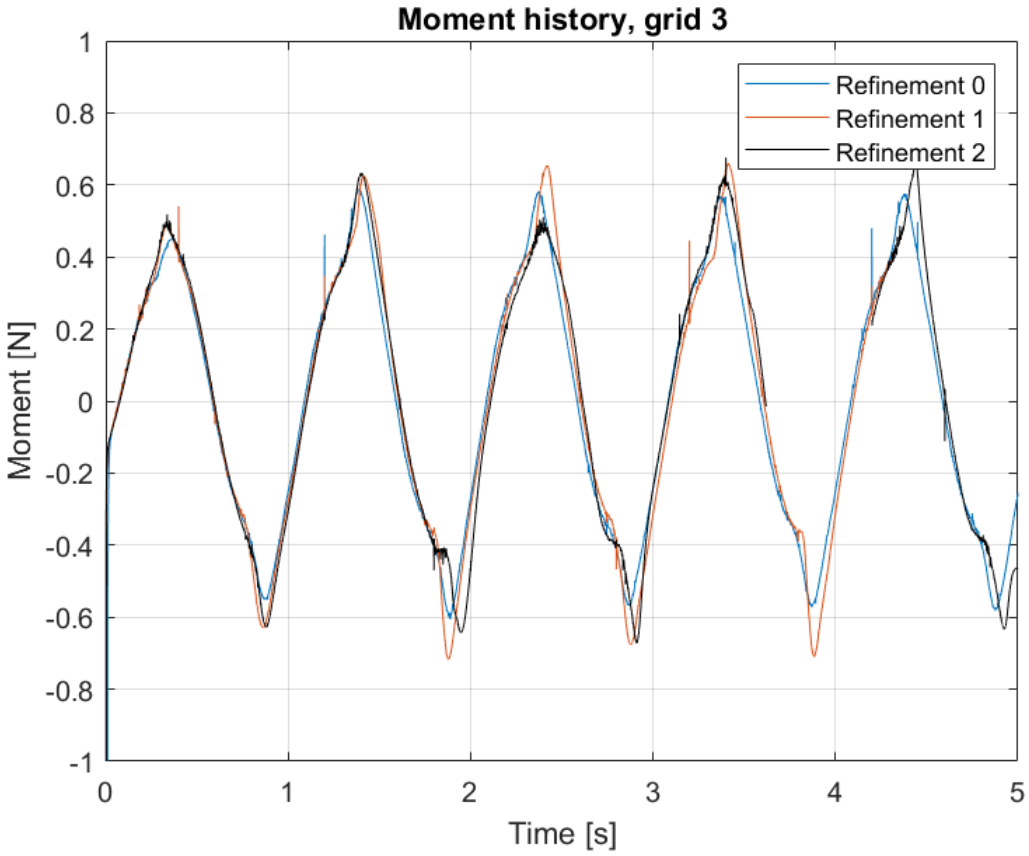

Figure 3: Moment history grid 3

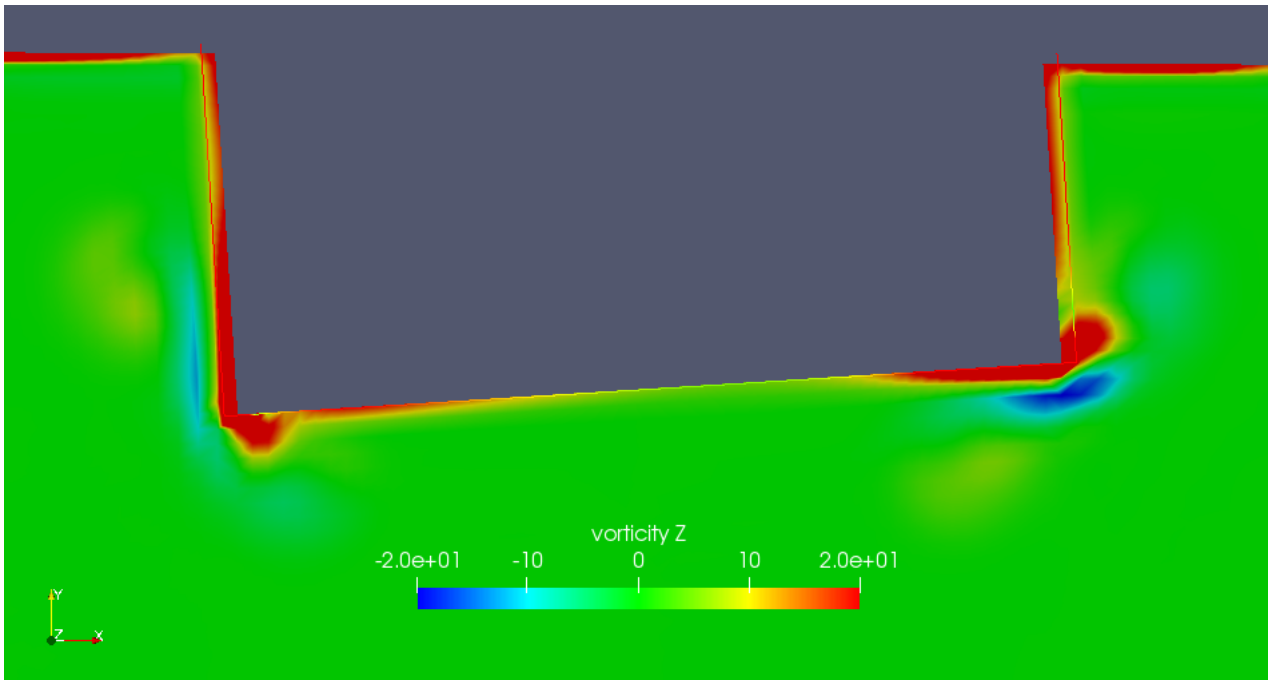

Figure 4: Z component of vorticity field for H-grid at T = 3.4 s.

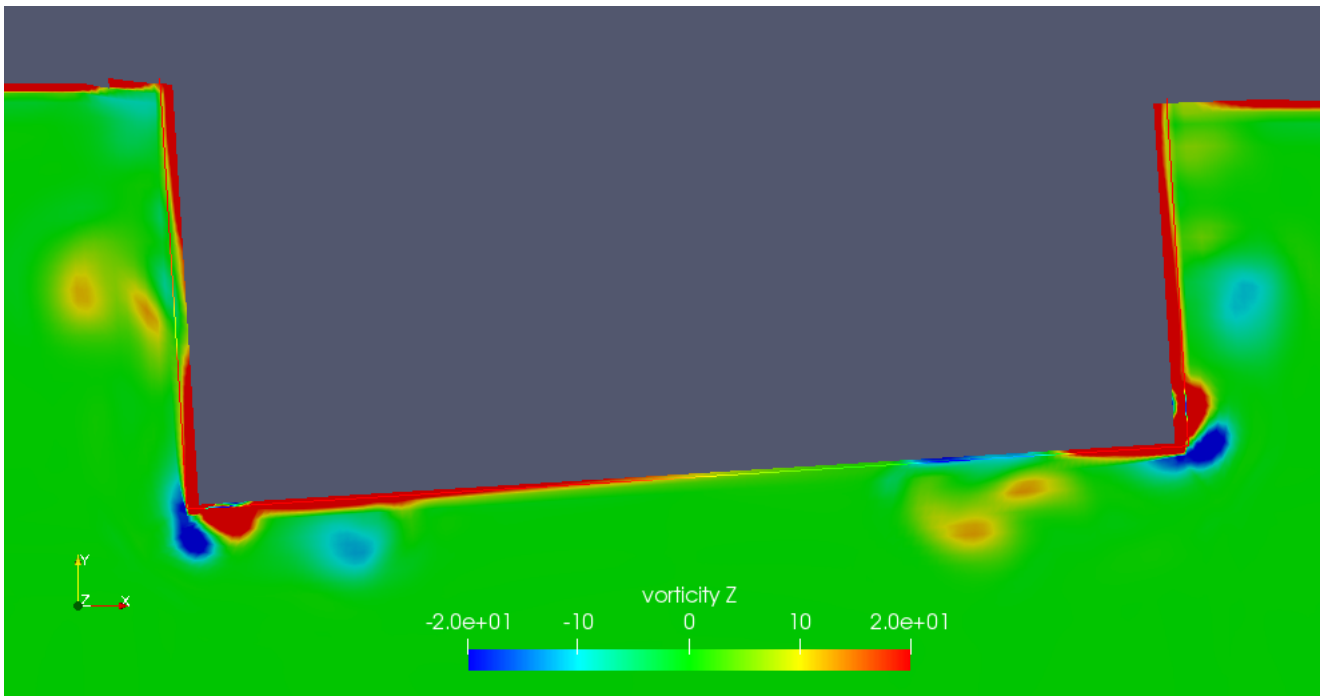

Figure 5: Z component of vorticity field for O-grid at T = 3.4 s.

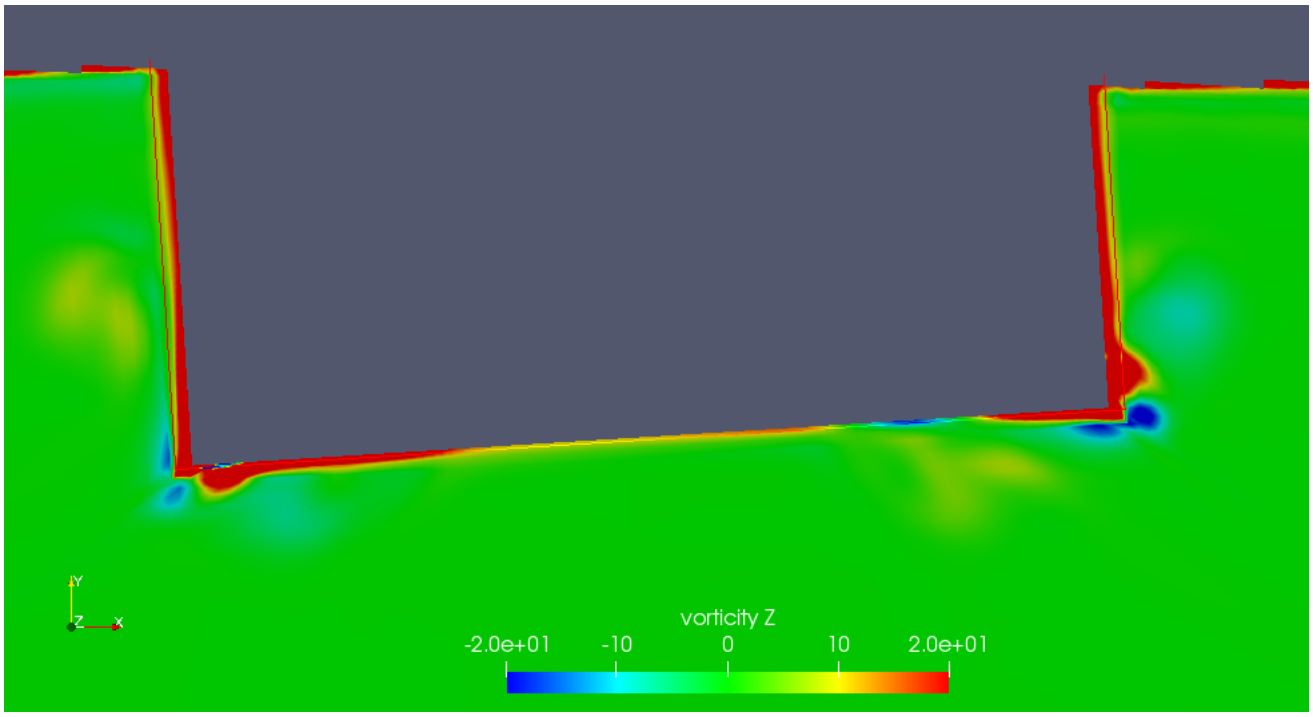

Figure 6: Z component of vorticity field for blockMesh made O-grid at T = 3.4 s.

.3 Appendix C - Free decay results

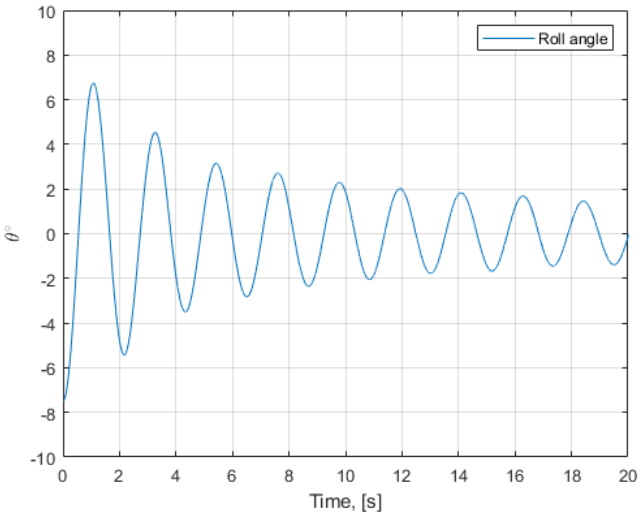

(a) BK0

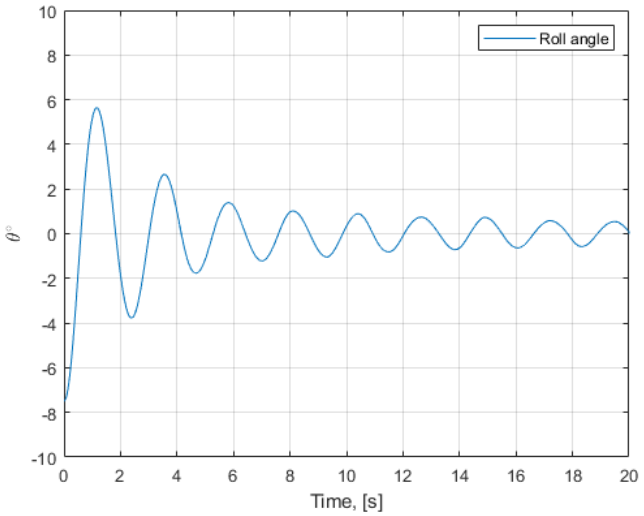

(b) BK2

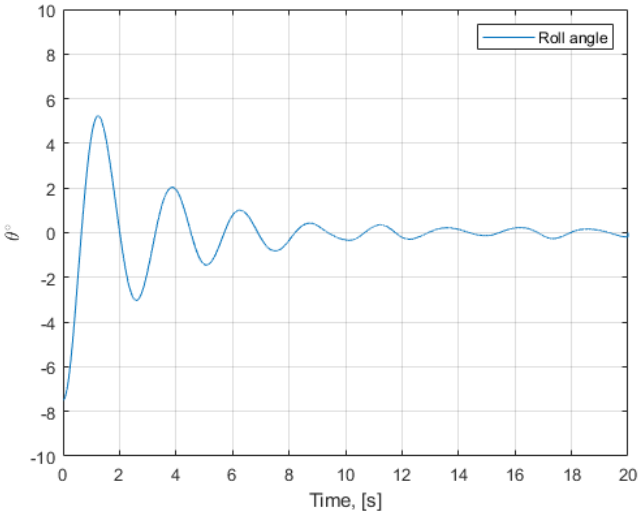

(c) BK4

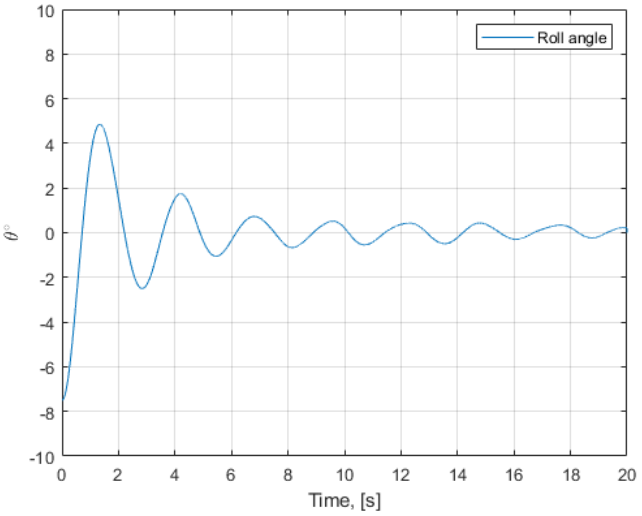

(d) BK6

Figure 7: Roll decay simulation for all sections at $\theta = 7.5$ °

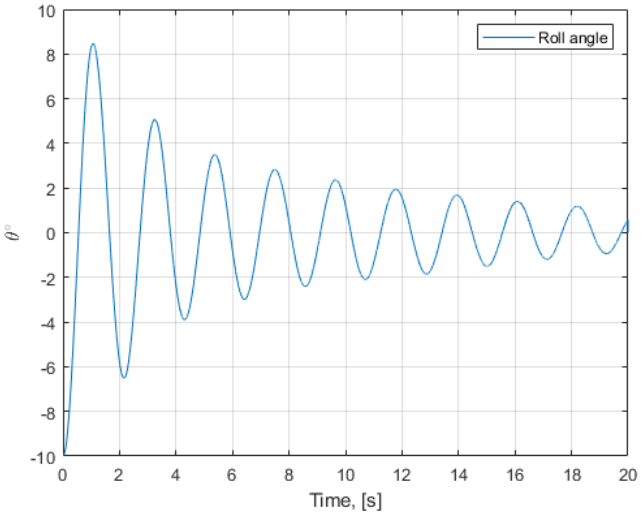

(a) BK0

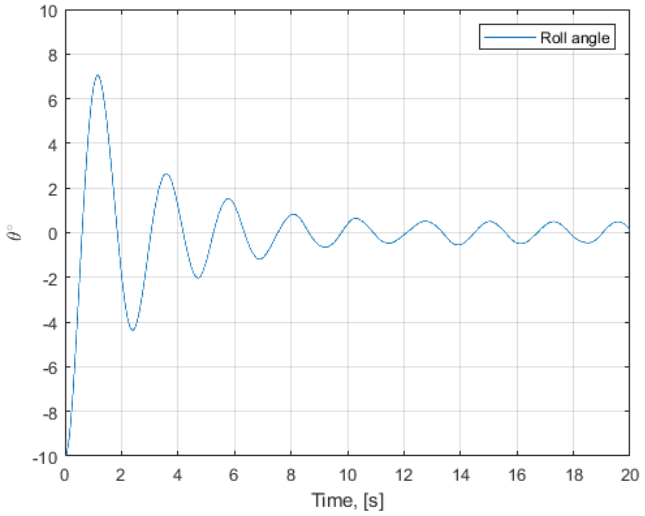

(b) BK2

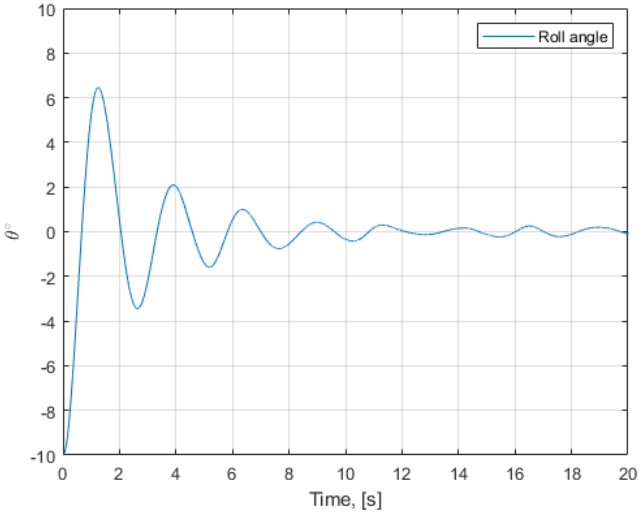

(c) BK4

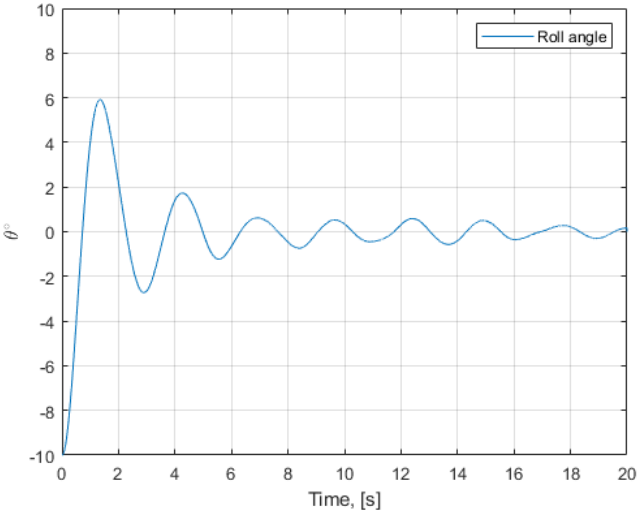

(d) BK6

Figure 8: Roll decay simulation for all sections at $\theta = 10$ °

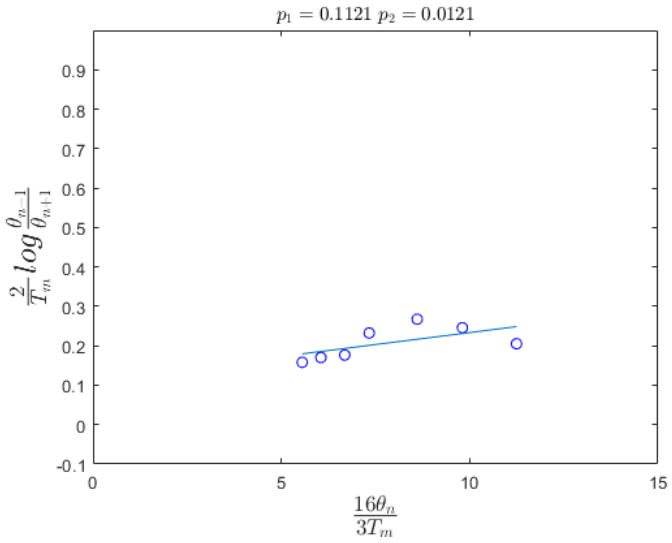

(a) BK0

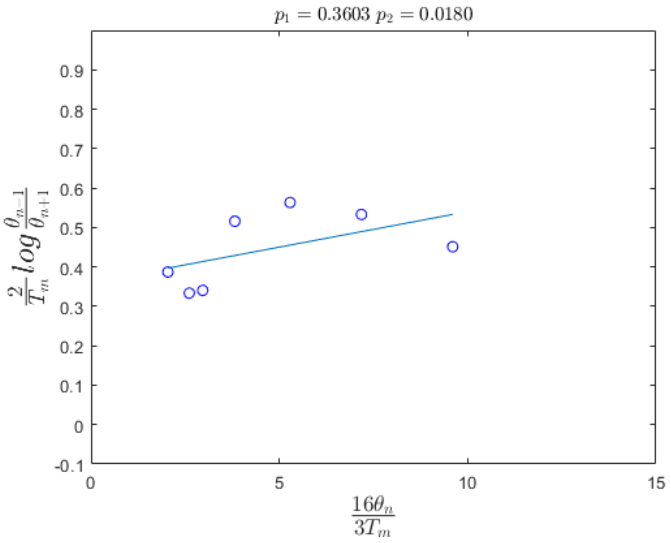

(b) BK2

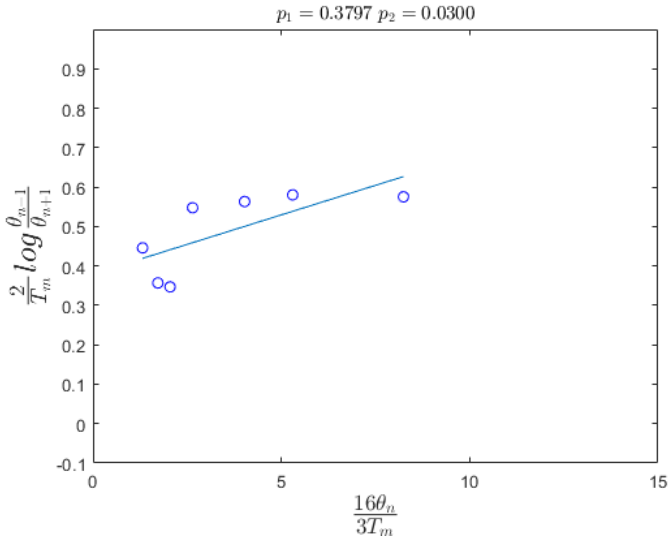

(c) BK4

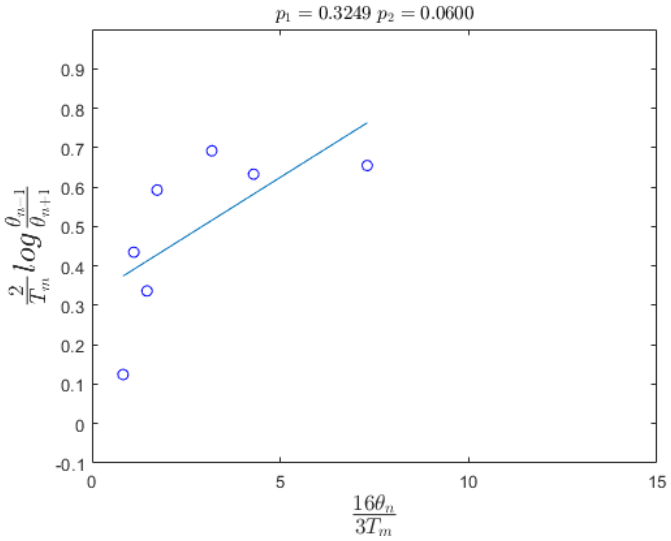

(d) BK6

Figure 9: The Faltinsen approach to estimate the damping coefficient p_1 and p_2. results for all sections at initial roll angle of 5°

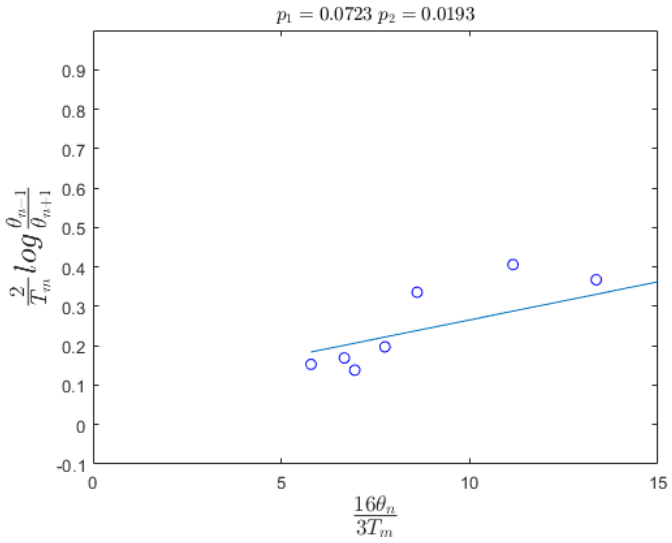

(a) BK0

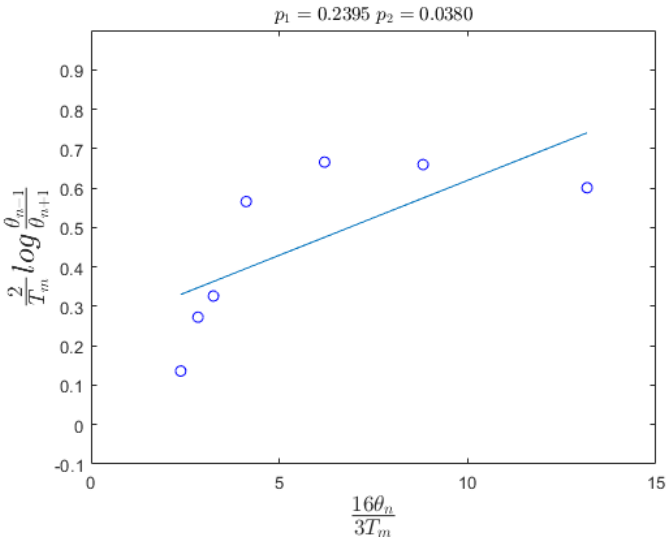

(b) BK2

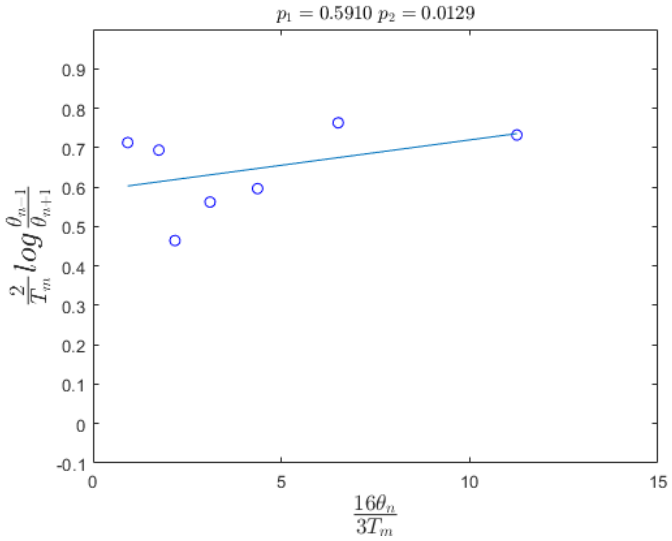

(c) BK4

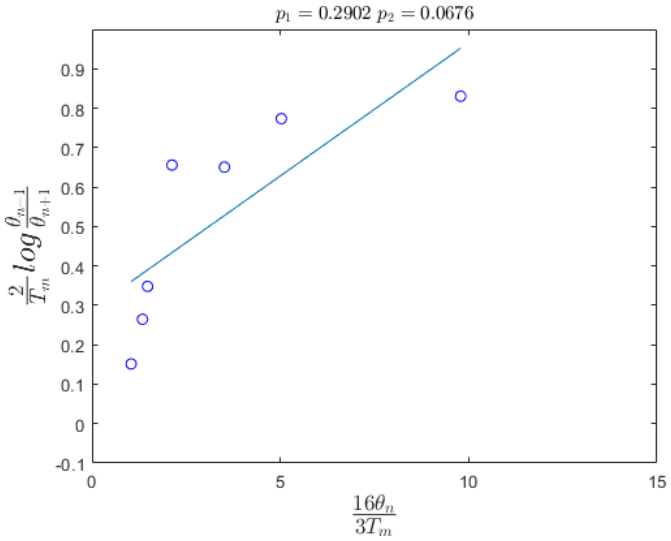

(d) BK6

Figure 10: The Faltinsen approach to estimate the damping coefficient p_1 and p_2. results for all sections at initial roll angle of 7.5°

Jensen

Numerical study on roll damping, relevant for FPSO platforms

NTNU
Norwegian University of
Science and Technology